11-13-2020

Bioscaffold Valve with and without Mechanically Conditioned Stem Cells for the Treatment of Critical Mitral Valve Diseases in the Young

Brittany A. Gonzalez
Florida International University, bgonz049@fiu.edu

FLORIDA INTERNATIONAL UNIVERSITY

Miami, Florida

BIOSCAFFOLD VALVE WITH AND WITHOUT MECHANICALLY CONDITIONED STEM CELLS FOR THE TREATMENT OF CRITICAL MITRAL VALVE DISEASES IN THE YOUNG

A dissertation submitted in partial fulfillment of the

requirements for the degree of

DOCTOR OF PHILOSOPHY

in

BIOMEDICAL ENGINEERING

by

Brittany A. Gonzalez

2020

To: Dean John Volakis
College of Engineering and Computing

This dissertation, written by Brittany A. Gonzalez, and entitled Bioscaffold Valve with and without Mechanically Conditioned Stem Cells for the Treatment of Critical Mitral Valve Diseases in the Young, having been approved in respect to style and intellectual content, is referred to you for judgement.

We have read this dissertation and recommend that it be approved.

_____
Nikolaos M. Tsoukias

_____
Arvind Agarwal

_____
Joshua D. Hutcheson

_____
Steve Bibevski

_____
Sharan Ramaswamy, Major Professor

Date of Defense: November 13, 2020

The dissertation of Brittany A. Gonzalez is approved.

_____
Dean John Volakis
College of Engineering and Computing

_____
Andres G. Gil
Vice President for Research and Economic Development
and Dean of the University Graduate School

Florida International University, 2020

DEDICATION

I dedicate my dissertation work to my loved ones. A special feeling of gratitude for my parents and sister, Rosemary, Jose and Bianca, who are my cheerleaders and never leave my side. Thank you for all that you do for me.

I dedicate this dissertation to my fiancé, George, for always encouraging me to do my best and reminding me that I can always get through anything I put my mind to. I thank you for being so patient, kind and understanding during my studies in graduate school and for always supporting me.

I also dedicate this work to my friend, Amirala, who always supported me throughout this PhD process; whether it be proofreading my writing, talking about results or discussing ideas. I appreciate our scientific and intellectual conversations but most of all I appreciate the friendship that grew out of our excitement for science.

I thank you all for the unconditional support and for being there for me throughout the entire doctorate program. None of this would be possible without you guys!

ACKNOWLEDGMENTS

I would like to thank the Biomedical Engineering Department for providing both professional and financial support, and the University Graduate School for awarding me with the Dissertation Year Fellowship to allow me to focus on the authoring of this dissertation. Significant portions of the research reported in this dissertation was funded by the American Heart Association (Award ID: 16GRNT31090009). Funding from the Miami Heart Research Institute is also gratefully acknowledged.

I would like to thank my advisor, Dr. Sharan Ramaswamy, for his support and guidance throughout my entirety time in the CV-PEUTICS Laboratory. Thank you for always challenging me and making me think critically and scientifically. I would like to acknowledge my committee for their support throughout the project and for providing me with knowledge in their various fields of expertise. I would like to especially thank Dr. Steve Bibevski for his immense help in teaching me and clarifying medical concepts, specifically when it came to our baboon surgeries. Thank you for taking the time to walk me through the surgeries step by step to make me feel like I was performing the surgeries with you.

I would also like to thank our team of cardiac surgeons, cardiologist and pathologist at Joe DiMaggio's Children Hospital and the veterinarians at Mannheimer Foundation, Inc. Thank you to my colleagues, Marcos, Asad, Tony, Andres and Jenniffer, who provided assistance, throughout different stages of the work presented in this dissertation.

ABSTRACT OF THE DISSERTATION

BIOSCAFFOLD VALVE WITH AND WITHOUT MECHANICALLY CONDITIONED STEM CELLS FOR THE TREATMENT OF CRITICAL MITRAL VALVE DISEASES IN THE YOUNG

by

Brittany A. Gonzalez

Florida International university, 2020

Miami, Florida

Professor Sharan Ramaswamy, Major Professor

Congenital heart diseases are the most common type of birth abnormality in the US. Infants with critical congenital valve disease have no established treatment-measure other than compassionate care options, owing to an absence of prosthetic valves in small sizes and their inability to support somatic growth. A regenerable valve would be appealing since these barriers could be overcome.

Porcine small intestinal submucosa (PSIS) bioscaffold was used to create valvular constructs with the possibility to grow overtime. PSIS bioscaffolds consisting of two different yarn-twist configurations (2ply and 4ply) were assessed for mechanical properties to determine which scaffold would withstand fatigue loading in a similar manner to the native heart valves. It was found that fatigued 2ply PSIS exhibited higher yield stress ($p<0.05$) and strain ($p=0.06$) compared to 4ply ones.

Next, a pilot study was investigated for implanting 2ply hand-made PSIS mitral valves into juvenile baboons (n=3) to assess their functionality and somatic growth longitudinally. Bioscaffold mitral heart valve function was assessed via echocardiography, while somatic growth was evaluated with a novel parameter, normalized aspect growth ratio (NAGR; ideal growth is 1), and via histological analysis after the valves were explanted. Our results showed trivial to mild regurgitation up to 17-months post-implantation demonstrating proper functionality of the PSIS mitral valves. The NAGR was found to be roughly 1 within the first 3 to 4 months, showing ideal growth. The PSIS mitral valve explants were found to develop extracellular matrix (ECM) at all explant time points (3-, 11- and 20-months). However, sudden valve failure occurred in all 3 subjects.

As a possible means to circumvent valve failure PSIS tubular mitral bioscaffold valves were subsequently seeded *in vitro* with bone marrow stem cells and exposed to pulsatile flow-induced oscillatory shear stresses in a perfusion bioreactor. It was found that our valve could produce ECM proteins significantly higher ($p<0.05$) than static control valves and also exhibited valve phenotypic characteristics (CD31 and α-SMA). Furthermore, the dynamic environment resulted in significantly higher ECM coverage on PSIS valves (61%, $p<0.05$). The allogeneic stem cells-seeded, bioscaffold mitral valves have the potential to accelerate *in vivo* valve tissue formation. We thus expect these oscillatory flow-conditioned valves to have longer-term function post-implantation compared to what was possible with the bioscaffold valves-alone.

TABLE OF CONTENTS

LIST OF TABLES

TABLES PAGE

LIST OF FIGURES

FIGURES PAGE

ABBREVIATIONS AND ACRONYMS

AA2P	Ascorbic Acid 2 Phosphate
ANOVA	Analysis of Variance
bFGF	Basic Fibroblast Growth Factor
BMCSs	Bone Marrow Stem Cells
BMP2	Bone Morphogenetic Protein 2
BSA	Body Surface Area
CCHVDs	Critical Congenital Heart Valve Defects
CHVDs	Congenital Heart Valve Defects
D	Annulus Diameter
DAPI	4,6-diamidino-2-phenylindole
E	Young’s Modulus
ECHO	Echocardiography
ECM	Extracellular Matrix
EMT	Endothelial-Mesenchymal Transformation
FDA	Food and Drug Administration
FESEM	Field Emission Scanning Electron Microscopy
hBM-MSCs	Human Bone Marrow Mesenchymal Stem Cells
hBMSCs	Human Bone Marrow Stem Cells
H&E	Hematoxylin and eosin
HSCs	Hematopoietic Stem Cells
IACUC	Institutional Animal Care and Use Committees
IDE	Investigational Device Exemption

KLF2A	Kruppel-like Factor 2a
LA	Left Atrium
LL	Leaflet Length
LV	Left Ventricle
Movat's	Russel-Movat Pentachrome
MSCs	Mesenchymal Stem Cells
MV	Mitral Valve
M2 Macrophage	Anti-inflammatory Macrophages
NAGR	Normalized Aspect Growth Ratio
NC	Neochordae
NK	Natural Killer Cells
OSI	Oscillatory Shear Index
PBS	Phosphate Buffered Saline
PECAM-1/CD31	Platelet Endothelial Cell Adhesion Molecule-1
PM	Papillary Muscles
PSIS	Porcine Small Intestinal Submucosa
SEM	Standard Error of Mean
SIS	Small Intestinal Submucosa
TAWSS	Time-averaged Wall Shear Stress
TEHV	Tissue Engineered Heart Valve
TGF-β	Transforming Growth Factor Beta
VECs	Valvular Endothelial Cells
VICs	Valvular Interstitial Cells

WSS	Wall Shear Stress
w/v	Weight per Volume
α-SMA	Smooth Muscle Actin
%RF	%Regurgitation Fraction

1. INTRODUCTION

1.1 Problem Statement

Congenital heart defects are the most common type of birth abnormality, affecting 8 out of 1,000 births in the US (www.aha.org). Despite distinct limitations, valve replacement is a successful technology for treating adults with critically diseased valves. On the other hand, infants with serious valve diseases have no established treatment-measure other than experimental or compassionate care options owing to an absence of prosthetic valves in small sizes and their inability to support somatic growth.

From a conceptual standpoint, a tissue engineered heart valve (TEHV) would be especially appealing since these barriers could be overcome; a TEHV can potentially provide for growth, self-repair, infection resistance and be a permanent approach for replacing defective heart valves (Stock, Vacanti et al. 2002). Scaffold selection is a critical component of TEHV development. The scaffold needs to be resilient to native hemodynamic cyclic loading conditions, degrade at a rate that matches *de novo* valve tissue growth and be pliable enough to facilitate valvular function. Soft tissue bioscaffolds possess these properties, but a protocol to optimize their usage in the TEHV application has not yet been identified. One such bioscaffold is porcine small intestinal submucosa (PSIS), which has recently gained popularity for assessment in cardiovascular applications (Badylak, Obermiller et al. 2003, Boyd, Johnson et al. 2010, Scholl, Boucek et al. 2010, Quarti, Nardone et al. 2011, Fallon, Goodchild et al. 2012, Hynes and Naba

2012, Witt, Raff et al. 2013, Gerdisch, Shea et al. 2014, Slaughter, Soucy et al. 2014), including heart valves (Pavcnik, Uchida et al. 2002, Pavcnik, Obermiller et al. 2009, Scholl, Boucek et al. 2010, Quarti, Nardone et al. 2011, Gerdisch, Shea et al. 2014, Bibevski and Scholl 2015, Mosala Nezhad, Poncelet et al. 2016, Bibevski, Levy et al. 2017).

PSIS, a biodegradable bioscaffold, has demonstrated the ability to recruit endogenous cardiovascular cells, leading to phenotypically-matched replacement tissue once the bioscaffold has completely degraded (Slachman 2014). Within our research group, our clinical colleagues have already shown that valves made from PSIS bioscaffolds have functioned flawlessly for over a year (clinical observations), in the compassionate care of pediatric patients. Even so, there have been reports of immune responses (Witt, Raff et al. 2013, Gerdisch, Shea et al. 2014, Mosala Nezhad, Poncelet et al. 2016) associated with PSIS. Therefore, seeding PSIS valves with bone marrow stem cells (BMSCs) before implantation may help to eliminate this immune response due to their immunomodulatory properties (Weber, Emmert et al. 2012, Gallina, Turinetto et al. 2015) but moreover, it will allow for differentiation of these BMSCs into valvular phenotypes to accelerate the regeneration once implanted.

To date, an objective and systematic study to evaluate PSIS valve growth potential and functional assessment has not been conducted. Support of somatic growth is a fundamental requirement of tissue-engineered valves in the young. However, efforts thus far have been unable to maintain this support long term. A

key event that will determine the valve's long-term success is the extent to which healthy host tissue remodeling can occur on the valve soon after implantation. The construct's phenotypic status plays a critical role in accelerating tissue remodeling and engineered valve integration with the host via chemotaxis. It is crucial that major extracellular matrix (ECM) components are present since all cells need the ECM in order to attach, grow and proliferate (Kusindarta and Wihadmadyatami 2018). The ECM will provide the proper surface and environment for support and anchorage of the cells, regulates and determines the cells' dynamic and behavior including: survival, proliferation, polarity, differentiation, adhesion, and migration (Kusindarta and Wihadmadyatami 2018). Moreover, the ECM, provides the mechanical support for the tissue and is involved in the growth mechanism, regenerative, and healing processes (Kusindarta and Wihadmadyatami 2018). Therefore, the purpose of this work is to achieve this task through a profound *in vitro* evaluation and concurrently conduct a pilot *in vivo* investigation on the valve's ability to support somatic growth in a juvenile, nonhuman primate model.

1.2 Specific Aims and Outcomes

We hypothesize that **mitral valve constructs comprising of mechanically conditioned bone marrow stem cells (BMSCs) seeded onto a porcine small intestinal submucosa (PSIS) bioscaffold, can provide robust function, support somatic growth and remain biocompatible, owing to: PSIS viscoelastic response, and *de novo* BMSC-secreted extracellular matrix (ECM)-to-host cell communications, respectively.** Our specific aims are:

Specific Aim 1: Assess static and fatigue mechanical responses of PSIS bioscaffold under two different textile assemblies, 2ply and 4ply relating to the laminated layers of two and four ECM fibers together, respectively. Non-fatigue and fatigue tensile tests were performed. Stress versus strain graphs were computed and different parameters were calculated, including Young's modulus (E), yield stress, yield strain and toughness.

Specific Aim 2: **Analyze the *in vivo* growth potential and functionality of the intact PSIS mitral valve temporally without cell-seeding or additional treatment measures.** A longitudinal echocardiographic (ECHO) PSIS mitral valve evaluation in baboons (n=3) until 20 months of age (implanted at 12-14 months of age) was conducted. At post-implant, all animals were sacrificed for direct evidence of growth, tissue integration with the host, phenotype of integrating cells and biocompatibility through histological evaluation.

Specific Aim 3: **Assess *de novo* ECM properties of acellular PSIS bioscaffolds seeded with BMSCs and subsequently conditioned with pulsatile flow-induced oscillatory shear stresses *in vitro*.** The BMSC-seeded PSIS valves were conditioned using a customized pulsatile flow, oscillatory shear stress-inducing mechanical conditioning protocol, that enhances the expression of valve regeneration biomarkers for mitral valve regeneration (Rath, Salinas et al. 2015, Williams, Nasim et al. 2017). The enhanced ECM-rich PSIS mitral valves were assessed for valvular ECM components and phenotype through histological and immunofluorescence evaluation.

2. LITERATURE REVIEW

2.1 Composition and Functionality of Mitral Valves

There are four valves in the heart, which function to promote unidirectional blood flow during the cardiac cycle. The mitral and tricuspid valves separate the atria from the ventricles, while the other two valves, aortic and pulmonary, separate the ventricles from the arteries (**Figure 1A**) (Hinton and Yutzey 2011). Our heart valve of interest is the mitral valve (MV), which connects the left atrium (LA) to the left ventricle (LV). The MV opens during diastole, allowing the blood to flow from the LA to the LV and conversely, closes during systole, preventing backflow to the LA (**Figure 1B**) (McCarthy, Ring et al. 2010).

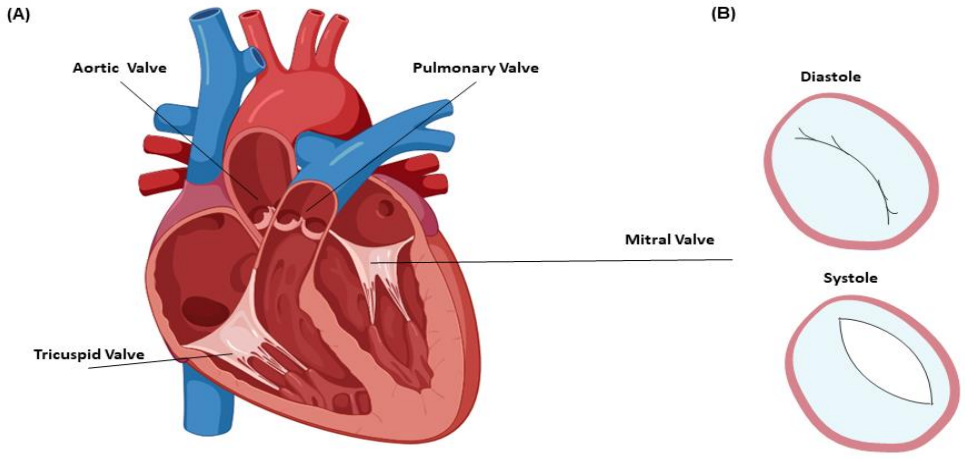

Figure 1: *Composition and functionality of the mitral valve***.** Cross-section of a heart with (**A**) the four valves focusing on (**B**) the mitral valve, where the valve is closed during diastole and opens during systole. Proper functioning of the valve allows for blood to flow from left atrium to left ventricle without backflow occurring.

The development of the MV is highly-complex and not fully understood. The developing MV is essentially a tube composed of extracellular matrix (ECM) surrounded by myocardial and endothelial layers (Dal-Bianco and Levine 2013).

The cardiac cushions are formed via endothelial-mesenchymal transformation (EMT), where endothelial cells migrate into the mesenchyme and become interstitial fibroblast cell types (Dal-Bianco and Levine 2013). The leaflets originate from the cushions followed by the papillary muscles and chordae. The MV is fully developed at 15 weeks and continues to grow with the developing organism (Dal-Bianco and Levine 2013).

There are four major components of the MV that are needed for proper function of the MV, which include the annulus, leaflets, chordae tendineae and papillary muscles attached to the LV wall (**Figure 2**) (Dal-Bianco and Levine 2013). An imbalance interaction between these key components can lead to dysfunctional MV, namely regurgitation, stenosis or a combination of both.

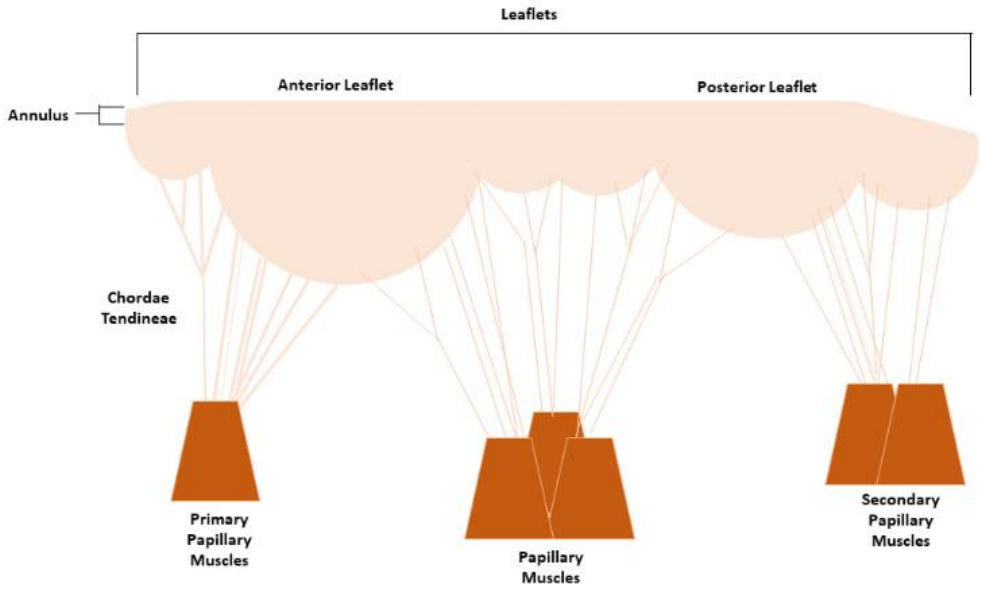

Figure 2: *Important features of the mitral valve*. Cross-section of the mitral valve focusing on the key components including the annulus, leaflets, chordae tendineae and papillary muscles. Each component is needed for the mitral valve to function properly. (Adapted from Carpentier A et al. Carpentier's Reconstructive Valve Surgery. From Valve Analysis to Valve Reconstruction. 2010 Saunders Elsevier)

The MV annulus, is the tissue structure that brings together the LA, LV and the MV leaflets. There are two portions of the MV annulus, the anterior and

posterior components. The anterior annulus is the flatter region of the annulus consisting of parallel collagen fibers (Dal-Bianco and Levine 2013). On the other hand, the posterior annulus is loosely anchored to the tissue, allowing for movement when contraction or relaxation occurs (Dal-Bianco and Levine 2013).

Similarly, the MV leaflet component has both anterior and posterior leaflets and are circumferentially attached to the annulus. The anterior leaflet has crossed collagen strands, suggesting tight anchoring, and is larger, longer and thicker than the posterior leaflet, thereby allowing for higher tensile load (Dal-Bianco and Levine 2013). The MV leaflet consists of three layers, the fibrosa/ventricularis, spongiosa and the atrialis, which have specific ECM components of collagen, water absorbing proteins and elastin, respectively. The collagen that are circumferentially oriented provide tensile stiffness; the radially oriented elastic fibers allow for tissue extension and recoil during the opening and closing of the valve; proteoglycans, water rich proteins, provide compressibility and integrity of the valve. This highly ordered ECM is critical for proper valve function. Two main cell types reside in the MV leaflets, endothelial and interstitial cells. The valvular endothelial cells (VECs) cover the blood-contacting surfaces and are sensitive to biomechanical stimuli, while the valvular interstitial cells (VICs) are mostly found in the central regions of the leaflet, which are quiescent in a mature valve and help to maintain normal valve ECM, but can also get activated to elicit altered ECM production in the event that the VICs sense abnormal mechanical stresses (Liu, Joag et al. 2007, Dal-Bianco and Levine 2013). Since blood flow is pulsatile, the

VECs on the ventricularis often experience unidirectional shear stress, while the fibrosa is strained and largely experiences oscillatory shear stress (Cheung, Duan et al. 2015).

Other important features of the MV are the chordae tendineae, which are fibrous strings that branch from the papillary muscles and attach to the leaflets, composed of tightly linked collagen and elastin. There are two types of chordae, primary chordae and secondary chordae (Dal-Bianco and Levine 2013). The primary chordae are thinner and are located at the tip of the leaflets, having a high concentration of collagen limiting its extensibility; conversely, the secondary chordae are thicker and are more extensible due to its tightly crimped collagen (Dal-Bianco and Levine 2013).

The last important components of the MV are the papillary muscles, lateral and medial, which originate from the left ventricle and are connected to the chordae attaching to the leaflets. The lateral papillary muscle usually has one head and is supplied with blood via the left circumflex and left anterior descending artery (Dal-Bianco and Levine 2013). On the other hand, the medial papillary muscle has two heads and is either supplied with blood from the right or circumflex coronary artery based on dominance (Dal-Bianco and Levine 2013). All these key components are complex and essential for the MV to function properly.

2.2 Biomechanics of the Mitral Valve

The valve structure-function relation is important to understand the mechanisms of valve homeostasis, development and disease progression (Hinton and Yutzey 2011). It is noteworthy to consider the physiological forces based on the valve position and hemodynamics, since the left side of the heart has higher pressures than the right side (Hinton and Yutzey 2011). Moreover, the structure, organization and leaflet thicknesses are different depending on the valve of interest (Brazile, Wang et al. 2015). There are three main loading stimuli affecting all valves, namely, flexure, fluid-induced shear and tension. Cyclic flexure occurs when the valve is opening and closing, shear originates from the blood flowing through the valves and cyclic tension occurs during valve closure (Hinton and Yutzey 2011).

The MV specifically is governed by the interaction between the MV annulus, leaflets, papillary muscles, chordae and LV. The closing forces involved in the MV include the LV contraction, basal myocardial rotation, mitral annulus and papillary muscle contraction along with tethering forces of the mitral annulus and papillary muscle-chordae interaction (Dudzinski and Hung 2014). A more simplified diagram of the forces exchanged between the papillary muscle tips and the MV are shown (**Figure 3**), with a force equilibrium equation demonstrating that the total papillary muscle force is equivalent to the combined forces of the chordae tendineae (closing forces) and the valvular-ventricular interaction forces (Askov, Honge et al. 2013). It has been found that the atrioventricular valves, including the MV, are

stiffer than the semilunar valves, with specifically the left-side leaflets being stiffer than the right-sided ones (Brazile, Wang et al. 2015). The MV was found to have the largest flexural rigidity and lowest bending modulus compared to all other valves, which can be correlated with the leaflet thickness and collagen alignment (less aligned), respectively (Brazile, Wang et al. 2015).

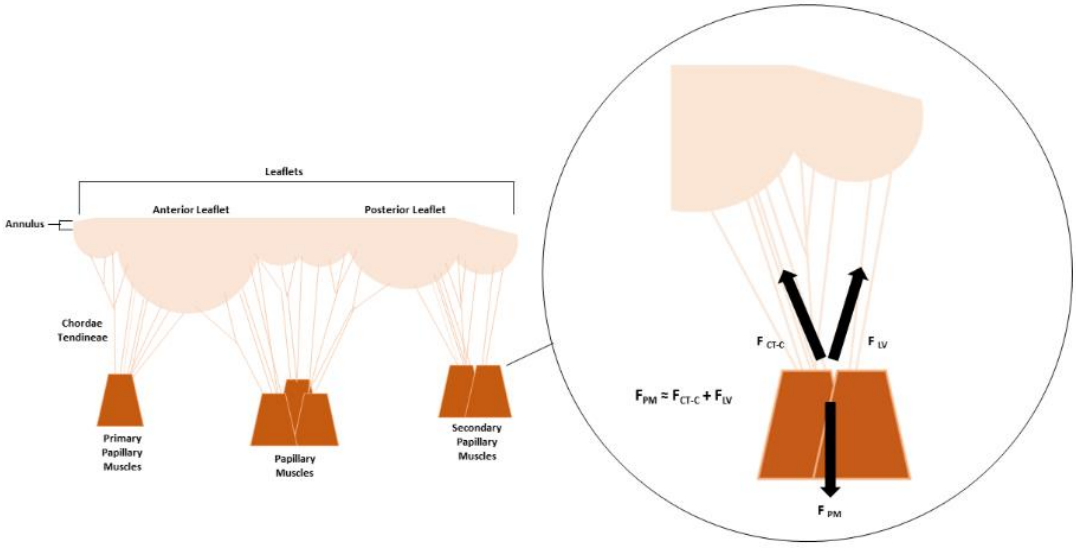

Figure 3: *Force exchange on the mitral valve components.* Cross-section of the mitral valve focusing on the interactions between the papillary muscles (F_{PM}), the chordae tendineae closing force (F_{CT-C}) and the valvular-left ventricle interaction force (F_{LV}), where $F_{PM} \approx F_{CT-C} + F_{LV}$ (Adapted from Askov J.B, et al. Evolving Technology/Basic Science. Significance of force transfer in mitral valve-left ventricular interaction: In vivo assessment. 2013. The Journal of Thoracic and Cardiovascular Surgery.)

2.3 Congenital Heart Valve Defects

Congenital heart valve defects (CHVDs) are diagnosed when there is a problem with the structure or function of the heart valve that is present at birth, which obstructs the normal blood flow. Congenital heart malformations are the most common type of defect present at birth, with CHVDs occurring in roughly 2% of live births, although the incidence is thought to be significantly higher since many cases remain subclinical and are unidentified (Hinton and Yutzey 2011). The two most common valves affected are the aortic and mitral valves, with mitral valve

prolapse being the most common (5% of the general population) (Hinton and Yutzey 2011). Other common MV diseases include regurgitation and stenosis. Regurgitation is when the valve does not close properly, leading to a backflow of blood. Stenosis, conversely, is when the valve cannot open properly, not providing the heart with enough blood flow. There are several types of CHVDs, that range from simple to complex and critical. The subset of focus is critical congenital heart valve defects (CCHVDs), specifically in the MV. Infants born with CCHVDs usually have low levels of oxygen soon after birth and need surgery within the first year of their birth (www.nhlbi.nih.gov).

2.3.1 Replacement Treatment Options for CHVDs

Valvular pathologies in infants and children are challenging cases. Valvular repair is usually preferred if possible, so that native tissue is still present and allows for growth. For these patients with CCHVDs, reconstruction may fail or is not feasible and so the only other option is replacement of the valve. There are three options of replacement for the mitral valve: homografts, bioprosthetic or mechanical valves, of which the most common selection being mechanical and bioprosthetic valves (Henaine, Roubertie et al. 2012). These replaced valves work well for the adult population, with each having certain advantages and drawbacks. Mechanical valves are very durable but require the need for life-long anticoagulants, while homografts and bioprosthetic valves have hemodynamics similar to native valve but are less durable and eventually degenerate (Etnel, Huygens et al. 2019). Moreover, homografts are limited in supply. These treatment

options do not suffice for infants with CCHVDs since artificial valves are manufactured in sizes of 18–30 mm diameter, while pediatric patients usually require a valve diameter of at most 15 mm, and frequently much less (Alsoufi 2014). Moreover, these patients need a valve replacement that can grow at a similar rate as their growth rate since they grow rapidly, which would eliminate the need for multiple reoperations. Therefore, a TEHV can potentially be an ideal treatment option for infants and pediatrics suffering from CCHVDs, where growth and biological integration is essential.

2.4 Regenerative Medicine Approaches for Heart Valves

Regenerative valve replacement options are needed mostly for the pediatric population, where growth and biological integration are key to proper function. These valve scaffolds should be biodegradable, biocompatible and non-immunogenic with added features of non-thrombogenic, non-obstructive and able to open and close properly for TEHVs (**Figure 4**) (Cheung, Duan et al. 2015). These scaffolds should ideally accommodate somatic growth and be able to remodel with the patient overtime. The TEHVs should withstand the mechanical properties required for the valve to function properly and adapt to the hemodynamic environment. Moreover, the TEHVs should promote cellular infiltration and differentiation to native valvular phenotype (Cheung, Duan et al. 2015). Therefore, the choice of scaffold and processing are vital to fulfill the TEHVs

requirements. There are several techniques that have been explored, including mold/suturing, electrospinning, 3D printing and decellularization.

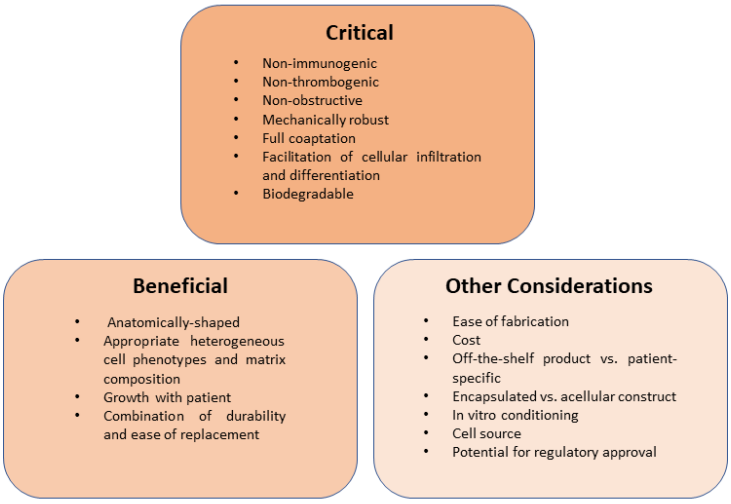

Figure 4: *Engineering criteria for heart valve fabrication***.** The critical components are listed, which are needed and essential for proper tissue regenerative heart valves. Furthermore, there are some recommendations and other considerations listed that may be beneficial but are not completely necessary, depending on the population of interest. (Adapted from Cheung, D.Y. et. al. Current progress in tissue engineering of heart valves: multiscale problems, multiscale solutions. 2015. Expert opinion on biological therapy.)

There has been interest in molding and suturing of both natural and synthetic materials to create TEHVs. One natural material used is purified collagen, which has been used to fabricate valve leaflets, as well as whole conduits with various cell types and matrix fiber alignments (Cheung, Duan et al. 2015). Fibrin is another popular natural material used to create TEHVs, since fibrinogen can be produced from blood and used to create fibrin hydrogels that are autologous (Cheung, Duan et al. 2015). The major problem with these biological proteins based TEHVs is that the leaflets cannot withstand the stresses that are applied once implanted. Similarly, synthetic materials have been used because they have the added advantage to be manipulated for certain mechanical and chemical properties and degradation rates (Cheung, Duan et al. 2015). These

different blends of synthetic material can then be seeded with cells before implantation. The main struggle for these TEHVs is to create a blend that is as similar as possible to the native valve mechanically and chemically, while degrading at a rate that is not too fast leading to structural incompetency but not too slow leading to a chronic immune response.

Other techniques that have been explored are electrospinning and 3D printing. Electrospinning allows for fine fibers to be created mimicking the native valve anatomy promoting cell growth and differentiation. Most electrospun materials used are polyester or elastomers, which create fibrous scaffolds (Cheung, Duan et al. 2015). 3D printing is used to create a TEHV that is anatomically and structurally similar to native valve tissue, using bioinks. These techniques are challenging for the same reasons mentioned above (synthetic materials used to mold and suture): balancing between mechanics, chemically structured and favorable degradation rate.

The last technique, which is of interest, is decellularization of bioscaffolds. These decellularized tissues can be either human-derived donor tissues, or animal-derived, although a majority are animal-derived due to availability. Further details about decellularized bioscaffolds are discussed below (Section 2.4.1).

2.4.1 Decellularization of Bioscaffolds

Decellularization is the process of using a tissue or organ and removing its cellular components while retaining the ECM structure and proteins (Cheung,

Duan et al. 2015). The cell removal can be done physically, chemically or with biological reagents (Cheung, Duan et al. 2015). Similar to bioprosthetic valves, decellularized heart valves provide hemodynamics mimicking the native heart valves. Decellularized heart valves have the added advantage of not being treated with glutaraldehyde, which allows for the cells to repopulate and remodel (Cheung, Duan et al. 2015). Moreover, these decellularized bioscaffolds reduce the immune response that leads to rejection of xenografts.

There are several contradicting outcomes associated with the use of decellularized valves. Some studies showed that decellularized valves showed immunogenicity and thrombogenicity (Bayrak, Tyralla et al. 2010, Zhou, Fritze et al. 2010, Cheung, Duan et al. 2015), while other valves did not show any immune response (Ota, Taketani et al. 2007, Arai and Orton 2009, Flameng, De Visscher et al. 2014, Cheung, Duan et al. 2015). Moreover, decellularized valves have shown potency and functionality in canine (Takagi, Fukunaga et al. 2006, Cheung, Duan et al. 2015), ovine (Akhyari, Kamiya et al. 2010, Cheung, Duan et al. 2015, Lauten, Laube et al. 2015), porcine (Honge, Funder et al. 2011, Cheung, Duan et al. 2015) and humans (Williams 2014, Cheung, Duan et al. 2015). Although there are contradicting results, there is no study for heart valves that have been objective and systematic. Therefore, exploring a decellularized bioscaffold, with and without further treatment is of interest, since it has an intact ECM and the added benefit to potentially grow, a key feature needed for patients with CCHVDs. Overall, decellularized TEHVs seem promising for valve replacement in the young.

2.4.2 Porcine Small Intestinal Submucosa (PSIS)

Decellularized bioscaffolds are of interest for TEHVs since these materials are composed of soft tissue ECM and are thus suited for enabling valve structural deformations. The primary biochemical constituents of the bioscaffold are collagen, glycoproteins, proteoglycans, mucins, elastic fibers, and growth factors (Hynes and Naba 2012). Bioscaffold valves have exhibited promising durability, growth, endothelialization, and absence of thrombus (Clarke 1999, Dohmen, Costa et al. 2005, Kim, Lim et al. 2006, Nejad, Blaser et al. 2016). A decellularized material that has recently received considerable attention for use in cardiovascular applications, which has received Food and Drug Administration (FDA) Investigational Device Exemption (IDE) for early clinical feasibility assessment, is PSIS (Sandusky Jr, Badylak et al. 1992, Robotin-Johnson, Swanson et al. 1998, Matheny, Hutchison et al. 2000, Rosen, Roselli et al. 2005, Ruiz, Iemura et al. 2005, White, Agnihotri et al. 2005, Yavuz, Geyik et al. 2006, Pavcnik, Obermiller et al. 2009, Bayrak, Tyralla et al. 2010, Boyd, Johnson et al. 2010, Scholl, Boucek et al. 2010, Gilbert, Gnanapragasam et al. 2011, Quarti, Nardone et al. 2011, Boni, Chalajour et al. 2012, Fallon, Goodchild et al. 2012, Hynes and Naba 2012, Padalino, Castellani et al. 2012, Eckhauser, Hannon et al. 2013, Poulin, Horlick et al. 2013, Stelly and Stelly 2013, Witt, Raff et al. 2013, Yanagawa, Rao et al. 2013, Cua, Kollins et al. 2014, Fallon, Goodchild et al. 2014, Gerdisch, Shea et al. 2014, Slaughter, Soucy et al. 2014, Sündermann, Biefer et al. 2014, Toeg, Abessi et al. 2014, Wallen and Rao 2014, Yanagawa, Rao et al. 2014, Zaidi, Nathan et al. 2014,

Bibevski and Scholl 2015, DuBose and Azizzadeh 2015, Padalino, Quarti et al. 2015, Soucy, Smith et al. 2015, Zafar, Hinton et al. 2015, Mosala Nezhad, Poncelet et al. 2016, Woo, Fishbein et al. 2016, Bibevski, Levy et al. 2017, Gonzalez, Pour Issa et al. 2020).

Small intestinal submucosa (SIS) is a biomaterial used for implantation in clinic for tissue engineering and regenerative medicine in arteries, bladder, intestinal tract, valve, esophagus and tendon (Wang, Chen et al. 2019). The structural composition of SIS consists mostly of collagen with traces of elastin, fibronectin, laminin, glycosaminoglycans and proteoglycans (Wang, Chen et al. 2019). These components have been linked to promoting healing, cell attachment on the ECM and inhibition of substrate degrading enzymes for collagen, glycoproteins and proteoglycans, respectively (Wang, Chen et al. 2019).

Of note, preclinical and clinical studies have reported both positive (Badylak, Obermiller et al. 2003, Boyd, Johnson et al. 2010, Scholl, Boucek et al. 2010, Quarti, Nardone et al. 2011, Hynes and Naba 2012, Slaughter, Soucy et al. 2014, Soucy, Smith et al. 2015) and negative (Pavcnik, Uchida et al. 2002, Pavcnik, Obermiller et al. 2009, Fallon, Goodchild et al. 2012, Poulin, Horlick et al. 2013, Witt, Raff et al. 2013, Gerdisch, Boyd et al. 2014, Padalino, Quarti et al. 2015, Zafar, Hinton et al. 2015, Mosala Nezhad, Poncelet et al. 2016, Woo, Fishbein et al. 2016) findings. Some of the major concerns of PSIS have been correlated with adverse immune response (e.g., chronic inflammation) or acute functional failure associated with construct integrity, such as tissue shrinkage

(Poulin, Horlick et al. 2013, Witt, Raff et al. 2013, Gerdisch, Shea et al. 2014, Padalino, Quarti et al. 2015, Mosala Nezhad, Poncelet et al. 2016, Woo, Fishbein et al. 2016). In contrast, early *in vivo* heart valve studies in the ovine model using PSIS have resulted in promising matrix repopulation with native cells, including surface endothelialization; however, ovine models are unable to consistently mimic the human responses for heart valves, since their transvalvular gradients are lower than that of humans (Pavcnik, Uchida et al. 2002, Pavcnik, Obermiller et al. 2009, Fallon, Goodchild et al. 2012, Mosala Nezhad, Poncelet et al. 2016). In human clinical trials, patients have been reported to have undergone surgical valve repair using PSIS, (Quarti, Nardone et al. 2011) in which trivial and mild regurgitation were observed (Mosala Nezhad, Poncelet et al. 2016). Furthermore, there is currently a clinical trial on PSIS (Cormatrix, Cor TRICUSPID ECM Valve, Roswell, GA) for dysfunctional tricuspid heart valves, where the purpose is to obtain initial insights on the ability to successfully implant the valve, determine clinical safety of the device and establish whether the device performs its intended use (clinicaltrials.gov). However, PSIS for pediatric applications requires the assessments of tissue remodeling capabilities and somatic growth overtime, which have not been investigated.

2.5 Enhanced Extracellular Matrix on Heart Valve Bioscaffolds via Cells

The goal of TEHVs is to permit cellular infiltration and then degrade, creating *de novo* tissue to provide the supportive structure for ongoing growth (Blum, Drews et al. 2018). The purpose of seeding a heart valve bioscaffold is to

provide enhanced ECM. Various types of cells have been used for seeding, with vascular endothelial, fibroblast, smooth muscle cells and stem cells being the most frequent (Blum, Drews et al. 2018). BMSCs are a source of autologous adult stem cells that are accessible and renewable (Au, Tam et al. 2008).

BMSCs are composed of two cell types, mesenchymal stem cells (MSCs) and hematopoietic stem cells (HSCs). MSCs are a viable and attractive options for TEHVs, since they are undifferentiated cells and can proliferate and differentiate into valvular phenotypes under certain biochemical and biomechanical stimuli (cell-cell and cell-ECM interactions). Furthermore, MSCs have unique immunological and repair characteristics (Weber, Emmert et al. 2012, Gallina, Turinetto et al. 2015), through the release of trophic factors, which make them an attractive option for *in vivo* implantations. These trophic factors stimulate neighboring parenchymal cells to start repairing damaged tissue and play a role in modulating the local immune system, enhancing angiogenesis, preventing cell death and positively simulating survival, proliferation and differentiation of the resident cells (Fu, Karbaat et al. 2017). Experimental studies demonstrated that treating infarcted animals with MSCs exerts functional benefits, including the promotion of vasculogenesis via paracrine signaling, the regulation of extracellular matrix components, and the induction of cell survival, which are mainly due to the cytokines and growth factors that MSCs secrete (Perez-Estenaga, Prosper et al. 2018). Furthermore, MSCs inhibit the activation and proliferation of T and B lymphocytes, reduce the cytotoxic activity of natural killer (NK) cells and promote

maturation of monocytes into anti-inflammatory type M2 macrophages (Perez-Estenaga, Prosper et al. 2018). HSCs are maintained by the bone marrow microenvironment, which allows the production of mature blood cells. HSCs are attractive in TEHVs as well because they can self-renew and differentiate into all functional blood cells (Bourgine, Klein et al. 2018). These properties of BMSCs make them an effective therapeutic tool for regeneration of the cardiac tissue.

2.6 Enhanced Extracellular Matrix on Heart Valve Bioscaffolds via Cells Conditioned in a Bioreactor

It has been shown that there is a need for bioreactors designed for improving TEHVs prior to implantation (Ramaswamy, Boronyak et al. 2014). Key factors in the neo-tissue formation include porosity, degradability, biocompatibility and mechanical properties of the scaffolds (Amrollahi and Tayebi 2016). It is vital to be able to mimic the physiological hemodynamics and culture conditions during *in vitro* tissue formation and development (Ramaswamy, Boronyak et al. 2014), which have been reported to enhance cell activity and tissue formation (Smith, Davies et al. 2001, Xing, He et al. 2004, Bilodeau, Couet et al. 2005, Ramaswamy, Boronyak et al. 2014). Hoerstrup et. al. developed a heart valve from a bioabsorbable polymer seeded with autologous ovine myofibroblasts and endothelial cells grown for 14 days in a pulse duplicator *in vitro* system under gradually increasing flow and pressure conditions. It was found that the optimal time to have the specimen in a bioreactor is 14 days, with an increase in extracellular matrix, specifically collagen (Hoerstrup, Sodian et al. 2000). Steady

fluid shear stress was found to differentiate MSCs to endothelial lineage from Wang et. al.'s study that used a custom-made parallel plate flow chamber that increased the expression of platelet endothelial cell adhesion molecule-1 (PECAM-1/CD31), which play a role in angiogenesis, platelet function and thrombosis, as well as the expression of von Willebrand factor (vWF), which is a blood clotting protein (Wang, Riha et al. 2005). Moreover, it has been found that pulsatile flow increases cell viability and orients the tissue forming layers in the direction of flow (Hoerstrup, Zund et al. 2000). To facilitate fluid-induced shear stress in the physiologically-relevant range for valves (3-5 dynes/cm^2) one specific bioreactor design utilized a cylindrical conduit configuration chamber to provide higher fluid velocities, allowing for higher shear stresses on the tissue specimen while remaining in laminar flow conditions (**Figure 5**) (Ramaswamy, Boronyak et al. 2014). Previous studies with this bioreactor demonstrated that BMSCs in a flex-flow (1 Hz and 850 mL/min) environment differentiated MSCs to a valve-like phenotype, with expression of endothelial (CD31) and myofibroblast (alpha smooth muscle actin; α-SMA) (Rath, Salinas et al. 2015); this phenotypic change was due to the presence of fluid-induced shear stress magnitudes and oscillatory shear stresses indicating that the flex-flow mechanical environment differentiates BMSCs to a valvular phenotype (Rath, Salinas et al. 2015). Fluid-induced shear stresses are known to be involved in the development of cardiovascular tissues and also be a mechanical regulator of stem cell differentiation (Williams, Nasim et al. 2017). It has been demonstrated that fluid-oscillating effects along with physiologically-relevant shear stress magnitudes (3-9 dynes/cm^2) allows stem

cells to produce *de novo* cardiac tissue (Williams, Nasim et al. 2017). Furthermore, it was found that a “sweet spot” of oscillatory shear index (OSI), or fluid oscillations, in the range of 0.18-0.23 induces valvular gene expression, with a significant upregulation in bone morphogenetic protein 2 (BMP2) and kruppel-like factor 2a (KLF2A), both valve developmental genes, as well as CD31 and α-SMA, which are valvular phenotypic genes (Williams, Nasim et al. 2017). The mechanisms of gene regulation due to oscillatory shear stress is not fully known, yet it is related to the ion channels that are mechanosensitive leading to activation [19], [87]. Therefore, in order to construct an optimized tissue engineered valvular

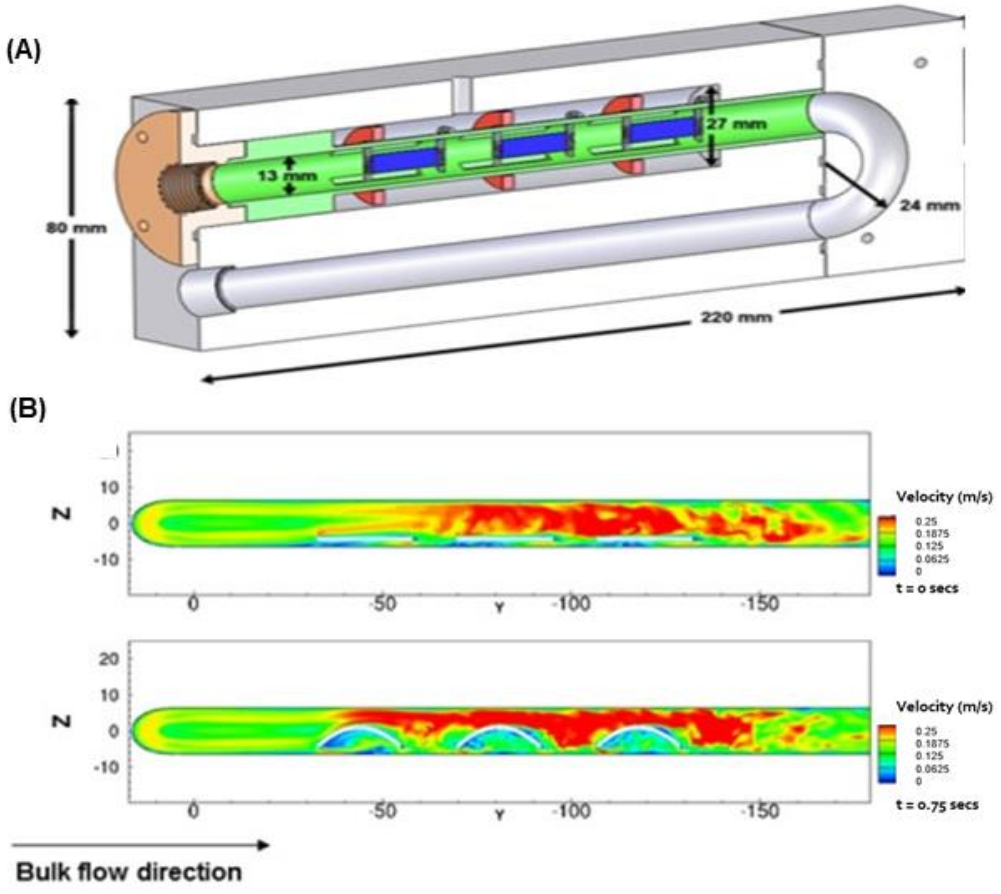

Figure 5: *Bioreactor design to provide high fluid velocities.* (**A**) Cylindrical conduit configuration chamber to provide (**B)** higher fluid velocities, higher shear stress and remaining laminar in flow (Re = 1376) from t = 0s to 0.75s [79].

replacement it is essential to target the shear stress magnitudes and OSI “sweet spot” when using stem cells to allow for proper differentiation to valvular phenotypes and ECM production.

2.6.1 Flow Environment for Heart Valve Regenerative Medicine

To develop TEVHs, it is generally accepted that mechanical forces innate to the cardiovascular system, namely flow, stretch and flexure, can optimize *in vitro de novo* tissue growth (Engelmayr Jr, Sales et al. 2006, Rath, Salinas et al. 2015, Salinas, Rath et al. 2016). To facilitate this mechanical conditioning, bioreactors are commonly used to dynamically culture engineered valve tissue constructs (Rath, Salinas et al. 2015, Salinas, Rath et al. 2016). The general approach to dynamically culture TEHVs begins with seeding of the cells on a scaffold of choice and placing them in a bioreactor that simulates the mechanical conditions to support valvular tissue formation and phenotype of interest. It has been shown that human bone marrow mesenchymal stem cells (hBM-MSCs) exposed to cyclic flexure and steady flow can produce robust collagen dense engineered tissues *in vitro* (Ramaswamy, Boronyak et al. 2014, Rath, Salinas et al. 2015). Moreover, these seeded hBM-MSCs were able to differentiate to both endothelial cells on the surface and activated interstitial cells deeper within the constructs, similar to the native valve, when exposed to a combination of physiologically-relevant cyclic flexure (1 Hz) and steady fluid-induced shear stress (4-5 dynes/cm^2) conditions (Rath, Salinas et al. 2015). The combination of cyclic flexure and steady flow (Flex-Flow) induces pulsatile and/or oscillatory flow patterns on the surfaces of TEVHs.

It has been shown that oscillatory flow conditions on developing valve tissues are important (Vermot, Forouhar et al. 2009, Salinas and Ramaswamy 2014, Salinas, Rath et al. 2016, Castellanos, Nasim et al. 2018). However, a physiologically relevant pulsatile flow waveform may induce oscillations similar to the conditions experienced in the native valve and mechanically condition these TEVHs. Indeed, hBM-MSCs have a significant upregulation of valve phenotypic gene expression, such as CD31 and α-SMA, while valve disease-relevant genes, including osteogenic marker TGFb1 were significantly downregulated after exposure to an aortic pulsatile flow profile (2D) for 48 hours (Williams, Nasim et al. 2017), in a monolayer culture.

Our group scaled our investigation to three dimensions utilizing hBM-MSC-seeded scaffolds that were mechanically conditioned using a physiologically relevant, aortic pulsatile flow waveform (Williams, Nasim et al. 2017). In particular, we subsequently assessed the resulting phenotypic changes to the engineered tissue constructs after being subjected to oscillatory shear stresses resulting from the aortic flow profile, in comparison to our previous work in which oscillatory patterns in the culture media was induced under a combination of steady flow and cyclic flexure, i.e., Flex–Flow (cyclic flexure of 1 Hz and steady fluid-induced shear stress of 4–5 dynes/cm^2). Notably, in the current study, the oscillations were solely fluid induced, without any structural deformation (e.g., cyclic flexure or stretch) of the specimens. He and Ku (He and Ku 1996) have previously shown that these fluid oscillations can be quantified using the oscillatory shear index (OSI; Equation

1). Similarly, wall shear stress (WSS) has been reported to affect differentiation of valve-specific phenotypes (Holliday, Ankeny et al. 2011). The time-averaged WSS (TAWSS) was used as a metric to quantify the physiological relevance of the shear stress magnitudes on the surface of the specimens (Equation 2).

EQUATION 1:

$$OSI = 0.5\left(1 - \frac{\left|\int_0^T \overrightarrow{WSS}\, dt\right|}{\int_0^T \left|\overrightarrow{WSS}\right| dt}\right)$$

EQUATION 2:

$$TAWSS = \frac{1}{T}\int_0^T \left|\overrightarrow{WSS}\right| dt$$

A physiologically relevant pulsatile flow profile that would elicit oscillatory shear stresses on MSC-seeded scaffold constructs could advance a TEHVs phenotype within the *in vitro* domain prior to implantation. Phenotypic matching of the implant with host tissues is an important attribute in subsequent *de novo* tissue remodeling *in vivo*, due to chemotactic events that are initiated by the implanted engineered extracellular matrix and cells, which may accelerate host tissue regeneration due to its niche (Hoshiba, Chen et al. 2016). Such an outcome is especially critical in situations like heart valve replacement in children, where support of somatic growth by the TEHV is critically needed.

In our previous work we reported that the samples from the Flex-Flow group exhibited a valve-like distribution of cells that expressed endothelial (CD31) and myofibroblast (αSMA) phenotypes on the surface and interstitial layers,

respectively (Rath, Salinas et al. 2015). It may correlate to the presence of oscillatory shear stresses (overall mean, OSI ~ 0.11) on the MSCs, induced during the time-varying flow on the sample surface, that was created via the cyclic flexure of the immersed samples in the steady flow environment (Rath, Salinas et al. 2015). More recently, we similarly found that physiological-relevant flow oscillations (overall, mean OSI ~ 0.18) that were directly created via the aortic flow waveform augmented the CD31 phenotype (Gonzalez, Perez-Nevarez et al. 2020). In contrast to Flex-Flow conditions, however, oscillatory flow without the concomitant flexural stresses serves to substantially reduce the α–SMA phenotype (Gonzalez, Perez-Nevarez et al. 2020). Therefore, oscillatory flow may promote controlled *in vitro* valve tissue regeneration, through enhancing the endothelial phenotype while restricting myofibroblast phenotypic expression. Since α–SMA is indicative of both normal and pathological tissue remodeling activity, it would therefore be more prudent to minimize α–SMA expression while augmenting other valvular markers that can be achieved via mechanical conditioning. However, since solid stresses may serve to also considerably increase α–SMA, a compromise can be achieved via the application of oscillatory fluid-induced stresses, without structural deformation of the specimens. Lastly, a very low level (relative to controls) of fibronectin expression found within the media, containing hBM-MSC-seeded scaffolds exposed to oscillatory flow, is suggestive of the potential for physiological relevant oscillatory shear stresses to minimize the risk of provoking transforming growth factor beta-mediated (TGF-β), valve remodeling activity following *in vivo* translation (Gonzalez, Perez-Nevarez et al. 2020).

However fundamentally, the ability of OSI conditions with physiologically-relevant magnitudes to enhance the stem cell secretion of extracellular matrix molecular components that may enhance valve tissue regeneration after construct implantation, remains unknown. If these molecules were to be deposited onto the scaffold, that may hold the key to facilitating a regenerable valve implant that can adequately function during the timeframe from child-to-adulthood, where somatic growth occurs, i.e., proportional valve growth with the growth of the child.

3. SPECIFIC AIM 1

Assess static and fatigue mechanical responses of PSIS bioscaffold under two different textile assemblies, 2ply and 4ply relating to the winding of two and four ECM fibers together, respectively.

3.1 Relevant Findings to Specific Aim 1

Previously, our laboratory tested bi-leaflet 4ply and 2ply PSIS valves (Pour Issa 2018) that were handmade from PSIS sheets (Cormatrix, Roswell, GA) as described before (Bibevski and Scholl 2015, Bibevski, Levy et al. 2017). These valves were sutured securely into Dacron conduits (**Figure 6**) and placed in the mitral position within a pulse duplicator system (ViVitro Labs, Victoria, BC). This system was used to test the hydrodynamic functionality of 4ply PSIS, 2ply PSIS, and bioprosthetic heart valves (Edwards Lifesciences, CA). It was found that for all heart rates and stroke volume combinations tested, the type of valve (bioprosthetic, 4ply and 2ply) had no significant effect on the mean diastolic pressures ($p>0.05$) (Pour Issa 2018, Gonzalez, Pour Issa et al. 2020). However,

for the % Regurgitation Fraction (%RF), the results were that the 4ply and 2ply PSIS valves were significantly higher ($p<0.05$) than the bioprosthetic valves (Gonzalez, Pour Issa et al. 2020). Specifically, the %RF for the bioprosthetic valve group was found to be significantly lower than the %RF in both the 2ply PSIS and 4ply PSIS valve group (Gonzalez, Pour Issa et al. 2020), but still within clinically relevant %RF limits (Sordelli, Severino et al. 2014). Therefore, interest arose as to which PSIS valve, 4ply or 2ply, would be the ideal option, which lead to the mechanical characterization of the PSIS bioscaffold (Specific Aim 1).

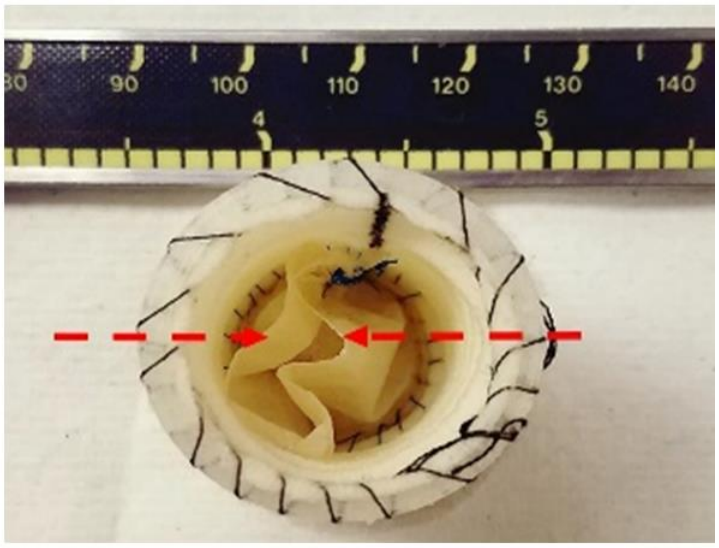

Figure 6: *PSIS valve sutured into Dacron conduit.* The PSIS scaffold created by hand [49] and sutured onto a Dacron conduit for hydrodynamic functionality testing. Red arrows signify the flaps of the PSIS mitral valve.

3. 2 Methodologies for Specific Aim 1

3.2.1 Mechanical Testing

3.2.1.1 PSIS Sample Preparation

PSIS specimens (4ply and 2ply; Cormatrix), were cut lengthwise from the manufacturing package into strips (3×1 cm^2, n=4/group). The thicknesses of the

samples were individually determined with calipers and recorded. The average thickness of the 4ply PSIS samples was 100±0.003mm, while the 2ply PSIS was 60±0.005mm.

3.2.1.2 PSIS Tensile Testing

Prepared mechanical test samples were incubated in 6 mL of 0.9% (w/v) saline solution for 50 hours at room temperature. The samples (3×1 cm^2, n=4/group) were then mounted in a mechanical testing instrument (ElectroForce 2300; TA Instruments, New Castle, DE) and calibrated (TuneIQ, WinTest software, version 7.0; TA instruments). The uniaxial tensile tests were run (in air) at a rate of 0.2 mm/sec with a total displacement of 11.5 mm (maximum displacement). Once completed, the samples were collected and immersed back into 6 mL of 0.9% (w/v) saline solution for further analysis.

3.2.1.3 PSIS Fatigue Testing

PSIS specimens (3×1 cm^2, n=4/group) were immersed in a 0.9% (w/v) saline bath (37°C) and placed between two grips for cyclic flexural fatigue testing of PSIS strips. For fatigue testing, the samples were subjected to a total cycling distance of 2.6 mm at a frequency of 29 Hz. The fatigue tests lasted 50 hours, consisting of 5.2×10^6 cycles, thereby simulating 6 weeks of pediatric mitral valve function. The fatigued samples were subsequently exposed to tensile testing with the same parameters that were utilized for the non-fatigue samples (Section 3.2.1.2).

3.2.1.4 Scanning Electron Microscopy

4ply and 2ply PSIS specimens were subjected to scanning electron microscopy. Within each group, two specimens had undergone cyclic flexural fatigue followed by tensile testing, while the other two had only undergone static tensile conditions. Evaluation of fracture surfaces upon tensile failure was carried out using a field emission scanning electron microscopy (FESEM; JEOL JSM 6330F, Tokyo, Japan) to determine the governing failure mechanisms in the specimens. Samples previously immersed in saline solution were dried for a period of 24 hours at ambient conditions prior to FESEM analysis. Due to the biological nature of the specimens, the samples were analyzed using a low voltage of 5 kV to minimize degradation.

3.2.2 Statistical Analysis

All results were reported as mean ± standard error of the mean. Mechanical testing results were statistically analyzed using a one-way analysis of variance (ANOVA), with a Tukey's post hoc test (Minitab, Inc., State College, PA). In contrast, the hydrodynamic testing was analyzed through a two-way ANOVA, where heart rate and stroke volume were considered blocking factors, that is, they are effective factors on the experimental outcome, but are themselves of no interest; a Tukey's post hoc test (Minitab, Inc.,) was performed whenever there was a significant factor ($p<0.05$). Statistical significance between any two given groups was found to have occurred when the p-value was less than 0.05 ($p<0.05$).

P-values within the range of 0.05 and 0.10 were considered marginally significant (Pritschet, Powell et al. 2016, Olsson-Collentine, Van Assen et al. 2019).

3.3 Results of Specific Aim 1

3.3.2 PSIS Mechanical Properties

3.3.2.1 Tensile Testing

From the tensile tests, the individual stress versus strain curves were plotted (MATLAB; Mathworks, Natick, MA) (**Figure 7**) to determine the mean Young's moduli (E), yield stresses, yield strains, and toughness for the PSIS 4ply and 2ply non-fatigued and fatigued samples (**Table 1**). Toughness was computed as the area under the stress–strain curve. The mean yield stress was found to be significantly different ($p<0.05$) among the groups assessed (**Table 1**). The significance between the 4ply and 2ply non-fatigue and fatigue samples was reported (**Figure 8**). Three statistically significant ($p<0.05$) differences were found between the groups: 4ply non-fatigue and 4ply fatigue, 2ply non-fatigue and 2ply fatigue, and 4ply fatigue and 2ply fatigue. Therefore, the mean yield stress of 4ply fatigue PSIS specimens was significantly lower in comparison to the 2ply fatigue PSIS specimens ($p=0.000$), and the mean yield stresses of the 4ply non-fatigue ($p=0.019$) and 2ply non-fatigue PSIS specimens were also found to be significantly lower compared to the 2ply fatigue PSIS specimens ($p=0.014$) (**Figure 8**). In addition, the mean yield strain was found to be marginally significantly higher ($p=0.06$) (**Table 1**). Therefore, a Tukey's post hoc test was performed on the mean

yield strain, which revealed that the mean yield strain of the fatigued, 2ply PSIS strips was significantly higher (p=0.045) than its fatigued, 4ply PSIS counterpart.

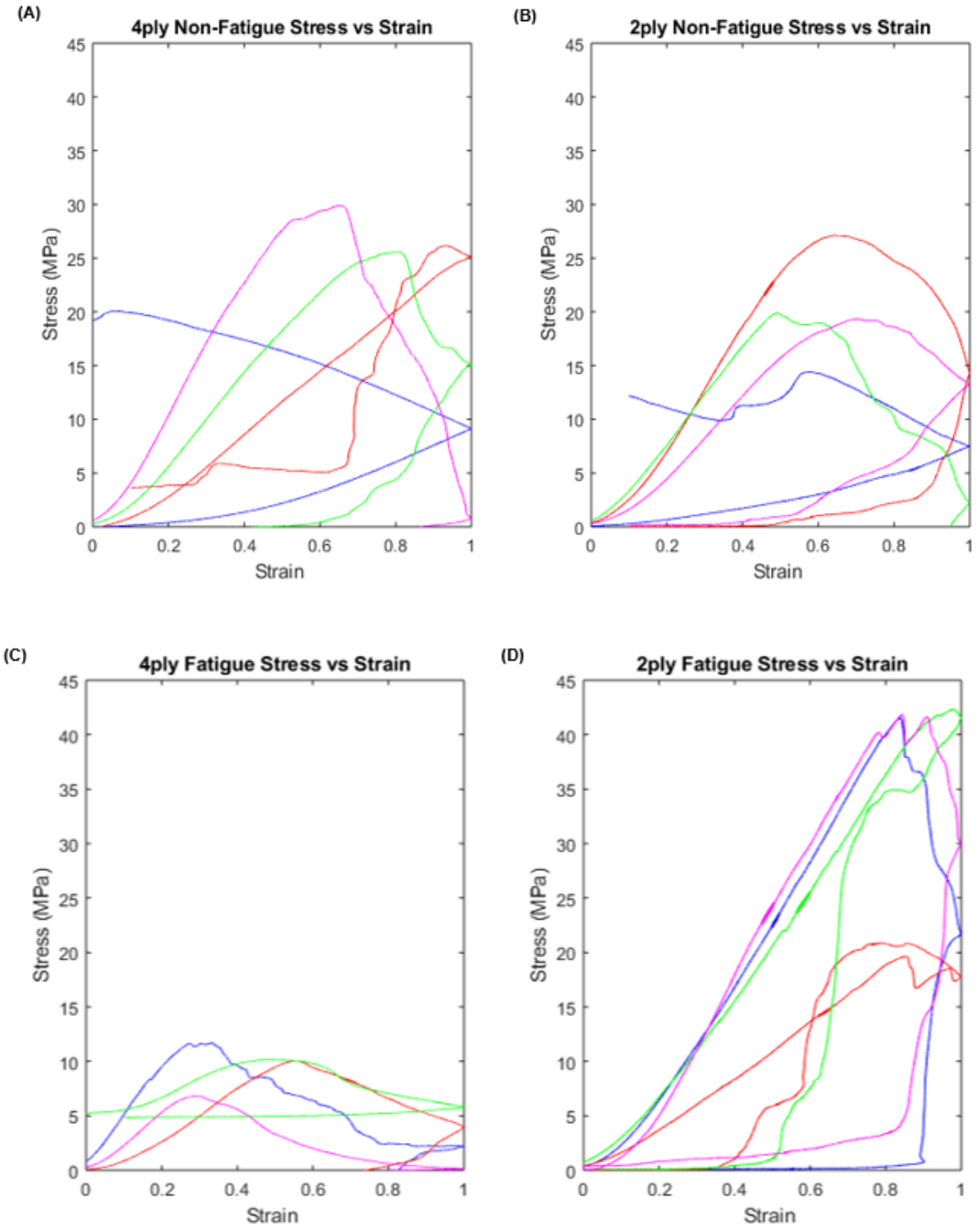

Figure 7: *Individual non-fatigue and fatigue tensile testing samples*. The stress versus strain curves of each PSIS strip tested, with each sample in a different color. The individual stress vs. strain graphs of each non-fatigue (**A)** 4ply and (**B)** 2ply PSIS. The individual stress vs strain graphs of each fatigue (**C)** 4ply and (**D)** 2 ply PSIS strips. n=4 per sample group.

All other groups were not significantly different from each other (non-fatigue 2ply and fatigued 2ply (p=0.350), non-fatigue 4ply and fatigued 2ply (p=0.375), non-

Table 1*: Summary of Mean ± SEM fatigue tensile property results for 4ply and 2ply PSIS specimens*. No significant difference (p>0.05) was seen in Young's Modulus, yield strains or toughness but a significant difference (p<0.05) was seen in yield stresses. Of particular interest were the differences observed between 4ply and 2ply PSIS fatigue samples. Statistically significance (p<0.05) was reported with an asterisk (*). Average yield stress of three comparisons were found to be significantly different (p<0.05): (4ply non-fatigue and 4ply fatigue), (2ply non-fatigue and 2ply fatigue) and (4ply fatigue and 2 ply fatigue) PSIS; the confidence intervals of the average differences between possible PSIS pairs and p-values for significant pairs was reported for yield stress (**Figure 8**).

PSIS Strip	Young's Modulus (MPa)	Yield Stress * (MPa)	Yield Strain	Toughness (MPa)
4ply Non-Fatigue	36.79 ± 8.32	25.43 ± 2.02	0.61 ± 0.19	11.12 ± 3.23
2ply Non-Fatigue	46.61 ± 4.55	20.23 ± 2.62	0.60 ± 0.05	11.18 ± 1.89
4ply Fatigue	30.13 ± 6.48	9.70 ± 1.03	0.41 ± 0.06	4.55 ± 0.79
2ply Fatigue	47.91 ± 8.88	36.68 ± 5.26	0.86 ± 0.04	11.85 ± 4.15

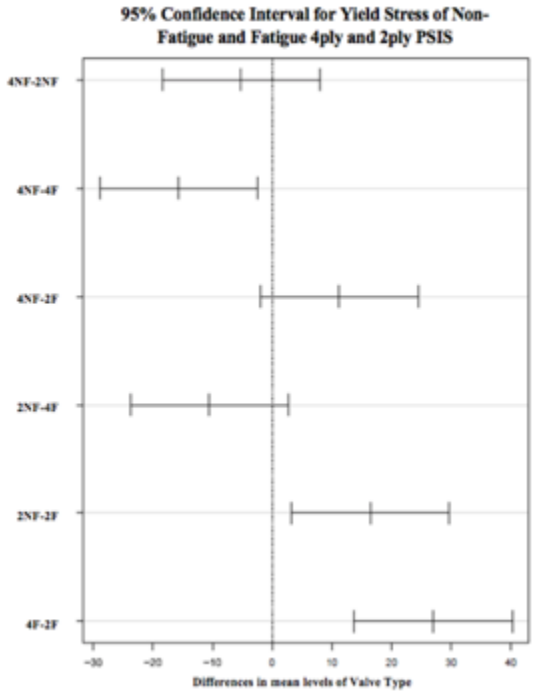

Figure 8: *95% Confidence intervals and significances for yield stress of PSIS.* Confidence intervals demonstrated the significant differences between the means of 4ply Non-Fatigue (4NF), 2ply Non-Fatigue (2NF), 4ply Fatigue (4F) and 2ply Fatigue (2F). Intervals that did not contain were considered significantly different (p<0.05). Therefore, 4NF-4F (p=0.019), 2NF-2F (p=0.014) and 4F-2F (p=0.00) were significantly different.

fatigue 2ply and fatigued 4ply (p=0.582), non-fatigue 4ply and fatigued 4ply (p=0.551), and non-fatigue 4ply and non-fatigue 2ply (p=1.000)).

3.3.2.2 Scanning Electron Microscopy

The 4ply PSIS non-fatigue samples that were imaged through FESEM showed dense fibers; however, there were cracks generated within the sample's surface (**Figure 9A**). These cracks were away from the failure regions of the samples. Although cracking occurred, the viscoelasticity of the fibers permitted the bridging of cracks before actual failure (**Figure 9B**). In contrast, the 4ply PSIS fatigued samples also had dense fibers, but no cracks were present at the surface

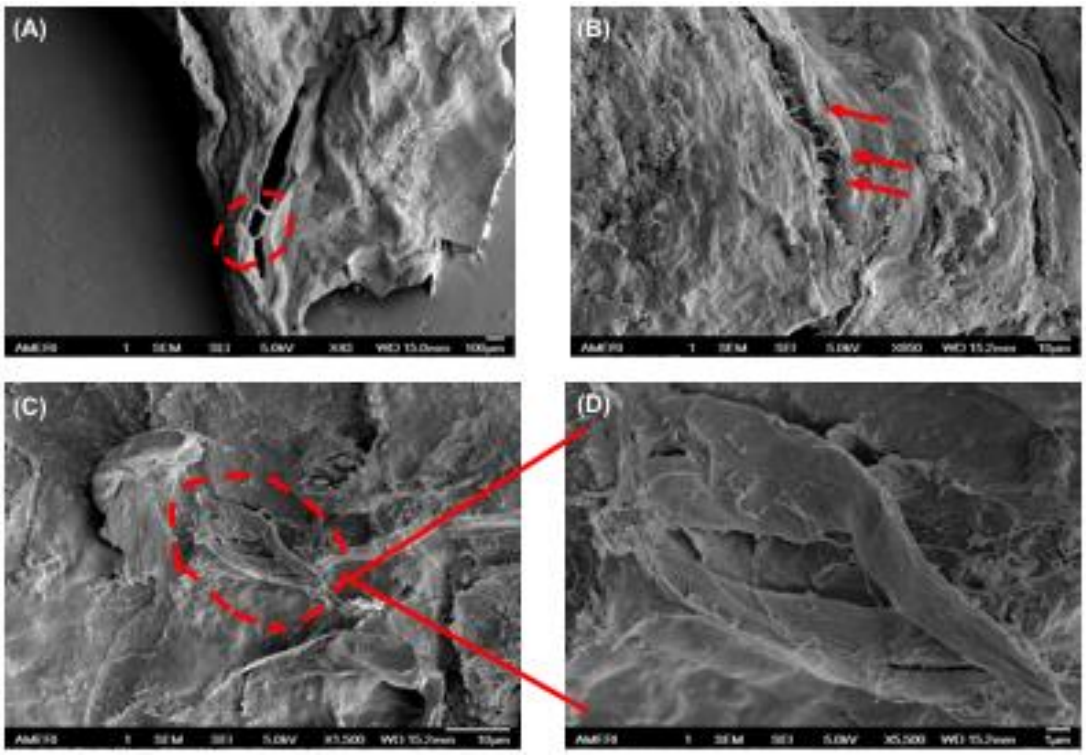

Figure 9: *SEM images of 4ply PSIS non-fatigue and fatigue samples.* Non-fatigue samples where (**A**) cracks are generated within the sample's surface away from failure regions and (**B**) viscoelasticity of fibers permits the bridging of cracks before failure. Fatigue samples where (**C**) no cracks are formed within the surface of the sample and (**D**) the presence of craze features, which are characteristic of fatigued failure, are shown throughout the failure region.

of the samples. However, there was the presence of craze features throughout the failure region, indicating shearing of fibers along the path of failure (**Figure 9C, D**).

The 2ply PSIS non-fatigue samples imaged through FESEM showed single fibers being dissociated from the specimen at fracture surfaces (**Figure 10A–C**). This shows the overall ductile nature of the whole structure. The 2ply PSIS fatigue samples, on the other hand, showed a distinguished damage in the fibers; this fiber pullout with surface damage could be attributed to the fatigue cycling (**Figure 10D, E**). The fibers also appeared more elongated and stretched compared to all other scaffolds (**Figure 10F**).

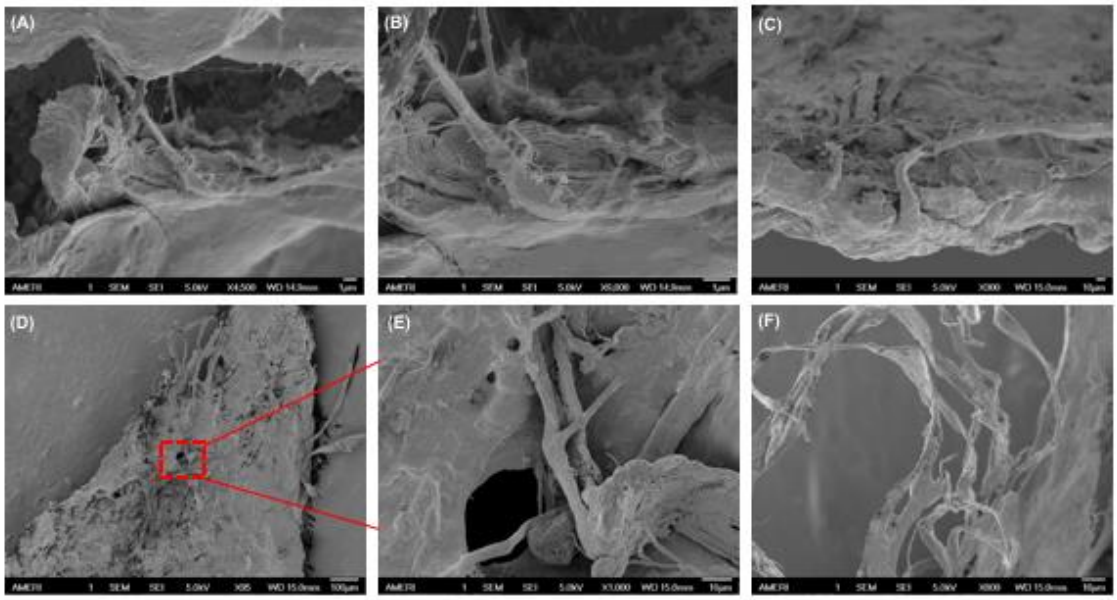

Figure 10: *SEM images of 2ply PSIS non-fatigue and fatigue samples*. Non-fatigue samples where (**A-C)** single fibers were dissociated from the specimen at fracture surfaces. Fatigue samples where (**D-E**) fatigue cycling caused fibers to pull-out of the surface and (**F**) to elongate.

3.4 Discussion

Biological scaffolds have been recently investigated for valve replacement (Rippel, Ghanbari et al. 2012, Cheung, Duan et al. 2015, Emmert and Hoerstrup

2016). The primary motivation in these investigations lies in the ability of bioscaffolds to be able to recapitulate valve tissue material responses and thereby facilitate unidirectional blood flow. In particular, PSIS is a degradable bioscaffold approved for early clinical studies (FDA-IDE) that facilitates gradual, yet organized tissue remodeling for cardiovascular applications (Sandusky Jr, Badylak et al. 1992, Robotin-Johnson, Swanson et al. 1998, O'Brien, Goldstein et al. 1999, Matheny, Hutchison et al. 2000, Badylak, Obermiller et al. 2003, White, Agnihotri et al. 2005, Toeg, Abessi et al. 2014, Mosala Nezhad, Poncelet et al. 2016). PSIS valves have been utilized in clinical trials with favorable results up to 10 years post-implantation (Dohmen, Lembcke et al. 2011).

However, despite this success, three central limitations persist. First, the clinical trials to date (Dohmen, Lembcke et al. 2011) have focused on pulmonary heart valve replacement, which does not address added material challenges in the systemic circulation such as the need for supplementary valve anchorage without compromise to function, increased strength, and an enhanced resistance to fatigue. Second, a regenerative strategy for valve replacement is most critically needed in pediatric patients where the somatic growth requirement can potentially be met; yet bioscaffold valve replacement strategies in humans have focused on adults to date.

Previous investigations relating to hydrodynamic assessment demonstrated that the mean diastolic transvalvular pressure was not affected by the type of valve being tested. In contrast, the %RF of both 4ply and 2ply mitral valves was found

to be significantly higher (p<0.05) in comparison to the bioprosthetic valves. This finding can be attributed to the unique strain hardening phenomena that we identified occurring exclusively on the 2ply PSIS material under cyclic fatigue loading conditions, thereby leading to leaflet stiffening. However, it should be noted that the leakage occurred for all valves was mild and is considered clinically acceptable.

Inspection of the PSIS specimen microstructure (**Figures 9**, **10**) provided in-depth insights into potential failure mechanisms of PSIS valve leaflets when subjected to fatigue loading conditions during the cardiac cycle, which could be classified into five progressive stages. Stage 1: appearance of crazes on the bioscaffold surface; Stage 2: surface microcracks, leading to fiber pullout on surface of the polymer; Stage 3: growth and coalescence of microcracks; Stage 4: macroscopic crack formation, including through the thickness of the valve leaflets; and Stage 5: crack propagation and catastrophic fracture as would be evidenced by holes or tearing of the valve leaflets.

The fatigue testing conducted in the current investigation revealed that the 4ply PSIS specimens were at the early stages of failure progression (**Figure 9**), specifically at Stage 1. In contrast, the 2ply PSIS specimens had progressed to Stage 2, since fibers had pulled out of the specimen surfaces (**Figure 10**). In addition, the fibers were subsequently recruited as was observed through fiber elongation (**Figure 10**). Indeed, fiber loading, following microfracture on the material surface, served to strengthen (p<0.05) and yet, simultaneously, toughen

(p>0.05) the material (**Table 1**), which is a known effect of craze propagation in polymers (Xu, Cheng et al. 2001, Yin, Cheng et al. 2017). The fatigued 2ply PSIS specimens ultimately exhibited a significantly higher yield stress (p<0.05) and a marginally-significant higher yield strain (p=0.06), respectively, compared to the unfatigued 2ply and 4ply and fatigued 4ply strips (**Figure 7** and **Table 1**).

Of note, in a direct statistical comparison between 4ply and 2ply (using Tukey's *post hoc* test) for mean yield strain, it was revealed that the fatigued 2ply strips were significantly different (p<0.05) than the fatigued 4ply specimens. Specifically, and somewhat surprisingly, both the mean yield stress and strain were found to be significantly higher (p<0.05) in the fatigued 2ply PSIS strips in comparison to the fatigued 4ply PSIS specimens. This may explain why the strain hardening and the craze-induced material enhancements of the fatigued 2ply PSIS specimens ultimately exhibited a higher yield stress (p<0.05) and yield strain (p<0.05), respectively (**Figure 7** and **Table 1**).

In conclusion, the current investigation revealed that the evolving material properties of the thinner 2ply PSIS bioscaffold under cyclic loading conditions robustly, but nonetheless temporarily supports valve function (in the order of a few months), in the treatment of critical congenital valve diseases in the young, where somatic growth is crucially needed. However, deterioration of PSIS valve function is likely to occur beyond this time frame if PSIS still remains as the dominant valve material and somatic growth is not accompanied by new host valve tissue in-growth.

The robust function of 2ply PSIS valves during the acute period is due to cyclic flexural fatigue-induced strain hardening, which leads to elevated strength, while microfracture and fiber pullout on the bioscaffold's surface increase the toughness of the material. These changes in the 2ply PSIS material properties allow to elongate on its own, thereby eliminating the need for cell infiltration and new valvular tissue growth soon after the valve would be implanted in the host. While 2ply and 4ply PSIS both undergo different rates of similar failure mechanisms and progression, from a practical standpoint, the 2ply PSIS bioscaffold would additionally reduce the demand on the host for volumetric *de novo* valvular tissue filling by half once implanted. However as stated earlier, endogenous cell recruitment and ECM secretory processes will nevertheless need to occur soon after the acute time frame to avoid valve failure.

4. SPECIFIC AIM 2

Analyze the *in vivo* growth potential and functionality of the PSIS mitral valve temporally without cell-seeding or additional treatment measures.

4.1 Methodologies of Specific Aim 2

4.1.1 In vivo Pilot Assessment of PSIS Mitral Valve Function and Growth

In a pilot assessment of 2ply PSIS valve function, three male juvenile (12 to 14 months old) hamadryas baboons (Papio hamadryas) underwent mitral valve replacement surgery. All procedures were performed in accordance with the

Institutional Animal Care and Use Committees from Florida International University (IACUC-16-036-CR02) and the Mannheimer Foundation, Inc. (IACUC no. 2015-07). All breeding, housing, and in vivo procedures were performed at the Mannheimer Foundation, Inc.

4.1.1.1 Surgical Preparation and Procedure for PSIS Mitral Valve Implantation

In brief, the juvenile baboons were sedated, intubated, and placed on a respiratory ventilator and given antibiotics an hour prior to the incision time. Next, each baboon was administered general endotracheal anesthesia, prepared and draped with normal sterile techniques (chlorhexidine-based solution). Echocardiography measured the native heart valve annulus and leaflet length to thereby create a custom-made bi-leaflet PSIS valve [14, 15]. Once prepared and draped, a right thoracotomy was performed, and the heart was exposed by pericardial incision and creation of a pericardial cradle. At that point, the baboon was heparinized, placed on cardiopulmonary bypass and cooled to 34°C (mild hypothermia). Thereafter, a left ventricular vent, antegrade cardioplegia needle, and caval snares were placed.

A cross-clamp was applied, while cold Custodiol (Essential Pharmaceutical, LLC., Durham, NC) cardioplegia was given antegrade; at the same time, topical cooling with ice protected the heart. The interatrial groove was dissected, and the left atrium was accessed through the free wall, whereby the mitral valve was visualized through the atriotomy. Next, the native valve was excised, including the chordal attachments, while the handmade PSIS valve of 2ply thickness was

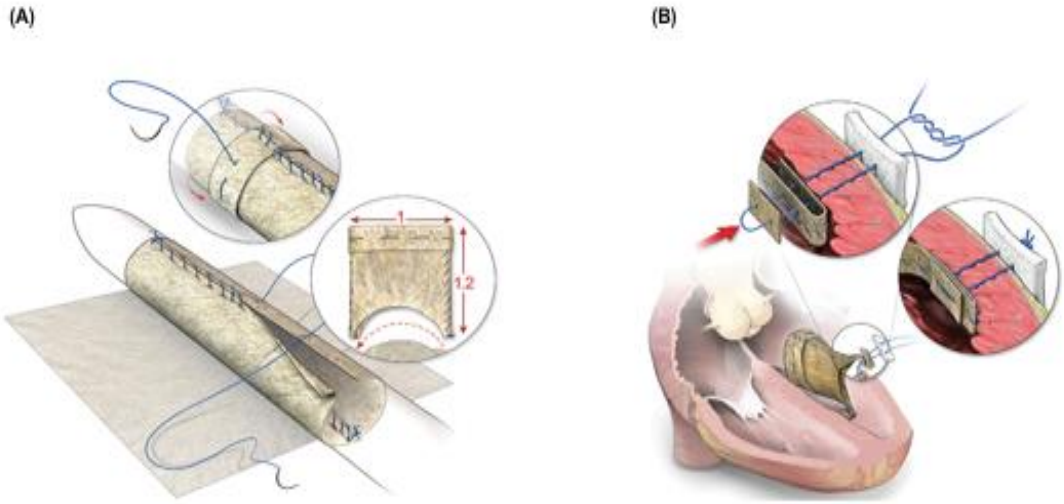

Figure 11: *Hand-made PSIS valve for mitral valve implantation.* **(A)** The assembly of a hand-made PSIS mitral valve using a dilator of specified diameter for implantation and (**B**) the attachment of the distal limbs of the mitral valve to the papillary muscles ([15] by permission of Oxford University Press).

implanted (**Figure 11A**; by permission of Oxford University Press [15]). This involved attachment of the distal limbs of the mitral valve to the papillary muscles or the immediately adjacent free wall and sewing of the orifice of the valve to the native annulus (**Figure 11B**; by permission of Oxford University Press [15]). The heart was then de-aired through the antegrade cardioplegia needle, and the cross-clamp was removed. The incisions were sutured to close surgical access points, and the animals were weaned from cardiopulmonary bypass for recovery. Anticoagulants (aspirin, 325 mg daily) were given to the baboons orally for 30 days following implantation of the 2ply PSIS mitral valve.

4.1.1.2 Echocardiography Monitoring of Juvenile Baboons with Implanted PSIS Mitral Valves

Echocardiographic (ECHO) assessments (LOGIQ e VET; GE Healthcare, Chicago, IL) were performed to evaluate the mitral valves for the baboons before valve replacement surgery, postoperatively immediately following PSIS replacement, 2 weeks' post-operation, and 1 (or 2) month(s) thereafter as needed. The ECHOs were completed using the standard two-dimensional, M-mode, and spectral and color Doppler imaging techniques, which are routinely applied in humans. With these ECHOs, qualitative data on the function (regurgitation) of the valves were assessed, as well as quantitative data such as leaflet length, atrium size and annulus diameter. The heights and weights were measured and accordingly, the body surface area (BSA) of the animal was determined. The BSA was calculated based on the DuBois equation used regularly for human pediatric patients, which is defined as: $BSA(m^2) = 0.007184 \times height(cm)^{0.725} \times weight(kg)^{0.425}$ (Orimadegun and Omisanjo 2014, Redlarski, Palkowski et al. 2016). Given the collected data from the ECHOs, a novel parameter, the normalized aspect growth ratio (NAGR, Equation 3; (Gonzalez, Hernandez et al. 2018)) was defined and computed based on the valve annulus diameter (D), valve leaflet length (LL) and the body surface area (BSA), where NAGR = 1 indicates ideal valve growth. Note that a linear rate of valve-to-somatic growth was assumed to occur as part of this NAGR definition.

EQUATION 3:

$$\text{NAGR} = \frac{\frac{(\frac{D}{LL})_{final}}{BSA_{final}}}{\frac{(\frac{D}{LL})_{initial}}{BSA_{initial}}}$$

4.1.1.3 Histological and Immunofluorescence Assessments of Explanted PSIS Mitral Valves

PSIS mitral valves were explanted from three baboons at 3-month, 11-month and 20-month post-implant. The timing of these explants was not intentional but rather, were a result of unexpected and sudden acute, critical PSIS mitral valve insufficiency or failure, that necessitated euthanasia of the animals. More specifically, the PSIS mitral valves failed due to endocarditis (3-, 20-month explant) that was unrelated to the valve and moderate adhesions leading to a hole in the posterior leaflet (11-month explant), both cases ultimately leading to a mechanical failure or chronic inflammation. The PSIS valves were subsequently fixed in 10% formalin (for 24 hours) immediately after explanation. The valves were then rinsed with PBS and embedded in a slow freeze process with optimal cutting temperature. The leaflets were then stored in -80°C overnight. The following day, the embedded samples were cut to a thickness of 16 μm (per slice) and placed on glass slides (TruBond 380; Newcomer Supply, Middleton, WI), which were set to dry at room temperature. 4,6-diamidino-2-phenylindole (DAPI; 1 mg/mL) fluorescent stain and Hematoxylin and eosin (H&E; Rapid Chrome H&E Frozen Section Staining Kit, Richard-Allan Scientific, Kalamazoo, MI) were used to determine the presence of

the cells and morphology on the explanted 3-month PSIS valve leaflets, while Movat's stain (Russel-Movat Pentachrome, Item no. KTRMP; American MasterTech Scientific, CA) was used to determine the different constituents of the leaflet tissues. Furthermore, detailed histological and immunohistochemistry stains were outsourced (Alizee Pathology LLC., Thurmont, MD) for tissue assessments of all three of our explanted PSIS mitral valves (3-month, 11-month and 20-month) along with native baboon valves and raw decellularized and acellular PSIS bioscaffolds. The tissue areas of focus included the leaflets, annulus, attachment points at the papillary muscles and neochordae. The histological stains of H&E and Movat's Pentachrome (Alizee Pathology LLC., Thurmont, MD) were performed. The immunohistochemistry stains included CD31, α-SMA, and Trophin (Alizee Pathology LLC., Thurmont, MD) for the phenotypic presence of endothelial cells, interstitial cells, and integration of the papillary muscles to neochordae and annulus of the valve to the myocardium, respectively. All qualitative assessments were independently confirmed by our team Pathologist (Dr. Elena Ladich, MD, Memorial Healthcare System, Hollywood, FL). Histological images were captured with bright-field microscopy (Zeiss, Axiovert 40 CFL, Maple Grove, MN; Olympus, BX43, Center Valley, PA) and immunofluorescence images were captured with confocal microscopy (Nikon Eclipse Ti, Minato, Tokyo, Japan).

4.1.1.4 Spatial Intensity Mapping of Explanted PSIS Mitral Valves

A Movat's image of the native mitral valve of a juvenile baboon (14 months old) was used as a reference image to all the image analysis of Movat's. The

reference image was then thresholded for brightness and contrast automatically (ImageJ, NIH Image, Bethesda, MD). This thresholded reference image was then saved and run against each image to normalize them through an in-house script (MATLAB, MathWorks, Inc., Natick, MA). Upon normalizing with respect to the reference, a color segmentation plugin was used (ImageJ, NIH Image, Bethesda, MD) and the different colors were chosen to distinguish the different ECM components of collagen, elastin, proteoglycans and fibrin. Once complete, the option of independent color channels was chosen, and Hidden Markov Model was used to determine the resulting percentage of the ECM concentration areas. The images were then processed for intensity of each component of interest (MATLAB, The MathWorks, Inc., Natick, MA) and used to find the ranges of the component, generating the spatial intensity maps of each ECM component. Each image was then converted from pixels to millimeters based on the corresponding magnifications (ImageJ, NIH Image, Bethesda, MD) to get the area of the image and multiplied by the intensity to get the respective ECM concentration in each image. The ECM concentrations were compared across all our samples according to the location of the tissue.

4.1.2 Statistical Analysis

Results were reported as average ± standard error of mean (SEM). The spatial intensity maps were compared based on location of the tissue and reported as specific ECM content (i.e. collagen, elastin, proteoglycans or fibrin) in analyzed image per total ECM content. The percentage of unfilled *de novo* tissue (i.e.

residual PSIS) were computed by determining the area of unfilled tissue by the total ECM content (ImageJ, NIH Image, Bethesda, MD). ECM concentrations and unfilled *de novo* tissue percentages were statistically analyzed using a one-way analysis of variance (ANOVA), with a Dunnett's test (Minitab, Inc., State College, PA) for the leaflet comparisons, a one-way analysis of variance (ANOVA), with a Tukey's post hoc test (Minitab, Inc., State College, PA) for the annulus comparisons and a two-sample t-test (Minitab, Inc., State College, PA) for the neochordae and papillary comparisons. Statistical significance between any two given groups was found when the p-value was less than 0.05 ($p<0.05$).

4.2 Results of Specific Aim 2

4.2.1 Echocardiography Monitoring of PSIS Mitral Valves

Our results show that up to 17-months post PSIS mitral valve implant in juvenile baboons (n=3) that the NAGR was roughly 1 during the first 2 months of implantation (**Figure 12**). This suggests that there is an ideal growth of the valve within these first 2 months, followed by progressive loss in the TEHV's ability to support somatic growth. These findings were compared to pediatric patients (NAGR of 0.89±0.20, n=3) and baboons (NAGR of 0.99±0.11, n=3, up to 4-months post-implantation) (Gonzalez, Hernandez et al. 2018). The NAGR was found to be roughly 1 in both species and was not significantly different ($p>0.05$) between the two groups. This finding suggests that the juvenile baboon's cardiovascular anatomical and physiological model meets the requirements for systematic and objective evaluation of the pediatric human response to bioscaffold valve.

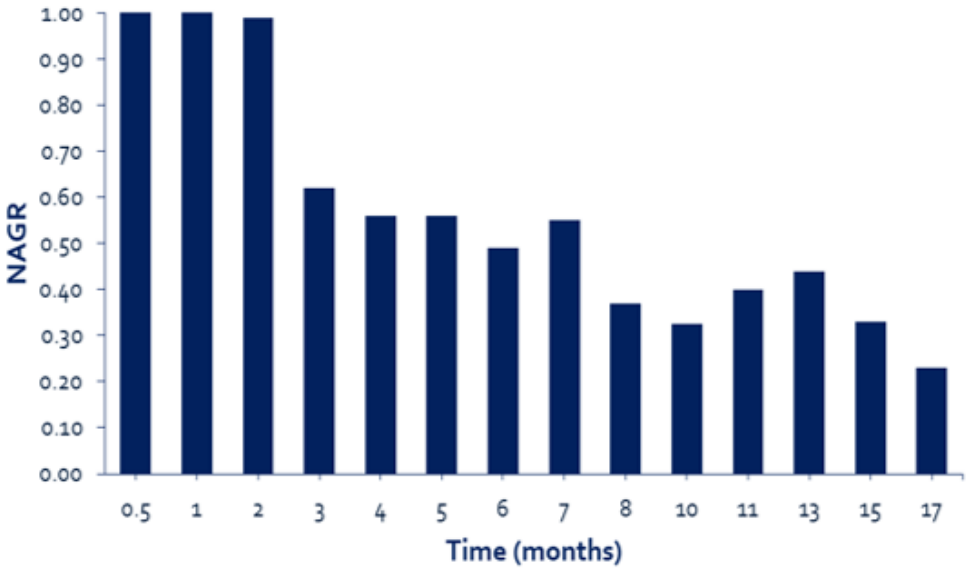

Figure 12: *Longitudinal PSIS Mitral valve assessment in baboons up to 17-months post-explant*. NAGR was found to be roughly 1 (i.e. ideal growth) at the beginning and then decreased due to the rapid growth of the baboon compared to the valve.

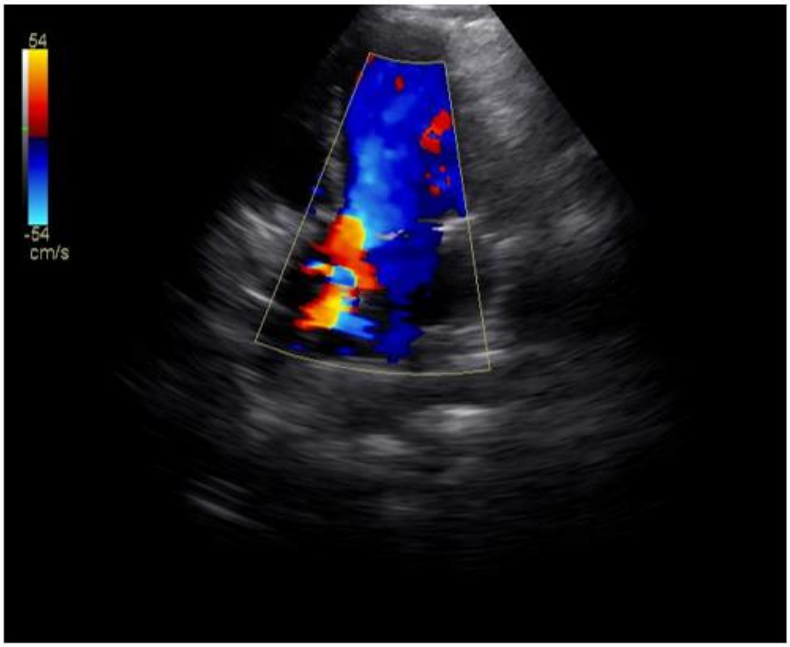

Figure 13: *Echocardiography monitoring of a juvenile baboon*. Echo of 16P29 at 3 months with a mild regurgitation. The area focused on shows the flow through the mitral valve. Red represents forward flow, while blue is the flow away from the transducer. A mixture of colors signifies forward and backward flow mixing (regurgitation).

ECHO images qualitatively assessed the function of the valves for each baboon. At each time point, the color Doppler imaging was performed to provide the regurgitation (**Figure 13**). The regurgitation was classified as trivial, mild, moderate or severe by a cardiologist. Throughout the study (17 months) the regurgitation was either trivial or mild, with an exception at 7 and 17 months, where it was moderate. Of note, severe regurgitation was never observed throughout the longitudinal ECHO monitoring period, demonstrating proper function of the implanted PSIS valves for the majority of the implantation period.

4.2.2 Histological and Immunofluorescence Assessments of Explanted PSIS

One PSIS mitral valve was explanted at 3-month post-implantation from one baboon for examination (**Figure 14**). The leaflet tissue was stained with DAPI to determine the live cells on the PSIS mitral valve leaflets. The implanted PSIS valve was comparable to the raw, un-implanted PSIS material, with cells only at the valve surfaces and a marginal presence of cells within the leaflet interstitial areas (**Figure 15A, B**); the cells present on the un-implanted PSIS material must be remaining porcine cells on the scaffold. It was revealed that endogenous cell

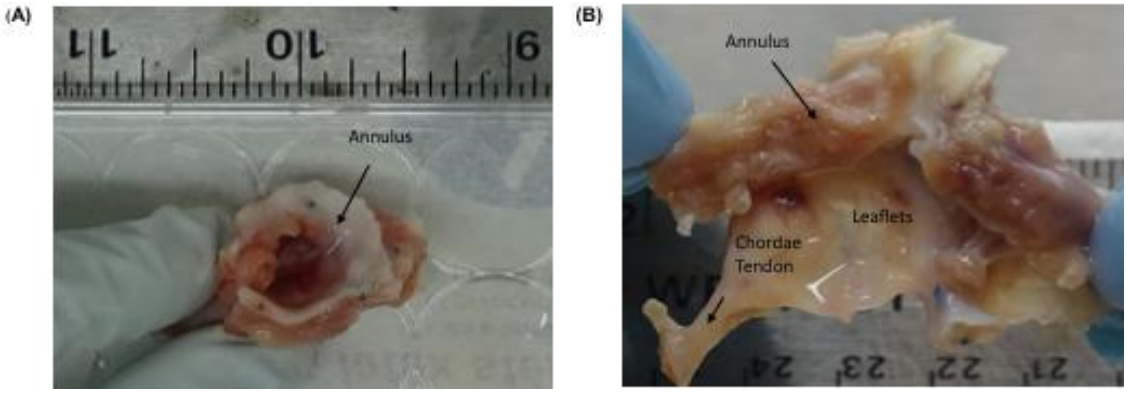

Figure 14: *Explant of baboon mitral valve 3-months post-implantation*. (**A)** Explant of the mitral valve with arrow signifying the annulus of the PSIS valve, while (**B)** signifies the annulus, chordae tendon and leaflet area of the explanted PSIS valve.

infiltration into the scaffold leaflet space *in vivo* was limited at this acute phase (3 months) of implantation (**Figure 15B**).

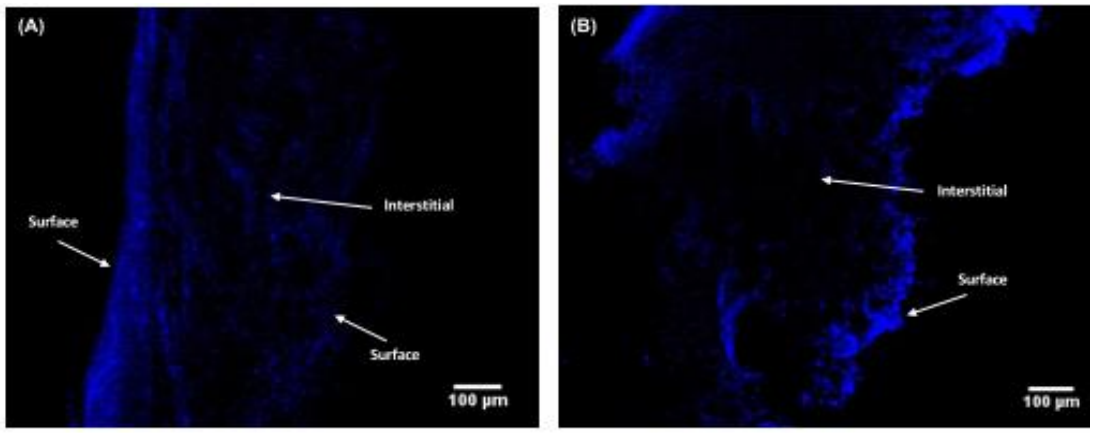

Figure 15: *Evidence of cells 90 days post-PSIS valve implantation*. Cells are seen on the surface (mucosa-mucosa) and minimally in the interstitial areas of both the (**A**) raw not implanted PSIS (remaining porcine cells) and (**B**) implanted PSIS mitral valve. There was a marginal evidence of cells found on the surface of both samples, raw and implanted PSIS, leading us to believe that the cells were retained on the decellularized scaffold and there was minimal infiltration of new cells. Florescent blue signifies staining of DNA, the nuclei of live and/or dead cells and debris. Magnification of 3.15X.

Similarly, histological assessment of the leaflets with Movat's staining revealed the morphological structure of the leaflets. The native PSIS material appeared in an orange-red color, signifying a muscle-like phenotype (**Figure 16A**). In contrast, the implanted PSIS material looked a dark-red color, representing a fibrin phenotype (**Figure 16B**). H&E staining confirmed the presence of the cells that remained on the PSIS scaffold before implantation on the surface (**Figure**

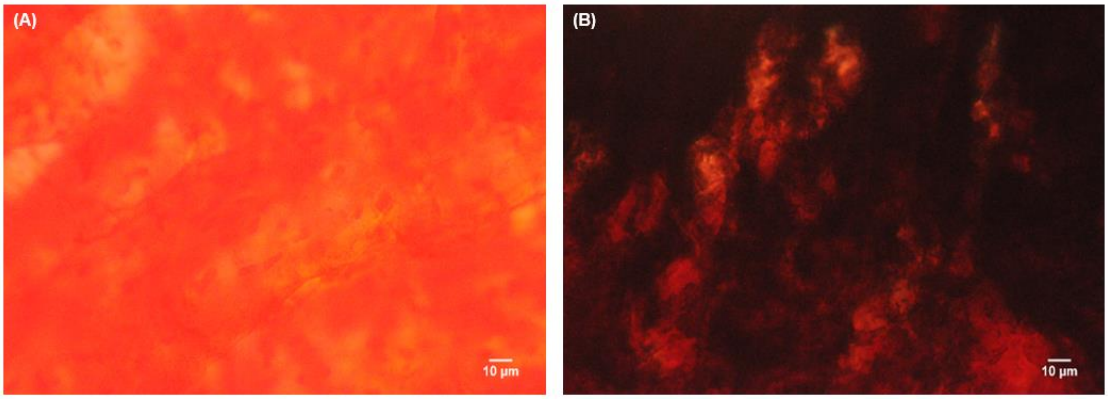

Figure 16: *In vivo (baboon) PSIS-mitral valve remodeling at 90 days post-implantation*. Movat's Pentachrome histology of a (**A**) raw not implanted PSIS and (**B**) implanted PSIS mitral valve (mucosa-mucosa surface). Yellow depicts a collagenous phenotype, orange-red represents a muscle phenotype and dark-red a fibrin phenotype. Magnification of 100x.

17A). Conversely, cells were located on the 3-month explant depending on the leaflet location (**Figure 17B, C**), with most of the cells appearing to be immune cells based on their morphology (**Figure 17B**).

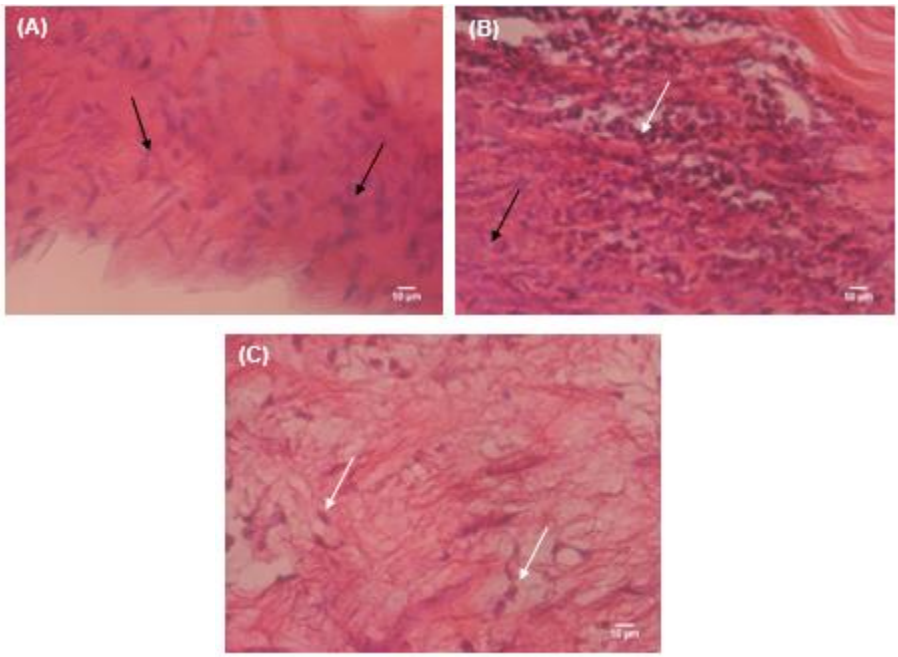

Figure 17: *In vivo (baboon) PSIS-mitral valve cellular infiltration at 90 days' post-implantation*. H&E histology of the surface of a (**A**) raw un-implanted decellularized PSIS and (**B, C**) implanted PSIS mitral valve (mucosa-mucosa surface) at two different leaflet spatial locations. The **A**) decellularized scaffold had porcine cells remaining on the surface of the bioscaffold, while the explanted valve (**B, C**) had remaining porcine cells from the bioscaffold as well as new native Baboon cells that are likely immune cells responding to the remnant porcine cells. For reference, note that pink stains for cytoplasmic filaments in muscle cells, intracellular membranes, and extracellular fibers, while purple stains for DNA or RNA in the cell nucleus and ribosomes, respectively. Black arrows signify cells remaining on bioscaffold; white arrows demonstrate wound healing response. Magnification of 100x.

More exhaustive histological and immunohistochemistry assessment were completed on all three baboon explants at 3-, 11- and 20-month post implantation (Alizee Pathology LLC., Thurmont, MD). Areas of interest of the PSIS mitral valves included the leaflets, annulus and integration point at the papillary muscles. The native juvenile baboon mitral valve (control) had cellular infiltration (**Figure 18A, D**) with presence of smooth muscle cells throughout the leaflet but primarily at the ventricularis layer (**Figure 18B, E**). Endothelial cells, on the other hand, were found

to be present on the outer surface of the leaflets (**Figure 18C, F**). The 3-month PSIS explanted valve seemed to have similar cellular infiltration with interstitial cells present (**Figure 19A-C**) and specifically the presence of smooth muscle cells at a fragment edge of the explant (**Figure 19D**). The presence of endothelial cells (CD31) on the leaflet was not seen to due limitations in cutting of the sample

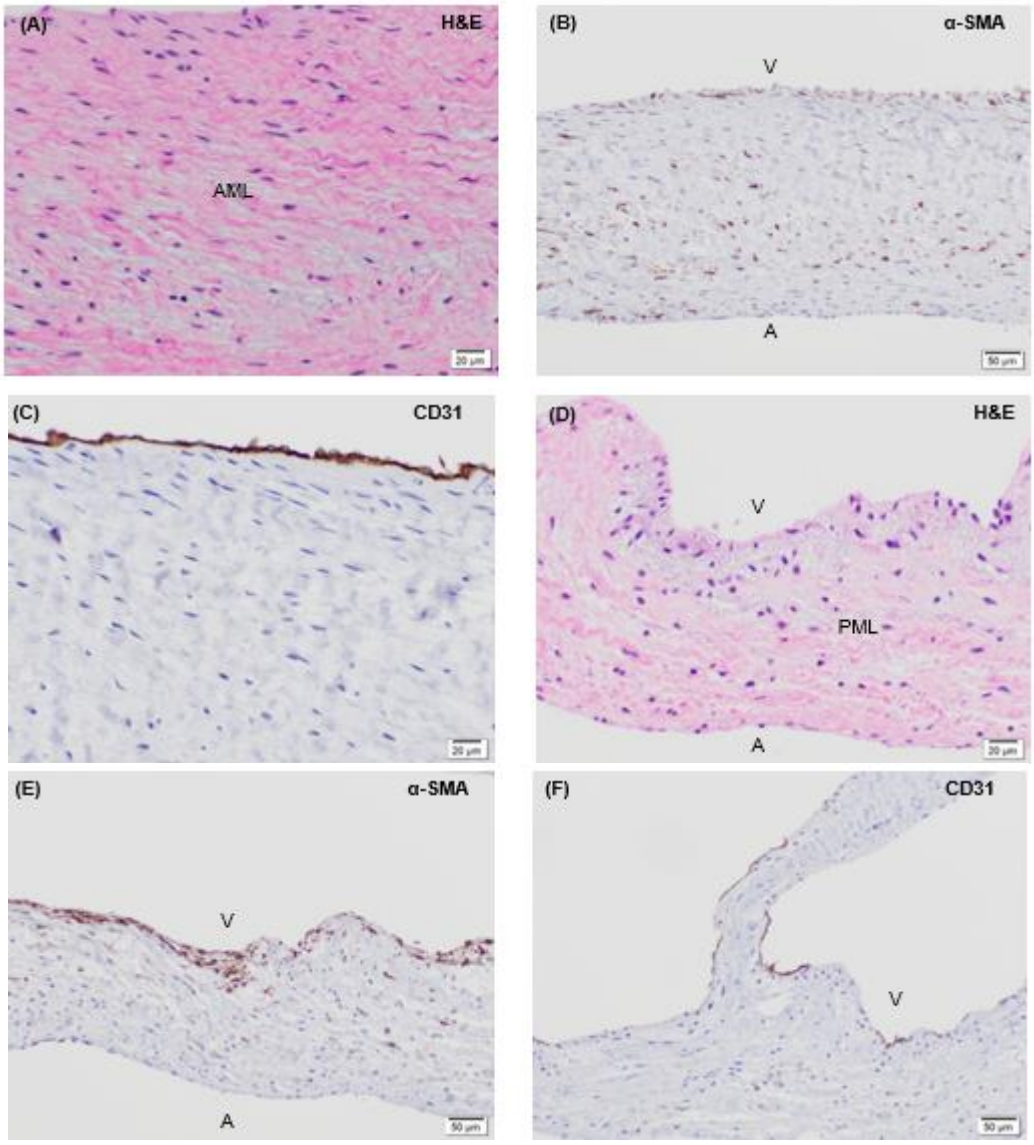

Figure 18: *Native juvenile baboon mitral valve explant at 14-months*. Native anterior (AML) and posterior (PML) mitral valve leaflets (**A**, **D**; H&E) at 40x demonstrating a normal presence of cells on the leaflet. Presence of α-SMA (smooth muscle cells) in brown (**B, E**; 20x) throughout the leaflets. Presence of CD31 (endothelial cells) in brown are also present lined at the outer surface of the leaflet (**C**-40x**, F**-20x). A depicts the atrialis and V depicts the ventricularis layers of the mitral valve.

overtime. Furthermore, an 11-month explant of a posterior PSIS mitral valve leaflet (**Figure 20A**) was assessed. Cellular infiltration was seen at the neoleaflet (**Figure 20A, C**) but there was also a chronic inflammatory response at the site of (**Figure 20B**) residual PSIS. Furthermore, calcification formed at the annulus of the valve (**Figure 20A**). Interestingly, the presence of smooth muscle cells was found on the explant similarly to the native valve. The smooth muscle cells were seen throughout the whole leaflet but preferentially on the ventricularis layer of the leaflet (**Figure 20D, E**). The presence of endothelial cells was found at the center of the leaflet in small vascular structures unlike the native baboon mitral valve (**Figure**

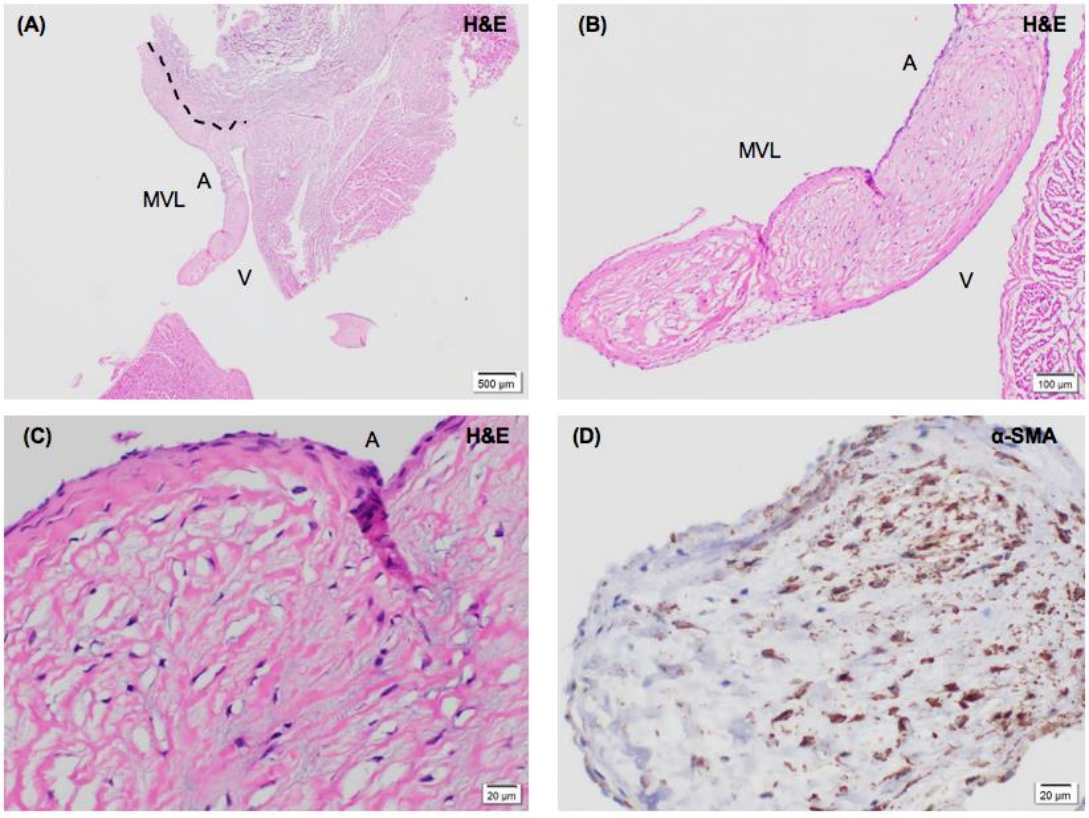

Figure 19: *PSIS mitral valve explant at 3-months post implantation in juvenile baboon.* Mitral valve leaflet (**MVL**) at low magnification of 2x (**A**; H&E) with underlying myocardium. Higher magnifications (**B**-10x, **C**-40x) showing presence of interstitial cells, proteoglycan (stains blue green) and endothelium. Presence of α-SMA (smooth muscle cells) in brown at the fragmented edge of the MVL (**F**-40x). A depicts the atrialis and V depicts the ventricularis layers of the mitral valve. Dotted line demonstrates annulus or the PSIS mitral valve.

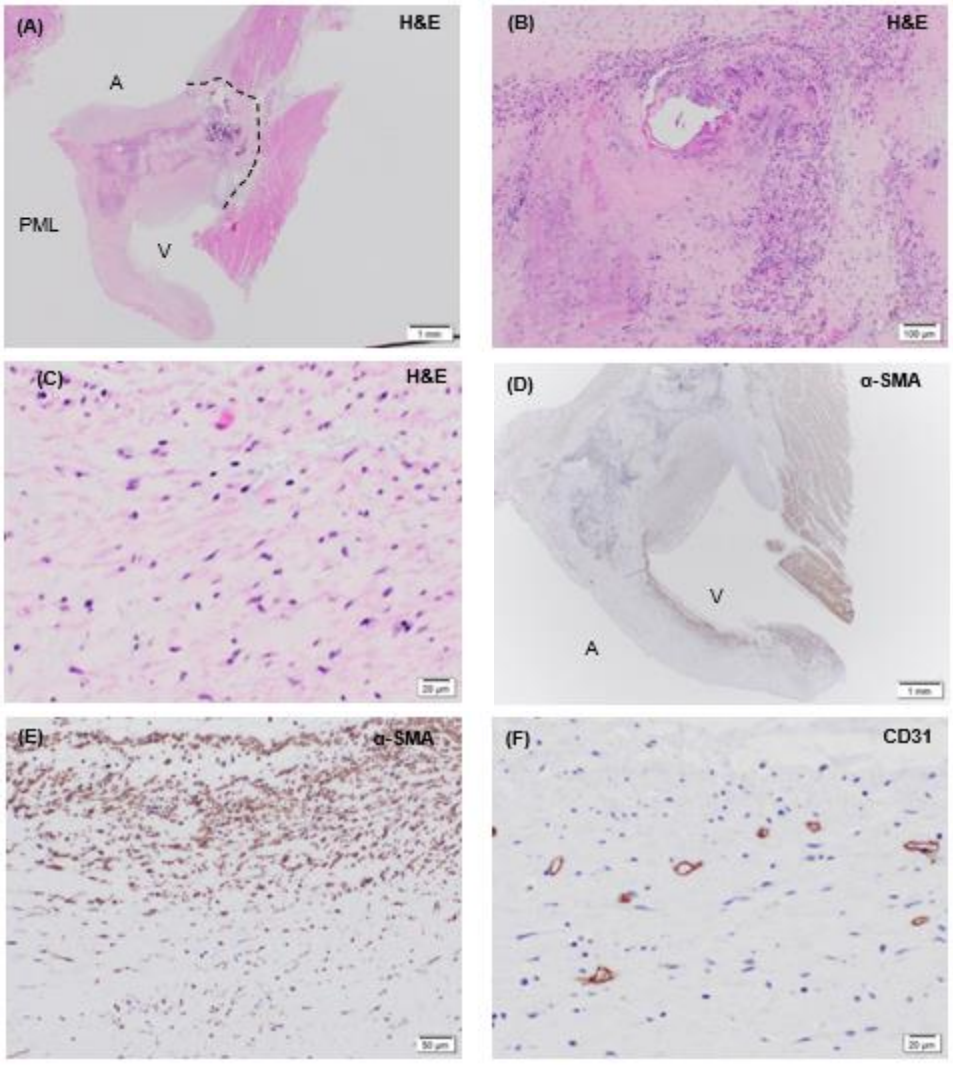

Figure 20: *PSIS mitral valve explant at 11-months post implantation in juvenile baboon.* Posterior mitral leaflet (**PML**) and annulus (dotted line) at 1.25x (**A**-H&E) with calcification and chronic inflammatory response including multinucleated giant cells (**B**-10x). Cellular infiltration of neo-leaflet (**C**-40x). Presence of α-SMA (smooth muscle cells) in brown (**D**-1.25x, **E**-20x) preferential on the ventricular surface and within neo-endocardial tissue but integrating into the center. Presence of CD31 (endothelial cells) in brown are also present at center of leaflet in small vascular structures (**F**-40x). A depicts the atrialis and V depicts the ventricularis layers of the mitral valve.

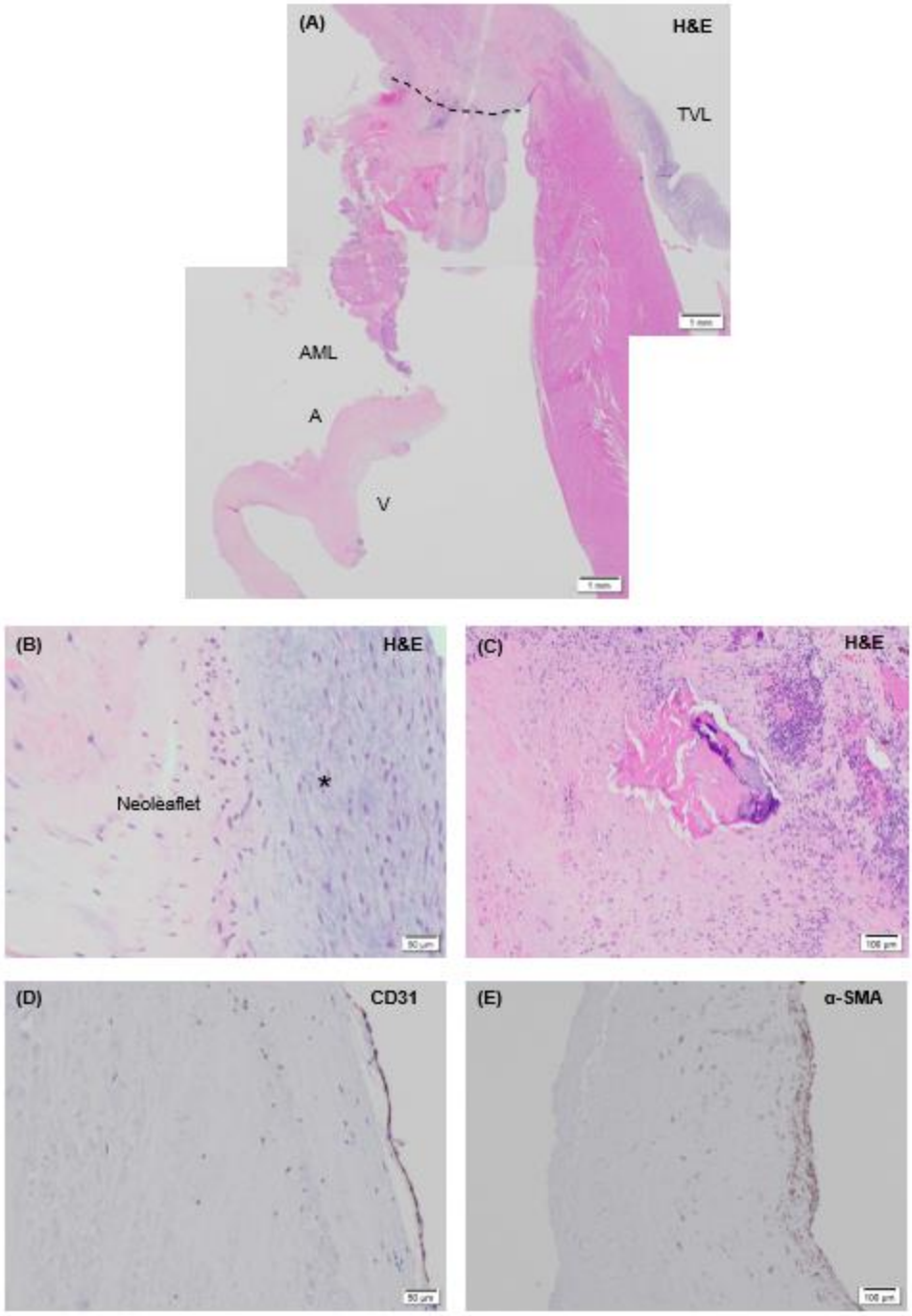

Figure 21: *PSIS mitral valve explant at 20-months post implantation in juvenile baboon.* Anterior mitral leaflet (**AML**) and annulus (dotted line) at 1.25x (**A-**H&E) with neo-endocardial tissue growth (asterisk; **B**-20x) and calcification and chronic inflammation at the annulus (**C**-10x). The native tricuspid valve leaflet (TVL) is also visible (**A**). Presence of CD31 (endothelial cells stain brown) are present at the surface of the leaflet (**D**-20x). There is also a presence of α-SMA (smooth muscle cells) in brown (**E**-10x) preferential on the outer surface but integrating into the center. A depicts the atrialis and V depicts the ventricularis layers of the mitral valve.

20F). Our last explant (20-month, cell unseeded PSIS valve), showed similar findings to our 11-month explant. The leaflet has physiological cellular infiltration (**Figure 21A, B**), however, chronic inflammatory response was observed at PSIS residual sites (**Figure 21C**). Calcification was also found at the annulus of the 20-month PSIS explant (**Figure 21A, C**). In the 20-month explant, endothelial and smooth muscle cells were present preferential on the outer surface of the valve (**Figure 21D, E**) resembling the native baboon mitral valve. Other images of the PSIS leaflet explants were taken that resulted in similar findings (**Appendix**).

4.2.3 ECM Assessment and Spatial Intensity Quantification of Explant PSIS Mitral Valves

To determine the ECM proteins on our PSIS explants, spatial intensity maps were computed based on our histological Movat's stained images. The native baboon mitral valve was computed first to determine a baseline trend of normal ECM growth. In the native baboon mitral valve (14 months of age) the leaflet was composed of four layers looking similarly to the atrialis, fibrosa, spongiosa and ventricularis (**Figure 22A**), with elastin at the atrialis and ventricularis layers. The valve leaflets were composed of 54 % collagen (**Figure 22B**), 15% elastin (**Figure 22C**) and 31% proteoglycans (**Figure 22D**). The explanted 3-month PSIS valve leaflet was mostly composed of collagen, with a 57% collagen composition (**Figure 23B**), scattered elastin (**Figure 23C**) and proteoglycans (**Figure 23D**) with 9% and 3%, respectively (**Figure 23A**). The 11-month PSIS mitral valve explant had matrix proteins of collagen, elastin, proteoglycans and fibrin present (**Figure 24A**). This

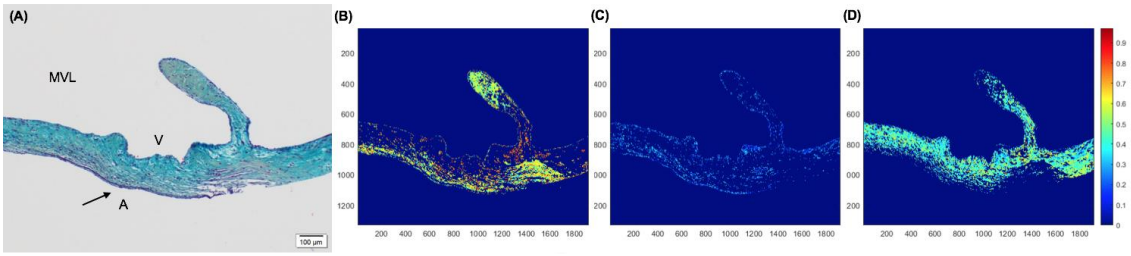

Figure 22: *ECM components of native juvenile baboon mitral valve explant at 14-months.* Native mitral valve leaflet (**MVL**) (**A**-10x; Movat's) demonstrating matrix proteins of collagen (**B**), elastin (**C**) and proteoglycans (**D**) (yellow/green, black, blue respective), with 54%, 15% and 31%, respectively of each ECM protein. Note elastic deposition along the atrialis layer (arrow). A depicts the atrialis and V depicts the ventricularis layers of the mitral valve.

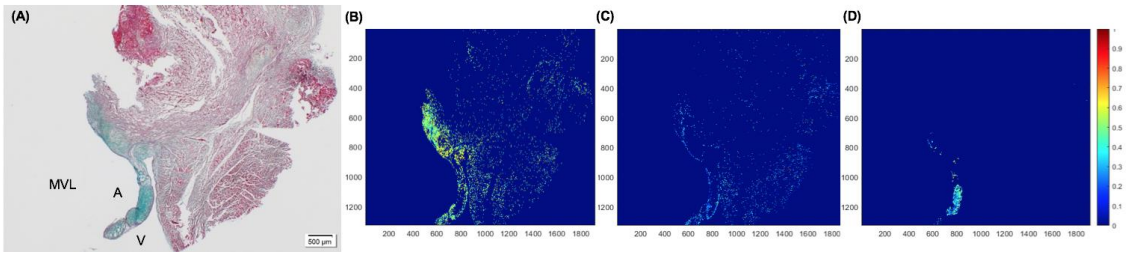

Figure 23: *ECM components of PSIS mitral valve explanted at 3-months post implantation.* PSIS mitral valve leaflet (**MVL**) (**A**-2x; Movat's) demonstrating matrix proteins of collagen (**B**), scattered elastin (**C**) and proteoglycans (**D**) (yellow/green, black, blue respective), with 57%, 9% and 3%, respectively of each ECM protein. A depicts the atrialis and V depicts the ventricularis layers of the mitral valve.

explant was mostly composed of 52% proteoglycans (**Figure 24D**) and 33% collagen (**Figure 24B**). The remaining ECM components were trace amounts of elastin (**Figure 24C**) and fibrin (**Figure 24E**) at 15% and 1%, respectively. Lastly, our 20-month explant was analyzed for ECM proteins showing similar rates of ECM protein (**Figure 25A**) as of our 11-month explant with 54% proteoglycans (**Figure 25D**), and trace amounts of elastin (**Figure 25C**) and fibrin (**Figure 25E**) at 6% and 3% ECM content, respectively. The collagen content was more abundant at 20-months of explant (**Figure 25B**), with a 61% collagen ECM content. Further histological images of native and PSIS baboon mitral valves were assessed for ECM content (**Appendix**) and the average ECM percentages of the leaflets ± SEM were calculated (**Table 2**). Based on our results, the native baboon valve leaflet

had 41% collagen, 12% elastin and 46% proteoglycans (**Table 2**). There was a relatively constant trend in collagen (45%, 40% and 49% for 3-, 11- and 20-month, respectively) throughout the time of implantation similar to the native baboon valve (**Table 2**). The same is true for elastin and proteoglycans at our longer time points

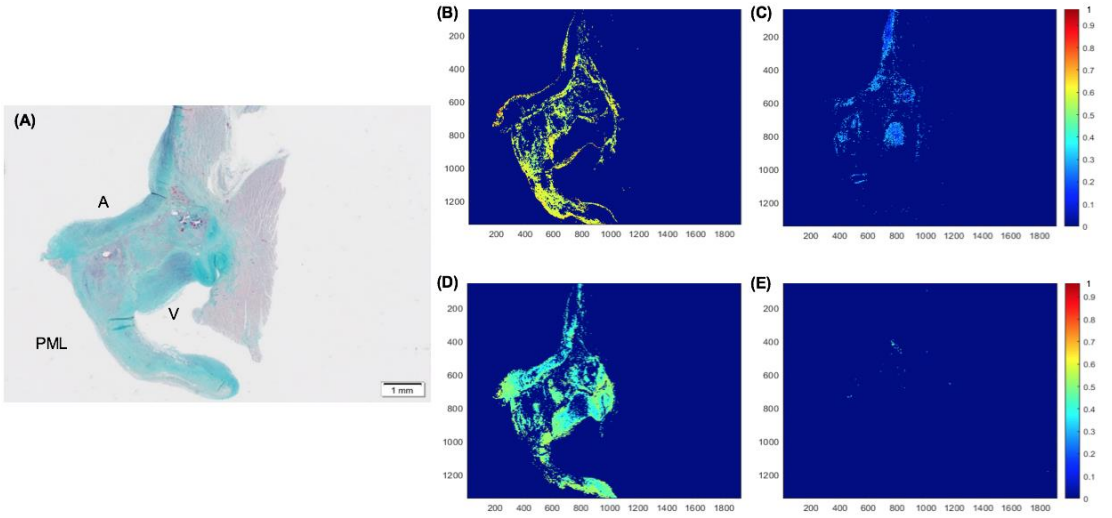

Figure 24: *ECM components of PSIS mitral valve explanted at 11-months post implantation.* PSIS mitral valve leaflet (**MVL**) (**A**-1.25x; Movat's) demonstrating matrix proteins of collagen (**B**), elastin (**C**), proteoglycans (**D**) and fibrin (**E**) (yellow/green, black, blue, dark pink respective), with 33%, 15%, 52% and 1%, respectively of each ECM protein. A depicts the atrialis and V depicts the ventricularis layers of the mitral valve.

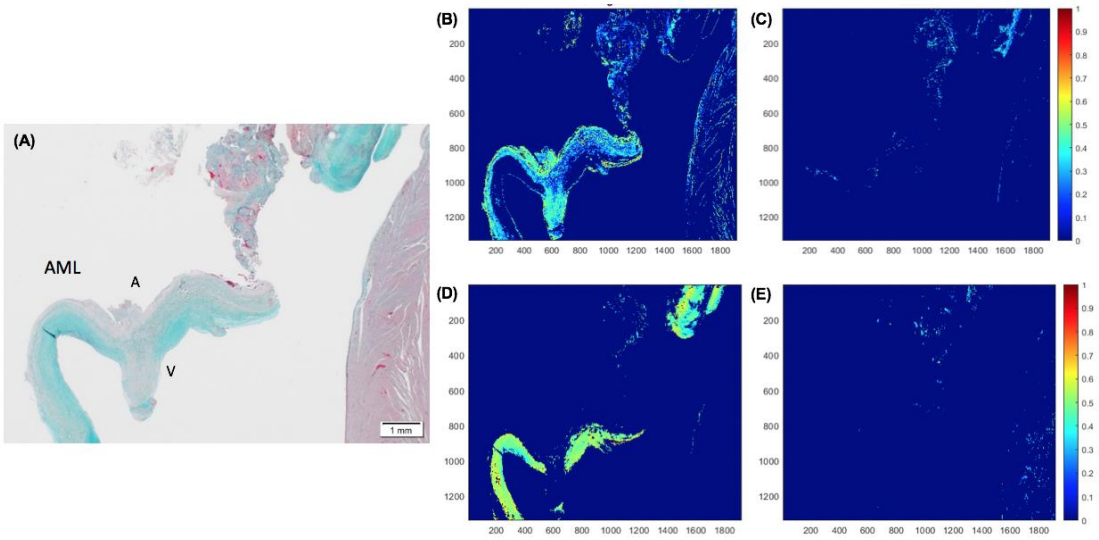

Figure 25: *ECM components of PSIS mitral valve explanted at 20-months post implantation.* PSIS mitral valve leaflet (**MVL**) (**A**-1.25x; Movat's) demonstrating matrix proteins of collagen (**B**), elastin (**C**), proteoglycans (**D**) and fibrin (**E**) (yellow/green, black, blue, dark pink respective), with 61%, 6%, 54% and 3%, respectively of each ECM protein. A depicts the atrialis and V depicts the ventricularis layers of the mitral valve.

of 11- and 20-month post implantation, where there are similar rates of elastin of 11% and 9%, respectively and proteoglycans of 48% and 40%, respectively (**Table 2**). On the other hand, the 3-month explant has insufficient growth of both elastin and proteoglycans of 7% and 24%, respectively, compared to the native baboon mitral valve (**Table 2**). No significant difference ($p>0.05$) was found between the groups for any ECM proteins (collagen, $p=0.77$; elastin, $p=0.28$; proteoglycans, $p=0.26$; fibrin, $p=0.05$). Although there was an abundant amount of ECM tissue, there was still an average of 2%, 3% and 4% of residual PSIS on the leaflets for 3-, 11- and 20-month explants, respectively (**Table 3**).

Table 2: Average *ECM components (%) ± SEM of baboon native and PSIS mitral valve explanted varying time points.* Various images per time point were assessed to determine the average percentages of each ECM component. It was found that the percentages of collagen and proteoglycans are comparable with minimal elastin. It is important to keep this percentage of ECM constant throughout regeneration. No significant difference was seen between any of the groups.

Baboon Valve Type	Area	% Collagen	% Elastin	% Proteoglycans	% Fibrin
Native Mitral Valve	Leaflet	41% ± 0.07	12% ± 0.02	46% ± 0.07	-
3-Month PSIS Explant	Leaflet	45% ± 0.11	7% ± 0.02	24% ± 0.21	-
11-Month PSIS Explant	Leaflet	40% ± 0.07	11% ± 0.02	48% ± 0.06	1% ± 0.00
20-Month PSIS Explant	Leaflet	49% ± 0.06	9% ± 0.01	40% ± 0.04	3% ± 0.01

Table 3: *Average % of unfilled de novo ECM (residual PSIS) of explanted PSIS mitral valve at various locations.* Various images per time point were assessed to determine the average percentages of unfilled de novo ECM (residual PSIS) remaining on the explant.

Baboon Valve Type	% Unfilled Tissue at Leaflet	% Unfilled Tissue at Annulus	% Unfilled Tissue at NC/PM
Native Mitral Valve	0%	-	-
3-Month PSIS Explant	2% ± 0.01	2% ± 0.79	-
11-Month PSIS Explant	3% ± 0.12	7% ± 0.10	1% ± 0.19
20-Month PSIS Explant	4% ± 0.46	3% ± 0.10	3% ± 0.04

The next area of interest was the annulus area of the mitral valves. The native juvenile baboon mitral valve was not collected during surgery due to limitations of tissue removal. Therefore, observations and comparisons were made only on the explanted PSIS annulus. For the annulus, the ECM content and integration of the PSIS annulus to the myocardium were assessed; troponin, which stains for muscle tissue, demonstrated integration between the two areas. All PSIS explants showed main ECM proteins of collagen, elastin and proteoglycans (**Figure 26A-C**) along with seamless integration at the annulus to the myocardium (**Figure 26D-F**). The 3-month explant was most abundant with collagen at the annulus and myocardium integration point, with 61% collagen content (**Figure 27B**), 15% elastin (**Figure 27C**) and the least ECM content of proteoglycans with 5% (**Figure 27D**). The 11-month explant had comparable amounts of collagen and proteoglycans, with 39% and 42%, respectively (**Figure 28A, B, D**). Elastin

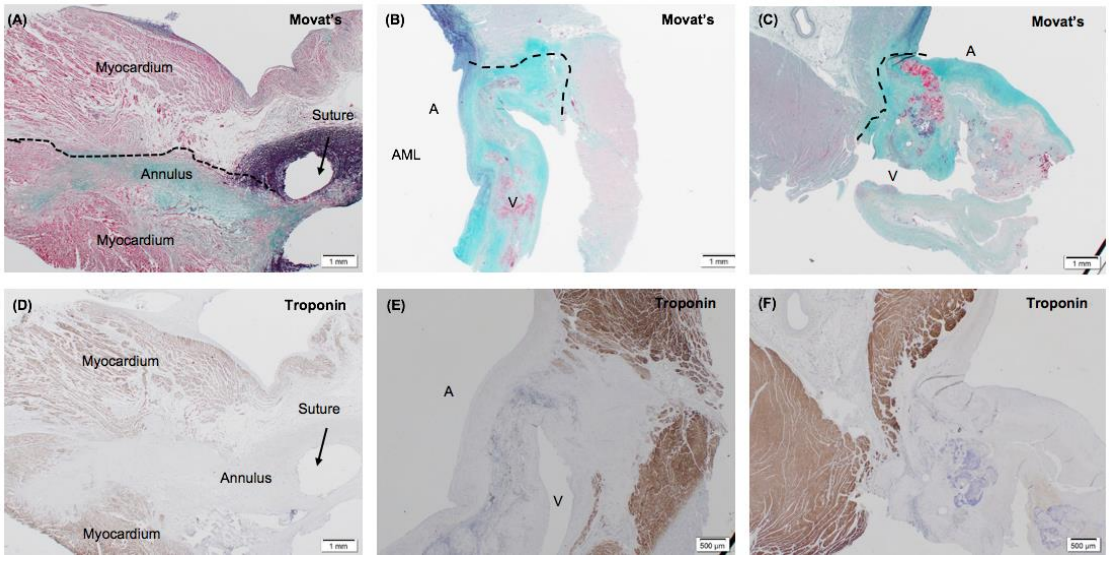

Figure 26: *PSIS mitral valve explanted at 3-, 11- and 20-months post implantation focused at the annulus.* PSIS mitral valve leaflet focused at the annulus (dotted lines) (**A, B, C**-1.25x; Movat's) demonstrating matrix proteins of collagen, elastin, proteoglycans and fibrin (yellow/green, black, blue, dark pink respective). A depicts the atrialis and V depicts the ventricularis layers of the mitral valve. Integration (**D**-1.25x, **E**, **F**-2x) is demonstrated between the annulus and surrounding myocardium via troponin staining.

(**Figure 28C**) and fibrin (**Figure 28E**) were seen in smaller amounts, with elastin content of 18% and fibrin content of 1%. The 20-month explant had a large area composed of fibrin, with a 18%, compared to the usual 1% seen in the other annulus areas (**Figure 29A, E**). The ECM content of collagen and proteoglycans (**Figure 29B, D**) are comparable with a larger presence of proteoglycans, with collagen content of 31% and proteoglycans with 47%. There were trace amounts of elastin, 4%, scattered throughout the annulus as well (**Figure 29C**). Further

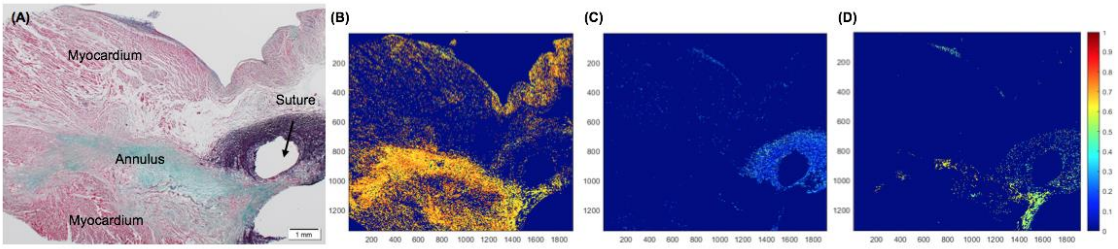

Figure 27: *ECM components of PSIS mitral valve explanted at 3-months post implantation focused at the annulus.* PSIS mitral valve leaflet (**MVL**) (**A**-1.25x; Movat's) zoomed at the annulus location demonstrating matrix proteins of collagen (**B**), elastin at the suture point (**C**) and proteoglycans (**D**) (yellow/green, black, blue respective), with 61%, 12% and 5%, respectively of each ECM protein.

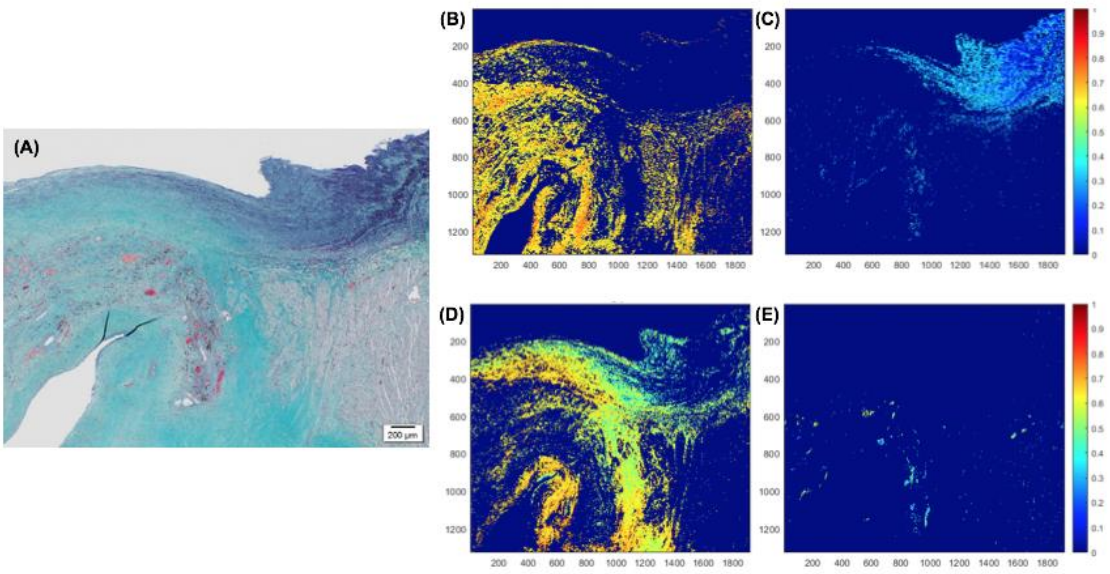

Figure 28: *ECM components of PSIS mitral valve explanted at 11-months post implantation focused at the annulus.* PSIS mitral valve leaflet (**MVL**) (**A**-4x; Movat's) zoomed at the annulus demonstrating matrix proteins of collagen (**B**), elastin at the edges (**C**) and proteoglycans (**D**) (yellow/green, black, blue respective), with 39%, 18% and 42%, respectively of each ECM protein. Trace amounts, 1%, of fibrin (**E**) present, with neo-vessel pockets.

histological images of PSIS baboon mitral valves were assessed for ECM content (**Appendix**) focused at the annulus and the averages of ECM ± SEM are reported (**Table 4**). The ECM content percentage of collagen was found to range between 41-61%, while elastin ranged from 6-12% (**Table 4**). The proteoglycans were low, at 5%, for the 3-month explant, while the 11-month and 20-month explants were at 44% and 38% (**Table 4**). The fibrin content increased over time, from no fibrin,

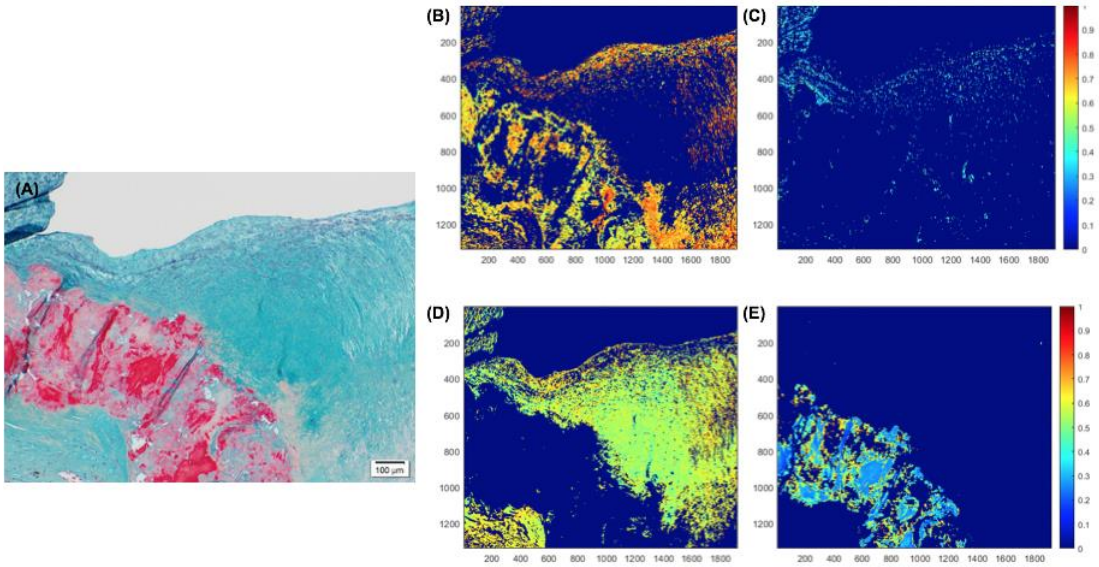

Figure 29: *ECM components of PSIS mitral valve explanted at 20-months post implantation focused at the annulus.* PSIS mitral valve leaflet (**MVL**) (**A**-10x; Movat's) zoomed at the annulus demonstrating matrix proteins of collagen (**B**), trace amounts of elastin (**C**) and proteoglycans (**D**) (yellow/green, black, blue respective), with 31%, 4% and 47%, respectively of each ECM protein. Trace amounts, 18%, of fibrin (**E**) present, with neo-vessel pockets.

Table 4: *Average ECM components (%) ± SEM of PSIS mitral valve annulus explanted at varying time points.* Various images per time point were assessed to determine the average percentages of each ECM component. The ECM % contents vary at each explant time point with no apparent trend. $^{*,+}$ signify a significant difference between groups.

Baboon Valve Type	Area	% Collagen	% Elastin	% Proteoglycans	% Fibrin
3-Month PSIS Explant	Annulus	61%	12%	5%$^{*+}$	-
11-Month PSIS Explant	Annulus	41% ± 0.04	14% ± 0.02	44% ± 0.03*	1% ± 0.00
20-Month PSIS Explant	Annulus	52% ± 0.07	6% ± 0.02	38% ± 0.05^{+}	4% ± 0.03

1% and 4% fibrin from 3-, 11- and 20-month explants. No significant difference ($p>0.05$) was found between the groups for all ECM proteins at the annulus (collagen, $p=0.25$; elastin, $p=0.10$; fibrin, $p=0.55$) expect for proteoglycans ($p=0.02$). The proteoglycans were found to be significantly lower in the 3-month explant compared to the 11- and 20-month explants. Overall there was an ample amount of ECM tissue but there was still an average of 2%, 7% and 3% of residual PSIS on the annulus area for 3-, 11- and 20-month explants, respectively (**Table 3**).

The last area of interest was the PSIS "legs" of the valve, which were sutured onto the papillary muscles (PM). These areas developed into neochordae (NC), which integrated with the papillary muscle overtime. The 3-month explant was not assessed due to removal of neochordae as histological cuts increased through the PSIS valve sample overtime. The 11-and 20-month explants demonstrated all ECM proteins assessed (**Figure 30A, B**) and seamless integration into the papillary muscles (**Figure 30C, D**). Analyzing the ECM content with spatial intensity maps, it was found that the 11-month explant (**Figure 31A**) was mostly composed of collagen with 70% ECM content (**Figure 31B**) followed by proteoglycans with 23% ECM content (**Figure 31D**). Collagen was found mostly at the base of the neochordae and papillary muscle integration point, while proteoglycans were found more at the neochordae. Trace amounts of elastin and fibrin were found with 7% and 1%, respectively (**Figure 31C, E**). The 20-month explant (**Figure 32A**) had similar ECM content compared to the 11-month explant

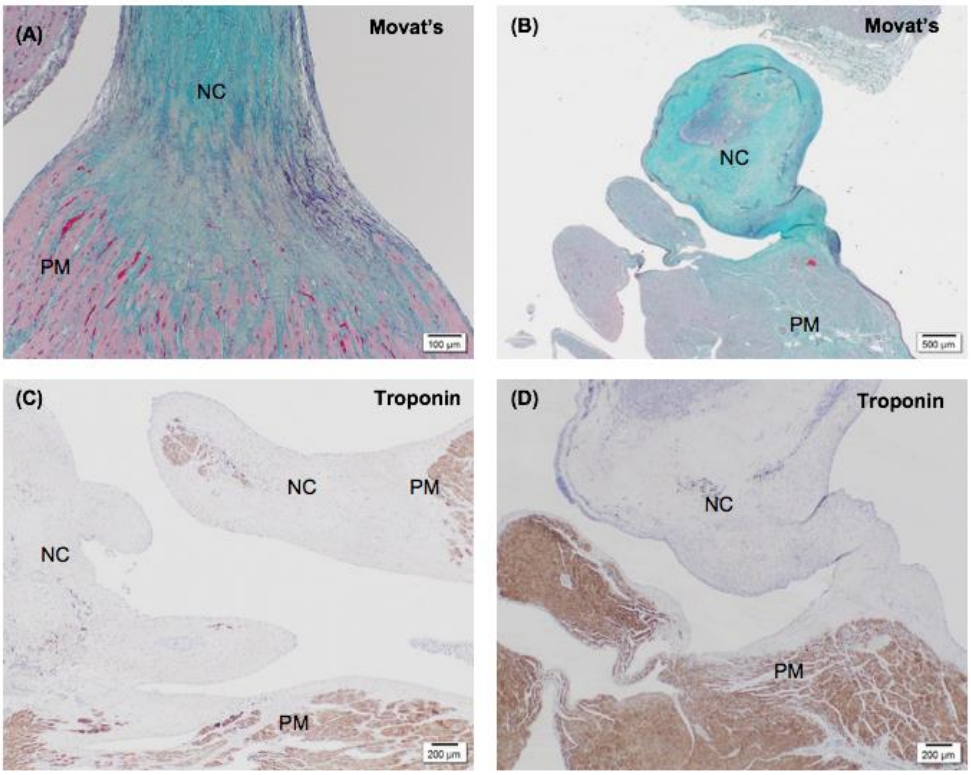

Figure 30: *PSIS mitral valve explanted at 11- and 20-months post implantation focused at the neochordae and papillary muscle point.* PSIS mitral valve focused at the papillary muscle showing neochordae formation (**A, B, C**-1.25x; Movat's) with matrix proteins of collagen, elastin, proteoglycans and fibrin (yellow/green, black, blue, dark pink respective) integrating (**D**-1.25x, **E**, **F**-2x) with surrounding papillary muscles via troponin staining.

with the most ECM content of collagen, followed by proteoglycans and elastin with 49%, 39% and 12%, respectively (**Figure 32B-D**). Further histological images of PSIS baboon mitral valves were assessed for ECM content (**Appendix**) focused at the neochordae and papillary muscle integration points and the average ECM contents ± SEM are reported (**Table 5**). Collagen ranged from 43-50%, elastin from 9-11%, proteoglycans from 37-47% and fibrin only present at our 11-month explant with 2% ECM content. No significant difference ($p>0.05$) was found between the groups for any ECM proteins (collagen, $p=0.41$; elastin, $p=0.48$; proteoglycans,

p=0.35; fibrin, p=0.24). Similar to the other areas of interest, there was an

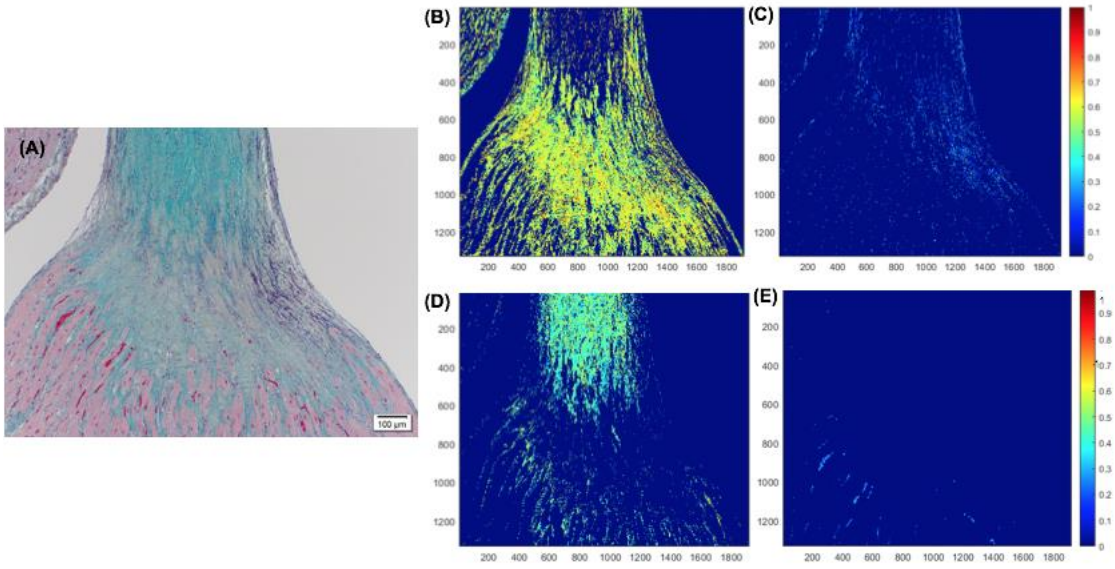

Figure 31: *ECM components of PSIS mitral valve explanted at 11-months post implantation focused at the neochordae and papillary muscle point.* PSIS mitral valve (**MVL**) (**A**-10x; Movat's) zoomed at the neochordae demonstrating matrix proteins of collagen (**B**), elastin (**C**) and proteoglycans (**D**) (yellow/green, black, blue respective), with 70%, 7% and 23%, respectively of each ECM protein. Trace amounts, 1%, of fibrin (**E**) present.

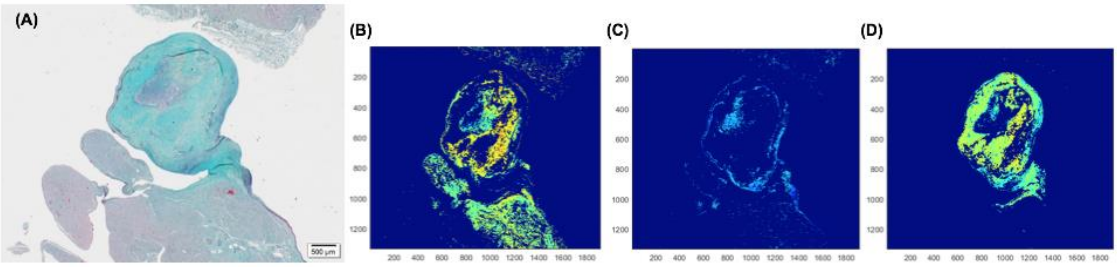

Figure 32: *ECM components of PSIS mitral valve explanted at 20-months post implantation focused at the neochordae and papillary muscle point.* PSIS mitral valve (**MVL**) (**A**-2x; Movat's) zoomed at the neochordae demonstrating matrix proteins of collagen (**B**), elastin (**C**) and proteoglycans (**D**) (yellow/green, black, blue respective), with 49%, 12% and 39%, respectively of each ECM protein.

Table 5: *Average ECM components (%) ± SEM of PSIS mitral valve neochordae and papillary muscle explanted at varying time points.* Various images per time point were assessed to determine the average percentages of each ECM component. The ECM % contents vary at each explant time point with no with comparable ECM content. No significant difference was seen between any of the groups.

Baboon Valve Type	Area	% Collagen	% Elastin	% Proteoglycans	% Fibrin
11-Month PSIS Explant	NC/PM	50% ± 0.06	11% ± 0.02	37% ± 0.07	2% ± 0.01
20-Month PSIS Explant	NC/PM	43% ±0.06	9% ± 0.01	47% ± 0.06	-

abundant amount of ECM tissue but there still was an average of 1% and 3% of residual PSIS on the integration point between the neochordae for 11- and 20-month explants, respectively (**Table 3**).

These results thus portray that our PSIS mitral valve integrated with the native surrounding cardiovascular tissue overall, but chronic inflammation occurred wherever there was residual PSIS matrix even after 20 months. These findings demonstrate that our 2ply PSIS valve could regenerate a neochordae that integrated with the papillary muscle but lacks the proper ECM content percentage throughout the regeneration process to support for proper valvular tissue growth.

4.3 Discussion

Valvular heart diseases continue to increase globally, including congenital heart defects (VeDepo, Detamore et al. 2017). Although an ideal heart valve prosthetic (without drawbacks) has been of interest and explored for decades, such a valve does not exist. Even more so for children, where the ideal pediatric valve is far greater in need, since there is an immense problem with patient-valve size mismatch and lack of somatic growth of the valves (VeDepo, Detamore et al. 2017).

A tissue engineered valve is a promising approach that would satisfy the unmet needs of currently available options, especially for children with congenital heart valve defects. There is much interest in decellularized tissues since its consists of biological components, which can ultimately impact positively the cells

to differentiate and provide a platform for the process of remodeling (VeDepo, Detamore et al. 2017). PSIS is a decellularized scaffold that has been used for tissue remodeling in various locations, yet the results have been mixed with positive (Badylak, Obermiller et al. 2003, Boyd, Johnson et al. 2010, Scholl, Boucek et al. 2010, Quarti, Nardone et al. 2011, Hynes and Naba 2012, Slaughter, Soucy et al. 2014, Soucy, Smith et al. 2015) and negative (Pavcnik, Uchida et al. 2002, Pavcnik, Obermiller et al. 2009, Fallon, Goodchild et al. 2012, Poulin, Horlick et al. 2013, Witt, Raff et al. 2013, Gerdisch, Boyd et al. 2014, Padalino, Quarti et al. 2015, Zafar, Hinton et al. 2015, Mosala Nezhad, Poncelet et al. 2016, Woo, Fishbein et al. 2016) outcomes.

In our pilot study, we implanted PSIS (Cormatrix, Roswell, GA) hand-made valves into juvenile baboons, with our clinical team, to investigate the functionality, somatic growth and regenerative capacities of the construct as an ideal treatment option for pediatric patients with critical congenital heart valve defects. It was found that our PSIS valves functioned well over time with mild to trivial regurgitation (**Figure 13**), which may be attributed to the NAGR. The NAGR was found to be nearly ideal (equal to 1) within the first couple of months (**Figure 12**), where the PSIS valve was growing at the same rate as the baboon (Gonzalez, Hernandez et al. 2018). As the time of implantation increased, the NAGR decreased and remained relatively constant, which could correlate to the rapid increase in the juvenile baboons' somatic growth compared to the growth of the PSIS valve (**Figure 12**).

It was also found that our PSIS mitral valves were able to regenerate the main ECM components of collagen, elastin and proteoglycans as well as integrate seamlessly with the host (**Figures 22-32**). Moreover, our PSIS mitral valve was able to recellularize, with predominantly smooth muscle cells (α-SMA$^+$ cells) and endothelial cells (CD31$^+$ cells) (**Figures 18-21**).

Our PSIS mitral valve leaflets at all explant time points (3-, 11-, 20-months) were able to regenerate ECM proteins similar to the native baboon mitral valve leaflets (**Figures 22-25**), with no significant difference ($p>0.05$) between the groups (**Table 2**). Even so, chronic inflammation and calcification were seen in the later time points (11-, 20-months) (**Figures 20, 21**), specifically at locations of residual PSIS (**Table 3**). This may be attributed to the remaining porcine cells on the decellularized PSIS scaffold (**Figures 15, 17**). These cellular residues trigger an inflammatory response following fibrin deposition, observed in trace amounts on the explants. A classic wound healing response would involve the migration of immune cells (Ellis, Lin et al. 2018) to the site of “injury”, in this case at the implanted PSIS mitral valve location.

Given the annulus area, the PSIS explants at our various time points regenerated ECM proteins and integrated well with the myocardium (**Figure 26**). No significance ($p>0.05$) was observed between the three explant groups in ECM protein contents except for proteoglycans; the 3-month explant had significantly lower ($p<0.05$) formation of proteoglycans (**Table 4**), which may have been a cause for failure, since proteoglycans are a major ECM component needed.

Proteoglycans play a role in the mechanical properties of the valve but also contribute to regulatory functions such as cell proliferation, differentiation and development (Baasanjav, Al-Gazali et al. 2011). The annulus areas at our later time points (11- and 20-months) contained fibrin (**Figure 28, 29**), especially at the 20-month explant (**Figure 29**). As mentioned, fibrin deposition is a common process of wound healing, however at this late time point (20-month explant) the presence of fibrin may have been related to the endocarditis, which ultimately led to failure. Endocarditis, an infection of the endocardium, causes lesions that are masses composed of fibrin, platelets and infecting organisms; this leads to a continuous inflammation resulting in ulcerations or perforations at these locations (Ashley and Niebauer 2004).

The last location of interest of the PSIS explants, the neochordae, also regenerated ECM proteins (**Figures 30-32**), with no significant difference ($p>0.05$) between the groups (**Table 5**). This area of the PSIS mitral valve recellularized and integrated seamlessly with the papillary muscle and the heart wall (**Figure 30**). Our finding compared to others studies, where complete re-endothelialization and recullularizarization was seen at attachment points (heart wall) but not on the valve leaflet surfaces (VeDepo, Detamore et al. 2017).

Overall, the decellularized PSIS mitral valve functioned well overtime and was successful in regeneration of ECM proteins and recellularization, especially since it appears that leaflet recellularization typically decreases as higher order animals are used for implant models (VeDepo, Detamore et al. 2017). It is believed

that to reach an ideal TEHV with the capability of mimicking the native heart valve ECM an optimal quantities of collagen and elastin is needed (~60% and 10% dry weight, respectively) (Eslami, Javadi et al. 2015). Therefore, the major problem seems to be the chronic inflammation that persists overtime due to the residual PSIS at all mitral valve explant locations (**Table 3**), not the level of ECM proteins. Hence, we speculate that a thin layer of baboon (i.e. host) ECM if produced on the decellularized PSIS mitral valves *in vitro* prior to implantation; will facilitate enhanced filling of exposed PSIS spatial locations (especially for the valve leaflets and annulus), hence allowing mitigation of the prolonged chronic response, and thereby leading to accelerated valve tissue regeneration *in vivo*.

5. SPECIFIC AIM 3

Assess acellular PSIS bioscaffolds seeded with BMSCs and subsequently conditioned with pulsatile flow-induced oscillatory shear stress to enhance somatic growth of *de novo* tissue *in vitro*.

5.1 Methodologies of Specific Aim 3

A custom-built, in-house “torpedo” bioreactor (**Figure 33**) is available in the CV-PEUTICS laboratory at Florida International University that can accommodate our tubular PSIS valves (CorTricuspid ECM valve, CorMatrix, Roswell, GA). The profile used is a square waveform with 17% positive flow and 83% negative flow direction (**Figure 34**), which provides a time-averaged wall shear stress (TAWSS) of 3.1 dynes/cm^2 and an OSI of 0.20.

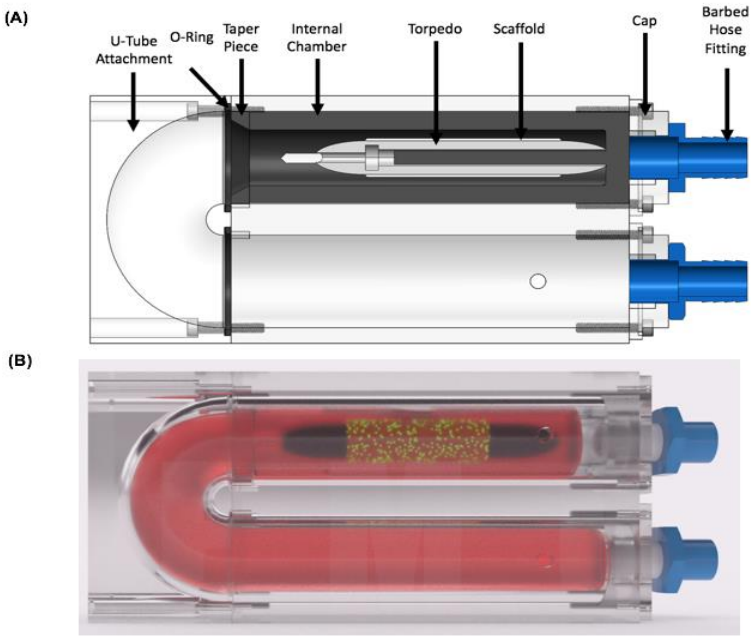

Figure 33: *Developed "torpedo" bioreactor*. **(A)** A design of our bioreactor with the major parts, including the torpedo and tube inlet and outlet. **(B)** Bioreactor schematic filled with cell culture media, the torpedo and a bioscaffold on the torpedo with seeded cells (green dots).

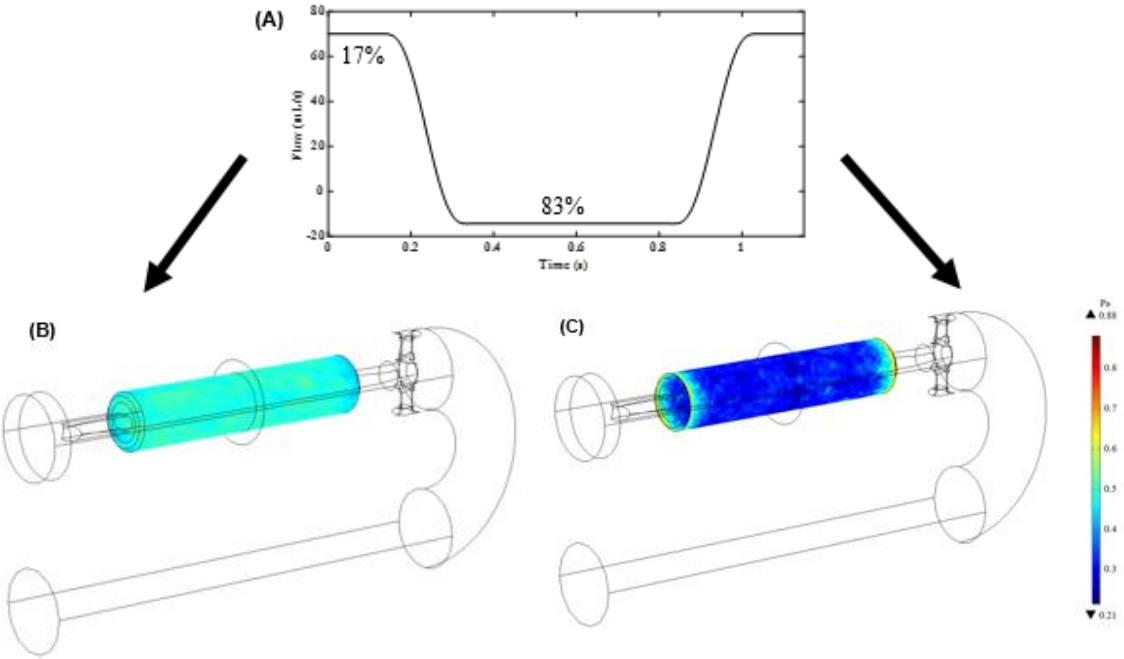

Figure 34: *CFD on our finalized torpedo bioreactor*. A **(A)** square waveform was used with a 17% forward and 83% backward flow. This waveform provided a **(B)** time-averaged wall shear stress (TAWSS) of 3.1 dynes/cm^2 and an **(C)** OSI of 0.20, both within the targets needed.

5.1.1 Cell Culture and Expansion of Bone Marrow Stem Cells

Human bone marrow stem cells (hBMSCs) (RoosterBio, Inc., Frederick, MD; catalog #: MSC-003) were cultured following the manufacturing protocol. In brief, the hBMSCs were freeze-thawed and transferred to a 50mL centrifuge tube, slowly adding (dropwise) 4 mL of prepared culture media (h-MSC High Performance Basal Medium (RoosterBio, Inc., Frederick, MD; catalog #: SU-005) and Media Booster GTX (RoosterBio, Inc., Frederick, MD; catalog #: SU-005) with 1% penicillin and streptomycin (Cytiva, HyClone™, Fisher Scientific, Pittsburgh, PA; Catalog #: SV300010). The cells were then centrifuged at 200 × g for 10 minutes. The supernatant was carefully removed and the cells were suspended in 45 mL of culture media and seeded into a T225 flask (Fisher Scientific, Pittsburgh, PA; Catalog #:10-126-63). Once confluent, the hBMSCs were harvested using 0.25% Trypsin-EDTA (1X) (Fisher Scientific, Pittsburgh, PA; Catalog #: 25200-056) and continuously passaged until a cellular growth of 28 x 10^6 cells (at passage 4).

5.1.2 Human BMSCs Seeded on PSIS Tubular Valves

The tubular PSIS valves (n=4) (CorTricuspid ECM valve, CorMatrix, Roswell, GA) were inserted onto a torpedo holder (n=2; n=2 PSIS valves per holder) (**Figure 35A**) and were then placed in a conical tube and rinsed with phosphate buffered saline (PBS) for 5 minutes. The valves on the torpedo were subsequently placed into a 50 mL vented conical tubes (Product # TP87050, TPP,

TubeSpin Bioreactor, Zollstrasse 7, CH-8219 Trasadingen, Switzerland), while the hBMSCs suspension (7 x 10^6 cells per PSIS valve; 14 x 10^6 cells in each conical tube) was then added to the conical tubes that contained the valves, while suspended in 45 mL of tissue culture media consisting of Dulbecco's modified Eagle's medium (DMEM; Corning, Fisher Scientific, Pittsburgh, PA; Catalog #: MT10013CV) supplemented with 10% fetal bovine serum (Corning, Fisher Scientific, Pittsburgh, PA; Catalog #: MT35010CV), 1% penicillin and streptomycin (Cytiva, HyClone™, Fisher Scientific, Pittsburgh, PA; Catalog #: SV300010), 2 ng/ml basic fibroblast growth factor (bFGF, Corning™; Fisher Scientific, Pittsburgh, PA; Catalog #: CB-40060) and 82 µg/mL ascorbic acid 2 phosphate (AA2P, Sigma-Aldrich, Fisher Scientific, Pittsburgh, PA; Catalog #: NC0602549) (**Figure 35B**). These tubes were then placed in a rotisserie (Labquake^{TM} Rotisserie Hybridization Rotators, Thermo Scientific, USA) at 10 RPM inside a cell and tissue culture incubator with 5% CO_2 and controlled humidity for 8 days.

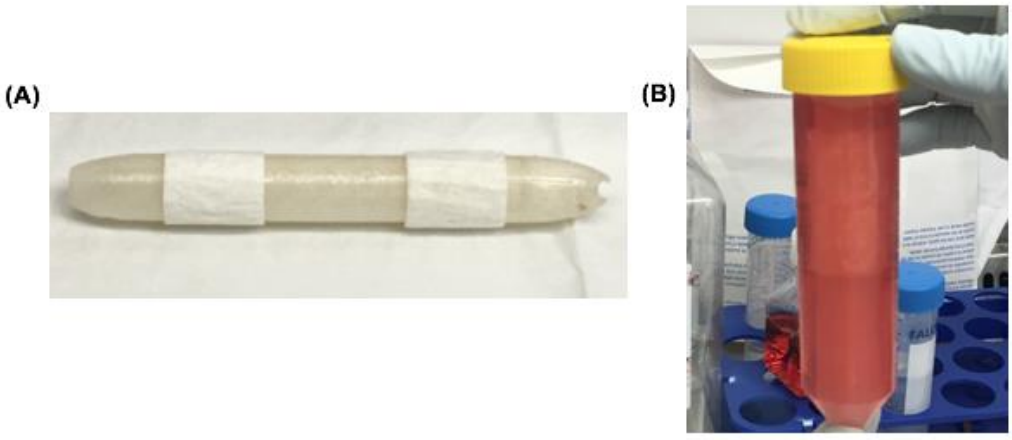

Figure 35: *Torpedo for MSC cell seeding of PSIS valve*. **(A)** Two valves placed on the torpedo and **(B)** transferred to a vented conical tube for 8 days in rotisserie.

5.1.3 Static and Dynamic Cell-Seeded PSIS Tubular Valves

After 8 days of seeding in the rotisserie, two tubular PSIS valves ("static" control group) on the torpedo were kept in rotisserie for another 14 days without media change. The other two tubular PSIS valves (dynamic group) on the torpedo were mounted into our new redesigned in-house torpedo bioreactor (**Figure 36**), similar to our previously used bioreactor for the purpose of conducting heart valve tissue engineering experiments (Ramaswamy, Boronyak et al. 2014, Rath, Salinas et al. 2015, Williams, Nasim et al. 2017), for 14 days.

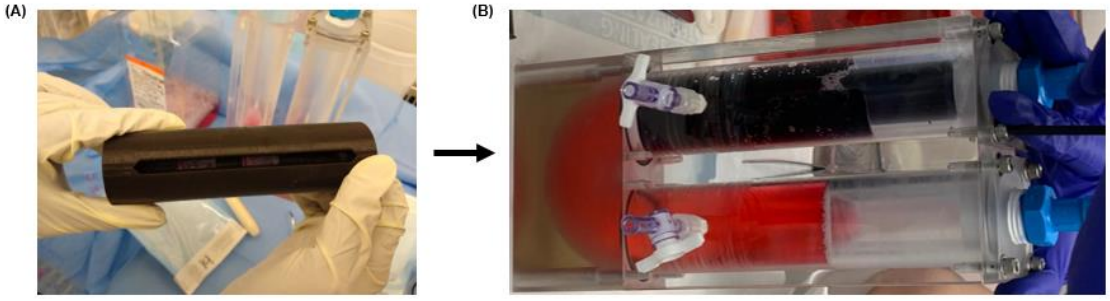

Figure 36: *Loaded "torpedo" bioreactor.* ***(A)*** Two PSIS valves on the torpedo holder, seeded with MSCs for 8 days in rotisserie, are placed in the outer housing. **(B)** These PSIS vales are then loaded into the torpedo bioreactor for 14 days.

5.1.4 Histological/Immunofluorescence Assessments of Static and Dynamic PSIS Tubular Valves

After 22 days (8 days seeding and 14 days stimulation), the PSIS valves (n=2 static; n=2 dynamic) were removed from rotisserie or from the torpedo bioreactor (**Figure 37**) and fixed in 10% (w/v) formalin immediately for 24 hours. The valves were then rinsed with PBS and embedded in a slow freeze process with optimal cutting temperature (Fisher HealthCare, Houston, TX; Catalog #: 4585). The embedded PSIS valves were then stored in -80°C overnight. The following day, the embedded samples were cut to a thickness of 16 μm (each slice)

and placed on glass slides (TruBond 380; Newcomer Supply, Middleton, WI), which were set to dry at room temperature.

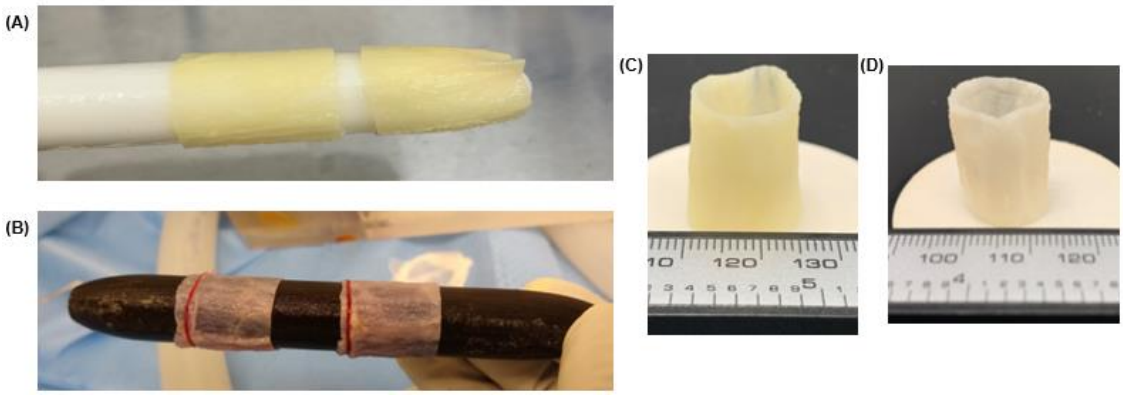

Figure 37: *PSIS valves post static and dynamic cultures.* ***(A)*** Two PSIS valves on the torpedo holder, seeded with MSCs for 8 days in rotisserie and kept in rotisserie for 14 days thereafter (static group). **(B)** Two PSIS valves on the torpedo holder, seeded with MSCs for 8 days and then loaded into the torpedo bioreactor for 14 days. (**C**) Static and (**D**) dynamic PSIS valves, respectively, removed from the torpedo holder after 22 days.

Hematoxylin and eosin (H&E; Rapid Chrome H&E Frozen Section Staining Kit, Richard-Allan Scientific, Kalamazoo, MI) was used to determine the presence of live cells and morphology of the PSIS valves, while Movat's stain (Russel-Movat Pentachrome; American MasterTech Scientific, Lodi, CA; catalog #: KTRMP) was used to determine the different constituents of the leaflet tissues. α-SMA (Invitrogen, Catalog #: 14-9760-82, anti-alpha smooth muscle actin antibody (0.5 mg/mL)) and CD31 (Invitrogen, Prod #: PA5-14372, anti CD31 antibody (0.5 mg/mL)) fluorescent stains (abcam, ab 150108 and ab150073 both 2 mg/mL, respectively) were use on the PSIS tubular valves to determine smooth muscle, interstitial and endothelial cells, respectively. 4,6-diamidino-2-phenylindole (DAPI; 1 mg/mL) fluorescent stain (Thermo Scientific™, Rockford, IL; Prod #: 62248) was used as a counterstain, staining the cell nuclei. Histological images were captured with bright-field microscopy (Zeiss, Axiovert 40 CFL, Maple Grove, MN) and

immunofluorescence images were captured with confocal microscopy (Nikon Eclipse Ti, Minato, Tokyo, Japan).

5.1.5 Spatial Intensity Mapping of ECM Components on the Static and Dynamic PSIS Tubular Valves

A Movat's image of the raw acellular PSIS strips (Cormatrix, Roswell, GA) was used as a reference image for all the image analysis of Movat's. The reference image was then thresholded for brightness and contrast automatically (ImageJ, NIH Image, Bethesda, MD). This thresholded reference image was then saved and run against each image to normalize them similarly through an in-house script (MATLAB, The MathWorks, Inc., Natick, MA) from our laboratory. Upon normalizing with respect to the reference, a color segmentation plugin was used (ImageJ, NIH Image, Bethesda, MD) and the different colors were chosen to distinguish the different ECM components of collagen, elastin, mucins and fibrin. Once complete, the option of independent color channels was chosen and Hidden Markov Model was used to determine the resulting percentages of the ECM concentration areas. The images were then scanned for intensities of each component of interest (MATLAB, The MathWorks, Inc., Natick, MA) and used to find the ranges of the component of interest, generating the spatial intensity maps of each ECM component. The ECM concentrations were compared between our static and dynamic PSIS valves.

5.1.6 Statistical Analysis

Results were reported as average ± standard error of mean (SEM). The spatial intensity maps were compared between the static and dynamic PSIS valve

groups for ECM content percentage (i.e. collagen, elastin, mucins or fibrin) and immunofluorescence intensity (DAPI, CD31 and α-SMA) per image. The percent area of unfilled tissue was also computed for both groups. All data was statistically analyzed using a two-sample t-test (Minitab, Inc., State College, PA). Statistical significance between any two given groups was found to have occurred when the p-value was less than 0.05 ($p<0.05$).

5.2 Results of Specific Aim 3

5.2.1 Morphological Assessments of Static and Dynamic PSIS Tubular Valves

The morphology and cellular content of both the static and dynamic PSIS valves were assessed with H&E. It was found that both the static and dynamic

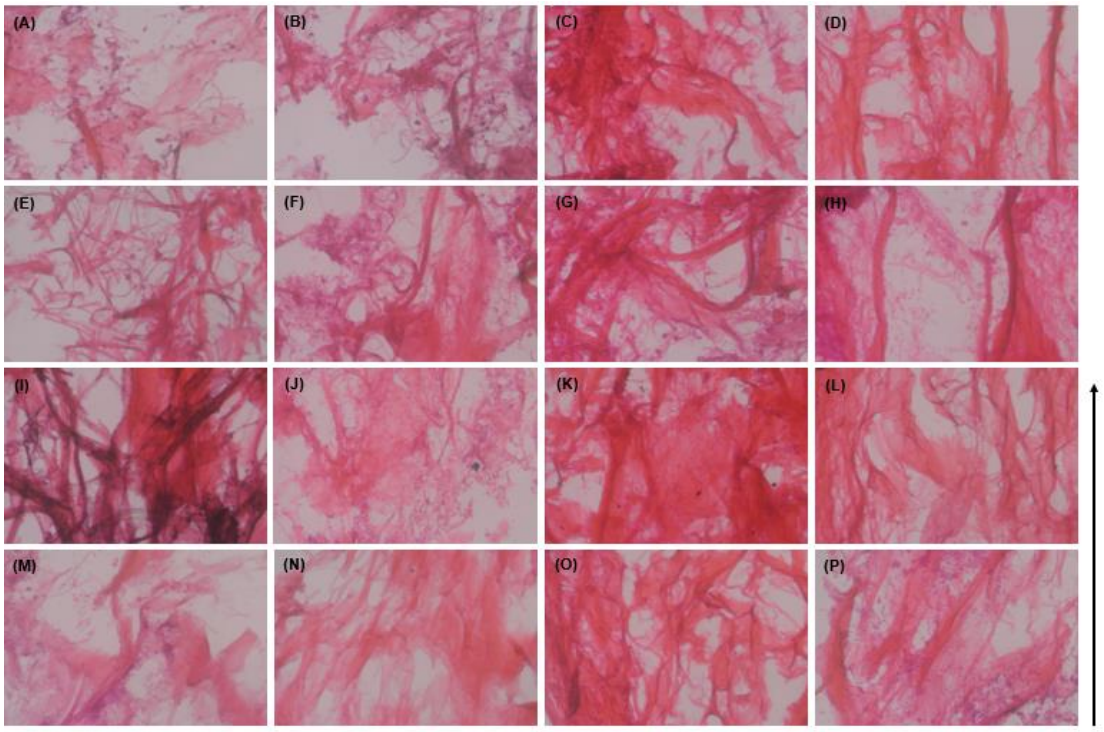

Figure 38: *Morphology and cellular infiltration of PSIS valves.* (**A-H**) Static and (**I-P**) dynamic PSIS valves were morphologically assessed via H&E staining. Both groups had cellular infiltration and tissue formation. The PSIS valves are denser in tissue as the depth increases from (**A, E, I, M**) 80 μm, (**B, F, J, N**) 176 μm, (**C, G, K, O**) 272 μm to (**D, H, L, P**) 368 μm. The (**A-H**) static group is scattered in orientation, while the (**I-P**) dynamic group oriented towards the direction of flow. The arrow signifies the direction of flow. Magnification 50x.

groups had the presence of *de novo* human tissues on the PSIS bioscaffold and had cellular infiltration (**Figure 38**). It appears that for both groups the layers of the PSIS valves towards the outer surface of the valve had less tissue and was disorganized (**Figure 38A, E, I, M**), although the dynamic group had more aligned tissue. With increasing tissue-depth, both groups became denser and more cells were seen (**Figure 38C-D, G-H, K-L, O-P**). The *de novo* tissue of the static PSIS valves seemed to be scattered in orientation (**Figure 38A-H**), while the dynamic PSIS valves oriented toward the direction of flow (**Figure 38I-P**).

5.2.2 Immunofluorescence Assessments of Static and Dynamic PSIS Tubular Valves

The differentiation of the hBMSCs towards endothelial cells and smooth muscle or interstitial cells, which populate the native vales, were assessed immunologically with anti-CD31 and anti-α-SMA antibodies. Similar findings to H&E were found when assessing for endothelial cells (CD31) with the tissue orientation, where the static group had scattered and disorganized tissue fibers (**Figure 39A-D**) while the dynamic group was oriented towards the direction of flow exposed on the PSIS valve constructs (**Figure 39E-H**). DAPI confirmed the presence of the cells; CD31 was expressed by the cells on the outer as well as inner layers in the static group (**Figure 39A-D**). As the depth increased (320 µm, 704 µm and 800 µm), CD31 was present embedded deep within the tissue (**Figure 39B-D**). The dynamic group expressed CD31 throughout the depth of the tissue (32 µm, 320 µm, 704 µm and 800 µm), with abundant expression deeper into the tissue (**Figure 39E-H**). Overall the presence of CD31 was found to be predominant

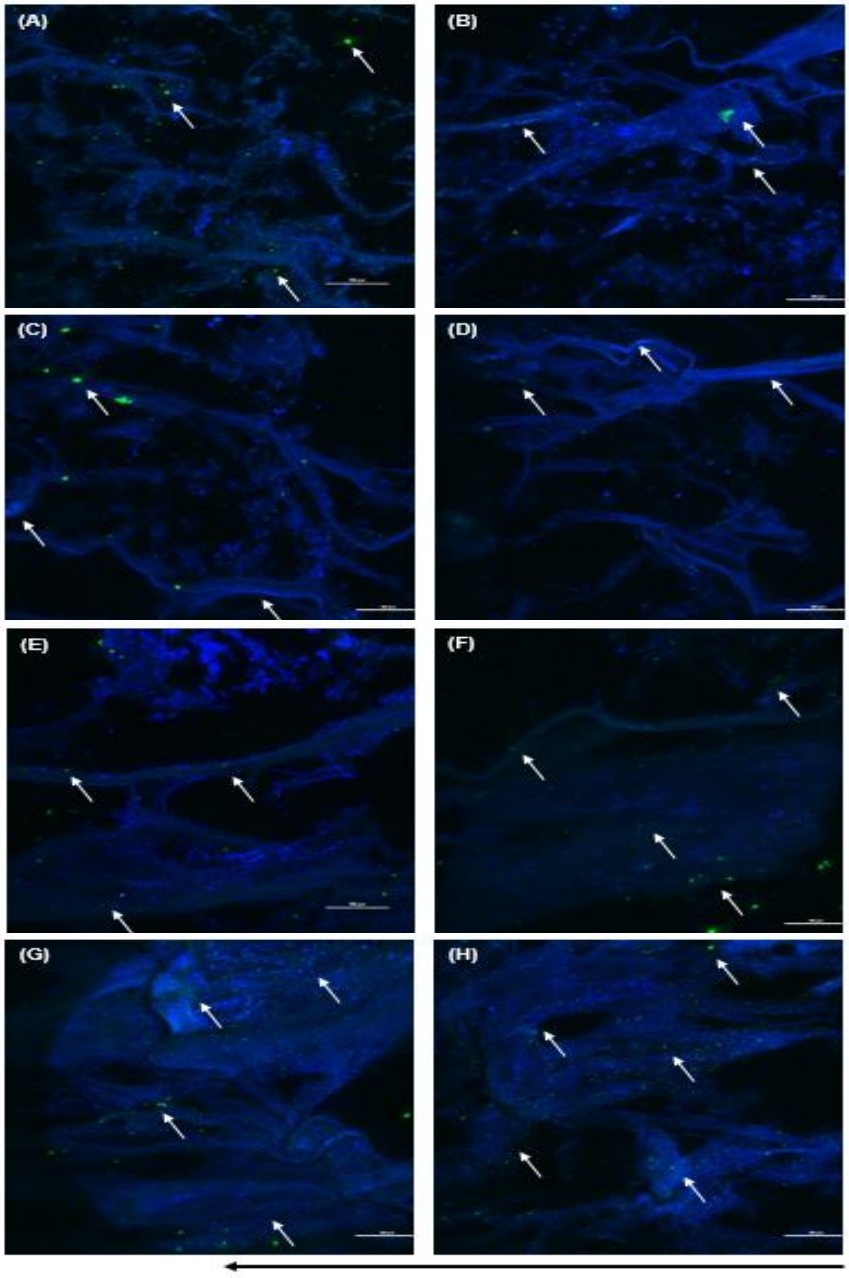

Figure 39: *Immunofluorescence assessment of cellular infiltration and presence of endothelial cells (CD31) on PSIS valves.* (**A-D**) Static and (**E-H**) dynamic PSIS valves were assessed via immunofluorescence staining of CD31. Both groups had cellular infiltration (DAPI- blue) and presence of CD31 (green). The (**A-D**) static group is scattered in orientation, while the (**E-H**) dynamic group oriented towards the direction of flow. The presence of CD31 is seen predominantly in the dynamic group (E-H) embedded in the tissue, with some presence in the static group (A-D) but more superficial at the surface. Images shown are at a depth of (**A, E**) 32 µm, (**B, F**) 320 µm, (**C, G**) 704 µm and (**D, H**) 800 µm. The long black arrow signifies the direction of flow. The smaller white arrows signify some areas with presence of CD31.

in the dynamic group compared to the static group (**Figures 39, 40, 41**), with an

average ± SEM intensity of CD31 of 0.06 ± 0.00 for static and 0.07 ± 0.01 for dynamic; note however that no significant difference ($p>0.05$) was found between the two groups ($p=0.32$).

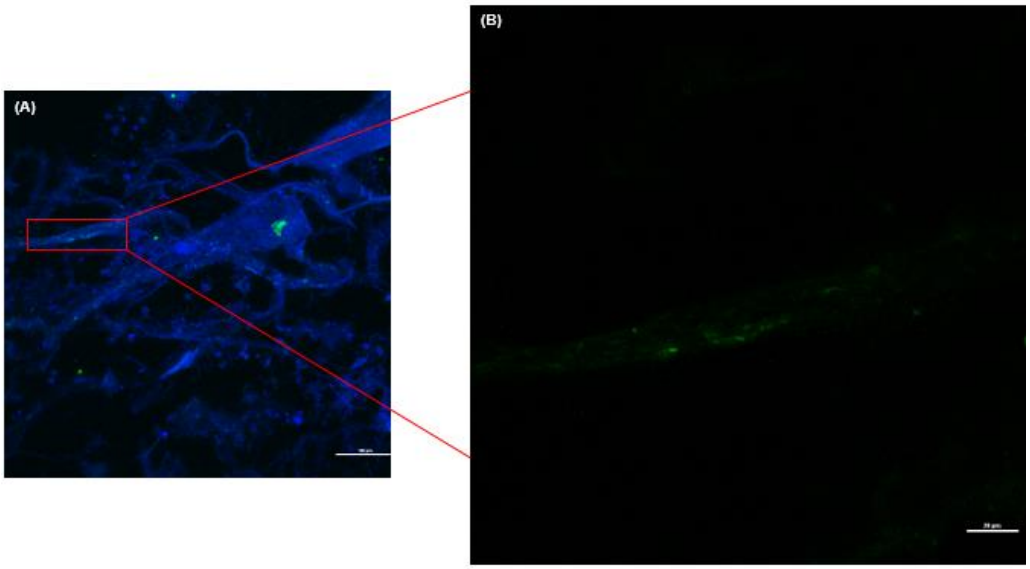

Figure 40: *Immunofluorescence assessment of presence of endothelial cells (CD31) on a static PSIS valve.* Image of a (**A**) static PSIS valve at a depth of 320 µm demonstrating the presence of cells (DAPI-blue) and CD31 (green). A magnified view (**B**) demonstrates the presence of CD31 embedded within the tissue.

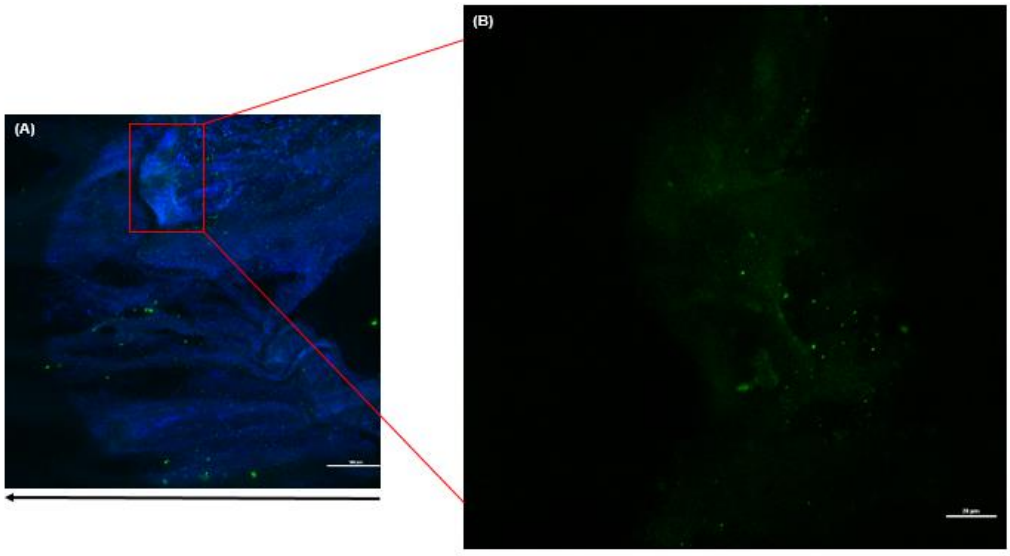

Figure 41: *Immunofluorescence assessment of presence of endothelial cells (CD31) on a dynamic PSIS valve.* Image of a (**A**) dynamic PSIS valve at a depth of 704 µm demonstrating the presence of cells (DAPI-blue) and CD31 (green). A magnified view (**B**) demonstrates the presence of CD31 embedded deep within the tissue. The arrow signifies the direction of flow.

When assessing for smooth muscle cells or interstitial cells (α-SMA), the

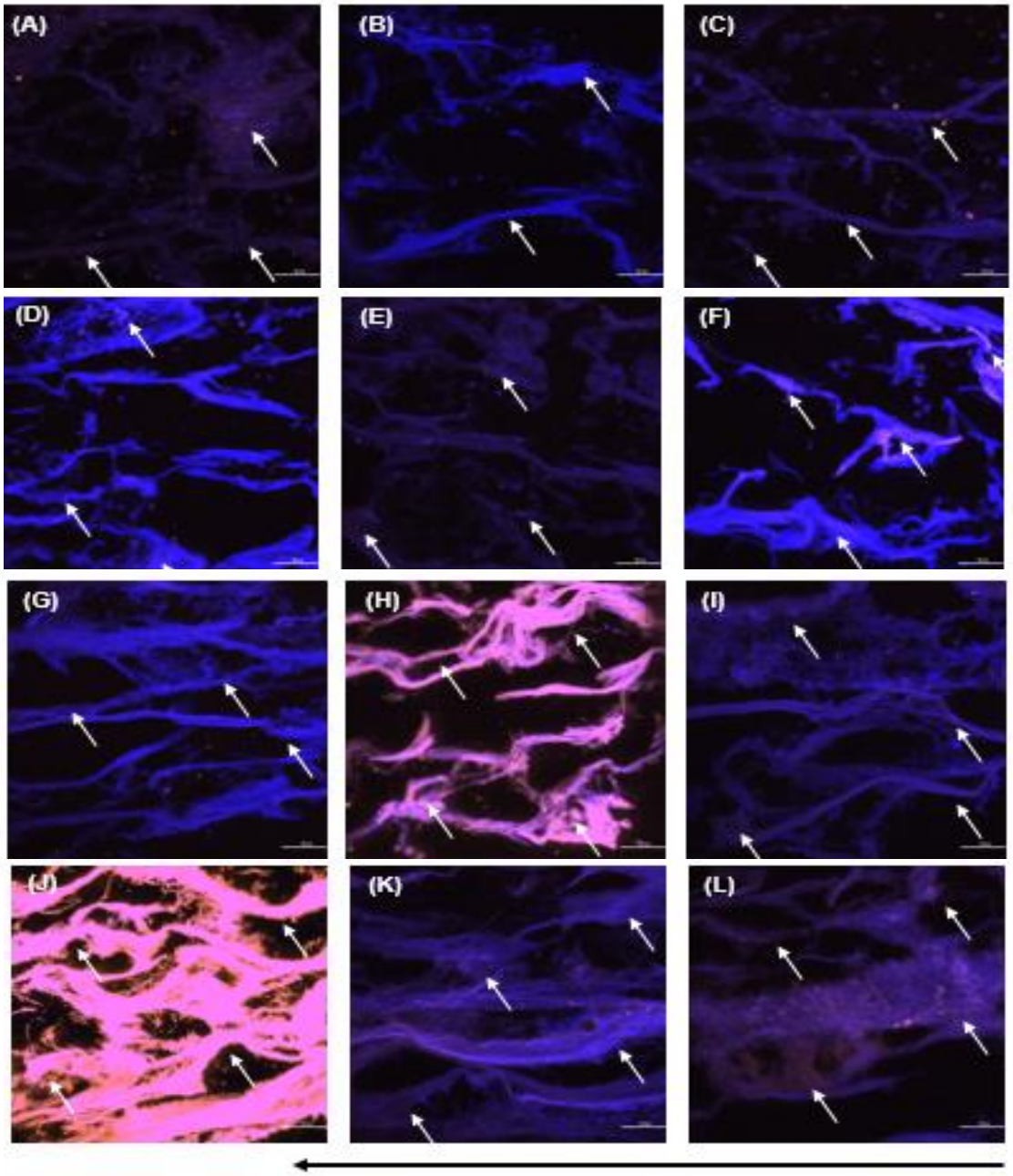

Figure 42: *Immunofluorescence assessment of cellular infiltration and presence of smooth muscle and interstitial cells (α-SMA) on PSIS valves.* (**A-F**) Static and (**G-L**) dynamic PSIS valves were assessed via immunofluorescence staining of *α-SMA*. Both groups had cellular infiltration (DAPI- blue) and presence of *α-SMA* (orange/pink). The (**A-F**) static group is scattered in orientation, while the (**G-L**) dynamic group oriented towards the direction of flow. The presence of *α-SMA* is seen predominantly in the dynamic group (G-L), but still seen in the static group (A-F) both embedded within the tissue. Images shown are at a depth of (**A, G**) 48 µm, (**B, H**) 240 µm, (**C, I**) 432 µm, (**D, J**) 528 µm, (**E, K**) 624 µm and (**F, L**) 816 µm. The long black arrow signifies the direction of flow. The smaller white arrows signify some areas with presence of *α-SMA*.

same trend continued with orientation of the tissue; the static group was disorganized (**Figure 42A-F**) while the dynamic group was organized and aligned with the direction of flow (**Figure 42G-L**). Similar to CD31, a presence of α-SMA

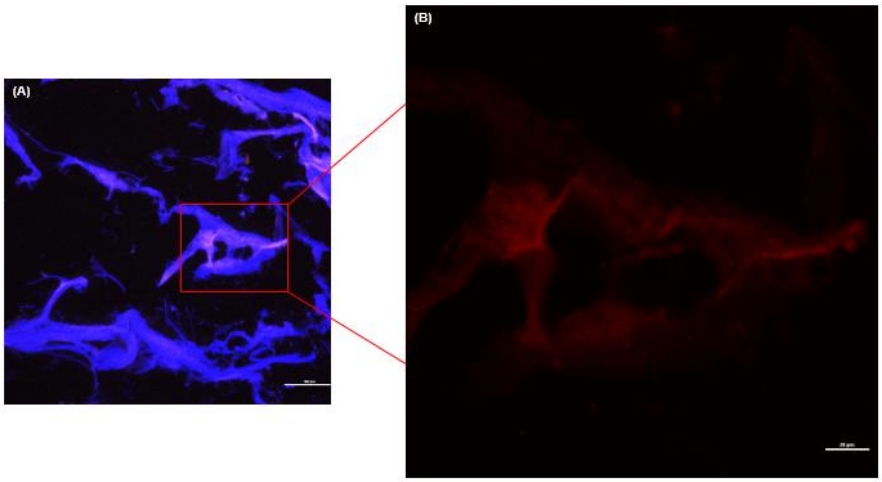

Figure 43: *Immunofluorescence assessment of presence of smooth muscle and interstitial cells (α-SMA) on a static PSIS valve.* Image of a (**A**) static PSIS valve at a depth of 816 µm demonstrating the presence of cells (DAPI-blue) and *α-SMA* (orange/red). A magnified view (**B**) demonstrates the presence of *α-SMA* embedded within the tissue.

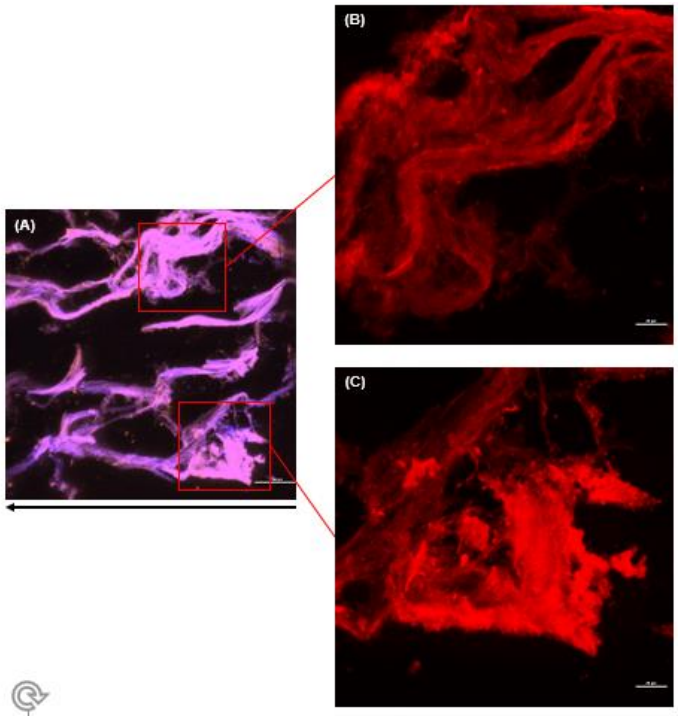

Figure 44: *Immunofluorescence assessment of presence of smooth muscle and interstitial cells (α-SMA) on a dynamic PSIS valve.* Image of a (**A**) dynamic PSIS valve at a depth of 240 µm demonstrating the presence of cells (DAPI-blue) and *α-SMA* (orange/pink). A magnified view (**B**) demonstrates the presence of *α-SMA (red)* embedded within the tissue.

and DAPI were found in both groups (**Figure 42**). Contrary to the findings of CD31, α-SMA was found to be embedded deep within the tissue at all depths of the PSIS valve (48 μm, 240 μm, 432 μm, 528 μm, 624 μm and 816 μm); this means that α-SMA was present at the outer and inner surface of the PSIS valves in both the static and dynamic groups (**Figure 42**). α-SMA was found to be more abundant in the dynamic group compared to the static group (**Figures 42, 43, 44**), with the depths of 240 μm, 528 μm and 816 μm demonstrating the most amplified presence of α-SMA (**Figure 42H, J, L and Figure 44**). The average ± SEM of α-SMA intensity was found to be 0.08 ± 0.00 and 0.25 ± 0.10 for the static and dynamic groups, respectively; note however that no significant difference ($p>0.05$) was found between the groups ($p=0.15$).

The average ± SEM intensity of DAPI (cells present) was computed as well from both CD31 and α-SMA images. The overall intensity of DAPI was 0.10 ± 0.01 and 0.15 ± 0.02 for static and dynamic groups, respectively. Interestingly, there was a significant difference ($p<0.05$) found between the two groups ($p=0.02$), with the dynamic group having a significantly higher intensity of DAPI (i.e. presence of cells).

5.2.3 ECM Assessment and Spatial Intensity Quantification of Static and Dynamic PSIS Tubular Valves

The ECM was assessed for both static (**Figure 45A-H**) and dynamic groups (**Figure 45I-P**) with Movat's histological stain. Movat's stains tissues to identify collagen, elastic fibers, fibrinoids, mucins, and nuclei in yellow, black, intense red,

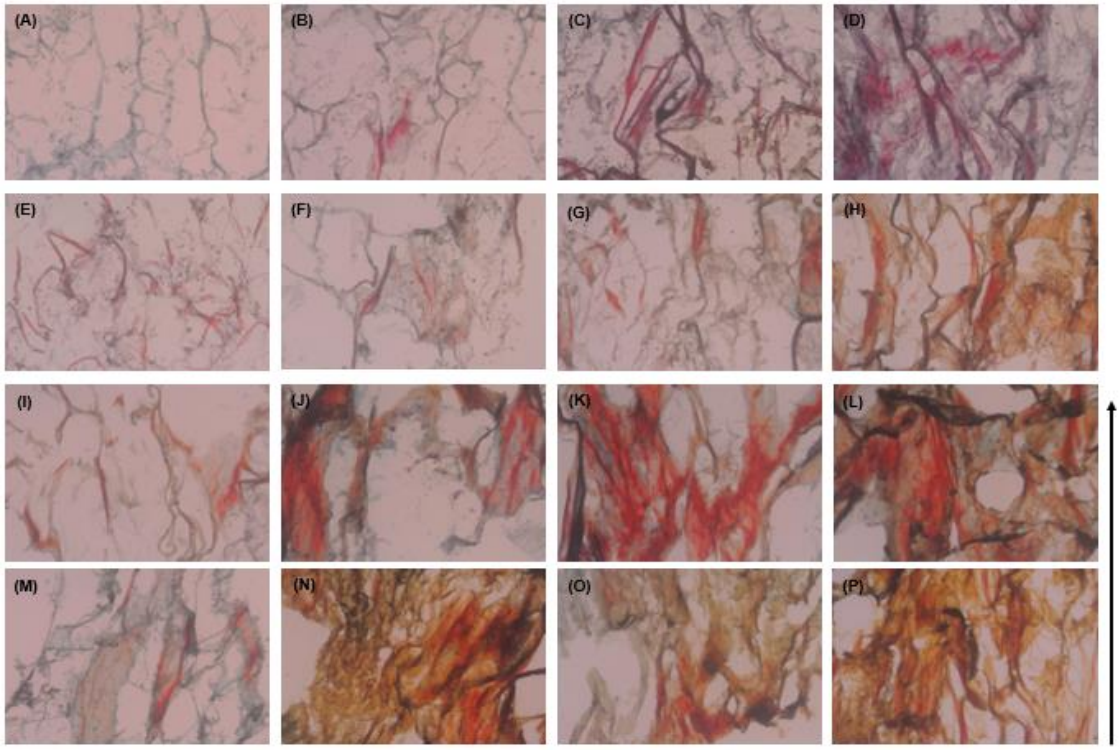

Figure 45: *ECM components of PSIS valves.* (**A-H**) Static and (**I-P**) dynamic PSIS valves were assessed for ECM components via Movat's staining. Both groups had presence of tissue formation. The PSIS valves are denser in tissue as the depth increases from (**A, E, I, M**) 16 µm, (**B, F, J, N**) 304 µm, (**C, G, K, O**) 592 µm to (**D, H, L, P**) 880 µm. The (**A-H**) static group is scattered in orientation, while the (**I-P**) dynamic group oriented towards the direction of flow. The arrow signifies the direction of flow. The following ECM components are present in the static group (**A-H**): mucins (blue), collagen (yellow) and fibrin (red); for the dynamic group (**I-P**) mucins (blue), collagen (yellow), fibrin (red) and scattered traces of elastin (black) are seen. Magnification 50x.

blue to green, and black, respectively. Tissue was found present in both groups, with a denser ECM as the depth increased (16 µm, 304 µm, 592 µm and 880 µm) towards the inner surface of the PSIS valves (**Figure 45**). The static group is mostly composed of mucins at the lower depths (outer surface of PSIS valves) (**Figure 45A, B, E, F**) with a combination of collagen, fibrin and elastin. As the depth increases, towards the inner surface of the PSIS valve, there was a predominant presence of collagen (**Figure 45C, D, G, H**). The dynamic group had less tissue substance at the outer surface of the PSIS valve (**Figure 45 I, M**) composed of mucins and collagen. As the depth increased towards the inner surface of the PSIS

valve (304 µm, 592 µm and 880 µm), the ECM became organized and aligned towards the direction of flow (**Figure 45J-L, N-P**). The presence of collagen and fibrin became more abundant and elastic fibers seem to be developing at these depths (**Figure 45J-L, N-P**).

To quantify the ECM content percentage of the PSIS valves, spatial intensity maps were computed. Spatial intensity maps were computed at different depths for the static group, with a depth of 16 µm (**Figure 46A**) and 304 µm shown (**Figure 46C**). It was demonstrated that the layer closer to the outer surface (depth of 16 µm) of the static PSIS valve was composed of 20% mucins with no presence (0%) of collagen or elastin (**Figure 46A, B**); the average ± SEM was found to be 20% ± 0.58 mucins at this depth for the static group. On the other hand, as the depth increased towards the inner surface of the PSIS valve, 9% mucins, 20% collagen, 1% elastin and 1% fibrin were present at a depth of 304 µm (**Figure 46C-G**); the average ± SEM values were found to be 11% ± 1.49, 17% ± 1.56, 3% ± 1.12 and 3% ± 0.85, respectively, for this depth. Similarly, the dynamic group was assessed for ECM content percentage, with the same depths of 16 µm (**Figure 47A**) and 304 µm (**Figure 47F**) shown. At a depth of 16 µm, there was a slight decrease in mucins compared to the static group with a 14% mucin content. Interestingly, the dynamic group had other ECM components present at this depth, including 16% collagen, 1% elastin and 4% fibrin (**Figure 47B-E**); specifically, an average ± SEM of 16% ± 1.44, 15% ± 0.67, 2% ± 0.73 and 4% ± 0.29 was present at 16 µm for mucins, collagen, elastin and fibrin, respectively. On the other hand,

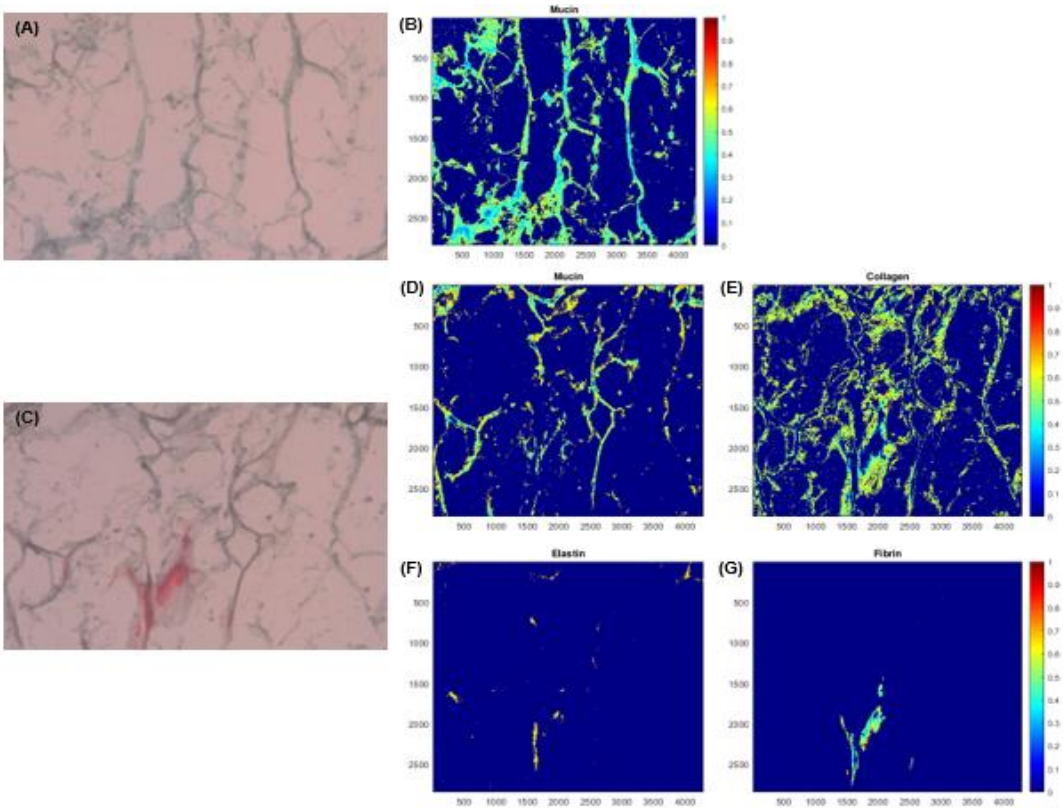

Figure 46: *ECM quantification of static PSIS valves.* (**A, C**) Static PSIS valves were assessed for ECM quantification via spatial intensity maps (**B, D-G**). Spatial intensity maps for these static PSIS valves at a depth of (**A**) 16 µm and (**C**) 304 µm were computed. At the outer surface of the PSS valve, there was (**B**) 21% mucins present with no other ECM components. At a larger depth, closer to the inner surface of the PSIS valve, there was a presence of (**D**) 9% mucins, (**E**) 20% collagen, (**F**) 0.6% elastin and (**G**) 1% fibrin. Magnification 50x.

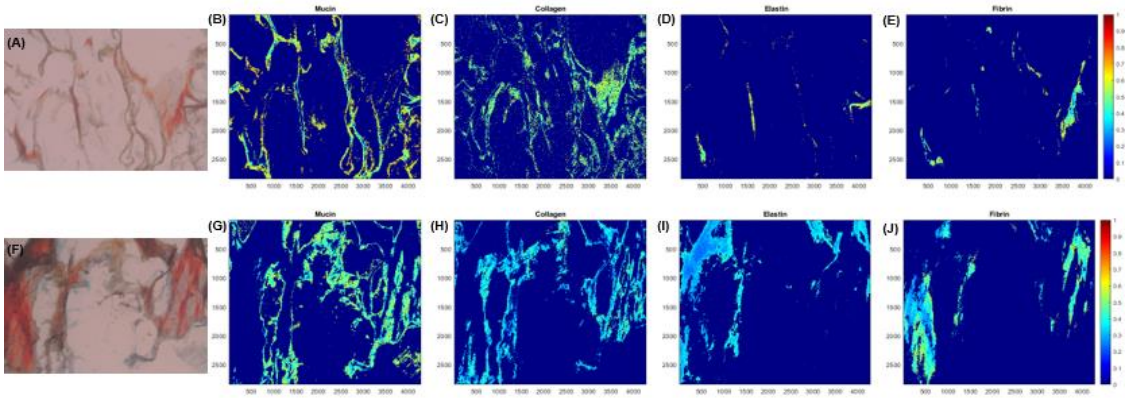

Figure 47: *ECM quantification of dynamic PSIS valves.* (**A, F**) Dynamic PSIS valves were assessed for ECM quantification via spatial intensity maps (**B-E, G-J**). Spatial intensity maps for these dynamic PSIS valves at a depth of (**A**) 16 µm and (**F**) 304 µm were computed. At the outer surface of the PSS valve, there was (**B**) 14% mucins, (**C**) 16% collagen, (**D**) 1% elastin and (**E**) 4% fibrin present. At a larger depth, closer to the inner surface of the PSIS valve, there was a presence of (**G**) 21% mucins, (**H**) 16% collagen, (**I**) 9% elastin and (**J**) 11% fibrin. Magnification 50x.

at a depth of 304 µm, the collagen content remained at 16%, while the mucins,

elastin and fibrin increased to 21%, 9% and 11%, respectively (**Figure 47G-J**); the average ECM content percentage ± SEM for this depth was found to be 21% ± 0.20 mucins, 12% ± 3.44 collagen, 6% ± 2.07 elastin and 9% ± 3.48 fibrin. Across the whole samples for both static and dynamic PSIS valves, the average ECM content percentages were computed. The static PSIS valves had an overall ECM content percentage of 18% ± 1.09 mucins, 19% ± 1.40 collagen, 4% ± 0.43 elastin and 7% ± 1.12 fibrin. The dynamic PSIS valves had an overall ECM content percentage of 21% ± 0.87, 19% ± 0.98, 8% ± 0.72 and 12% ± 0.85 of mucins, collagen, elastin and fibrin, respectively. It was found that the ECM percentage content was significantly different ($p<0.05$) for all ECM components assessed except collagen (no significant difference; $p=0.63$). The dynamic PSIS valves had a significantly higher ECM content percentage of mucins ($p=0.01$), elastin ($p=0.00$) and fibrin ($p=0.00$). Furthermore, the average percent of "unfilled" *de novo* ECM ± SEM was computed across the whole samples (**Table 6**). The static group had 53% ± 2.84 unfilled *de novo* tissue formation, while the dynamic group had 39% ± 1.83 (**Table 6**); a significant difference ($p<0.05$) was found between the groups, where the dynamic group had a significantly higher ($p=0.00$) amount of *de novo* tissue formation *in vitro*.

Table 6*: Average % of unfilled de novo ECM on in vitro PSIS tubular valves.* Various images throughout the depth of the samples were assessed to determine the average percentages ± SEM of unfilled de novo ECM on the PSIS tubular constructs. A significant difference ($p<0.05$) was found between the two groups. * signifies a significant difference.

PSIS Valve Group	% Unfilled Tissue Formation
"Static" Control	53% ± 2.84*
Dynamic	39% ± 1.83*

5.3 Discussion

Congenital heart valve defects in the young have no viable treatment options currently available mainly due to limitations in current artificial valve sizing options and their inability to support somatic growth. Regenerative medicine using TEVHs may provide long-lasting solutions since TEVHs can facilitate provisions for somatic growth, biological repair, and remodeling. Decellularized scaffolds have been of interest, since they are composed of biological materials, which can ultimately impact positively the cells to differentiate and provide a platform for the process of remodeling (VeDepo, Detamore et al. 2017). The problem with these decellularized scaffolds is that they are limited in recellularization once implanted (VeDepo, Detamore et al. 2017). Therefore, seeding of these biological constructs may promote enhanced recellularization. MSCs are one of the most promising and suitable cell types for regeneration since they can differentiate into endothelial and interstitial-line cell subtypes, which reside in heart valves. The microenvironment of these cells includes both biochemical factors and hemodynamic forces that influence differentiation. However, a standard reproducible protocol to develop a valvular construct to be used *in vivo* for longitudinal purpose is lacking (Dan, Velot et al. 2015).

Our torpedo bioreactor with a profile of a square waveform with 17% positive flow and 83% negative flow direction (**Figure 34**) provided a TAWSS of 3.1 dynes/cm^2 and an OSI of 0.20 proved feasible for regenerating a thin layer of tissue on our PSIS tubular valves that oriented towards the direction of flow

(**Figures 38, 45**); interestingly, our “static” and dynamic groups did not have significantly different ($p<0.05$) presence of CD31 or α-SMA, both markers of cells found in the native mitral valve, although there was a higher intensity for both in the dynamic groups. It was found that our dynamic PSIS tubular valves had a significantly higher ($p<0.05$) robust ECM composed of mucins, elastin and fibrin (**Figure 45**); no significant difference ($p>0.05$) was found between the groups for collagen production. Mucins, collagen and elastin play a critical role in the structure and function of the PSIS mitral valve; furthermore, elastin and fibrin are key in the process of regeneration. The role of mucins, specifically proteoglycans, is of great discussion and remains to be clarified (Wang, Lu et al. 2019). Proteoglycans play a significant role in ischemia and pressure overload-related cardiac remodeling, regulate ECM composition and organization and influence leukocyte adhesion and migration during the inflammatory process (Wang, Lu et al. 2019). Elastin is not produced easily *in vitro*, but we have demonstrated it is feasible in both our “static” control (~4%) and dynamic (~8%) groups. The proper amount of elastin to mimic the native heart valve is roughly 10% dry weight (Eslami, Javadi et al. 2015) and since elastic fibers are difficult structures to repair or regenerate (Kothapalli and Ramamurthi 2009) it would be of interest to have a tissue that has ~8% elastin (dynamic group). Elastin is believed to be crucial in accelerating valve regeneration rates after implantation, since elastin is a known driver of chemotaxis and beneficial tissue remodeling (Daamen, Veerkamp et al. 2007). Fibrin is important for blood clotting, cellular and matrix interactions, inflammation, wound healing and angiogenesis (Laurens, Koolwijk et al. 2006). Furthermore, fibrin increases MSC

viability and causes phenotypic changes in MSCs to endothelial cells (Zhang, Wang et al. 2006). This may be the reason why we found a significantly higher ($p<0.05$) amount of cells in our dynamic group compared to our static group (**Figures 39, 42**). Therefore, a higher concentration of these ECM proteins that covers more tissue (less % *de novo* tissue unfilled) would be beneficial in regeneration (i.e. the dynamic group); the dynamic group was found to be significantly higher ($p<0.05$) than the static group in filling the scaffold with *de novo* tissue. This demonstrated that physiologically-relevant magnitudes of both fluid-induced oscillations and shear stresses allowed for the development of enhanced heart valve matrix but did not have as much as an effect on differentiation and phenotypic changes.

Given findings, the PSIS tubular valves can be seeded with MSCs (similar to the host) and exposed to pulsatile flow-induced oscillatory shear stresses in our torpedo bioreactor to “coat” the valves with a thin layer of robust ECM (same tissue-type as the host) to use for implantation. These PSIS tubular valve would be acellular instead of a decellularized valve, meaning that there will be fewer porcine cells on the scaffold to begin with. Furthermore, the torpedo bioreactor PSIS tubular valves would assist with significantly higher ($p<0.05$) engineered tissue filling by 61% (**Table 6**) before implantation (compared to “static” controls), resulting in a reduced risk of chronic inflammation that can lead to valve failure.

6. DISSERTATION CONCLUSIONS

6.1 Conclusion

In conclusion, the current investigations revealed that the evolving material properties of the thinner 2ply PSIS bioscaffold under cyclic loading conditions robustly, but nonetheless temporarily support valve function (in the order of a few months), for the treatment of critical congenital valve diseases in the young, where somatic growth is crucially needed. Moreover, our PSIS hand-made valves were able to recruit endogenous cells and secrete sufficient ECM for 3-, 11- and 20-month post implantation. The valves functioned well overtime but led to failure due to a chronic inflammation, which may be correlated to the residual porcine cells in the implant. Based on our findings of robust *de novo* tissue formation on our PSIS tubular valves exposed to pulsatile flow-induced oscillatory shear stresses, allogeneic BMSCs can be seeded on our PSIS valves before implantation to secrete a thin layer of baboon (i.e. host) ECM (significantly higher filling of 61% of the valve , compared to “statically” cultured valves; $p<0.05$) so that once implanted, there are less areas of residual PSIS, thereby enabling more effective prevention of a prolonged chronic inflammatory response, thus increasing the probability of accelerated *in vivo* valve tissue regeneration and hence, the overall success of integration of this tissue engineered mitral heart valve in the host.

This work has provided a profound insight into how oscillatory shear stress-conditioned stem cells can enhance ECM properties on a bioscaffold material.

Moreover, it has provided us with a better understanding of the *in vivo* tissue regeneration, growth and biocompatibility as well as the *in vitro* tissue formation due to physiologically-relevant oscillatory flow (OSI=0.20) mechanically-conditioned stem cells. In addition, we demonstrated the importance of bioscaffold choice as well as stem cell inclusion and offer a real chance of translating this work to the clinic in the next decade. Our end goal is to utilize our proposed strategy as a permanent, effective treatment for critical congenital valve diseases in pediatrics, which currently has no viable treatment options.

6.2 *Limitations and Future Work*

With our proposed tubular BMSC seeded PSIS valve exposed to pulsatile flow-induced oscillatory shear stresses there is a chance that the cells remain on the PSIS bioscaffold before implantation. The concern of implanting engineered heart valve tissues with the stem cells intact is that this could lead to *de novo* tissue overgrowth and fusion with native cardiovascular structures, which could lead to catastrophic loss of valve function (Zilla, P., et al., 2020). Therefore, we are working on a decellularization protocol to be able to remove the BMSCs from the engineered valve tissues, while keeping the produced ECM structure unaltered so that no cells remain on the PSIS tubular valve. In the near future, we are also scheduled to perform upcoming surgeries on juvenile baboons (n = 2) that will be implanted with our ECM-enhanced (and potentially decellularized) valves with the underlying PSIS tubular bioscaffold. The, somatic growth support-potential and functionality of these implanted ECM-enhanced, tissue engineered mitral heart

valves will subsequently be assessed longitudinally and non-invasively via echocardiography.

REFERENCES

Akhyari, P., et al. (2010). "In vivo functional performance and structural maturation of decellularised allogenic aortic valves in the subcoronary position." European Journal of Cardio-Thoracic Surgery **38**(5): 539-546.

Alsoufi, B. (2014). "Aortic valve replacement in children: options and outcomes." Journal of the Saudi Heart Association **26**(1): 33-41.

Amrollahi, P. and L. Tayebi (2016). "Bioreactors for heart valve tissue engineering: a review." Journal of Chemical Technology & Biotechnology **91**(4): 847-856.

Arai, S. and E. C. Orton (2009). "Immunoblot detection of soluble protein antigens from sodium dodecyl sulfate-and sodium deoxycholate-treated candidate bioscaffold tissues." The Journal of heart valve disease **18**(4): 439-443.

Ashley, E. A. and J. Niebauer (2004). Cardiology explained, Remedica.

Askov, J. B., et al. (2013). "Significance of force transfer in mitral valve–left ventricular interaction: In vivo assessment." The Journal of thoracic and cardiovascular surgery **145**(6): 1635-1641. e1631.

Au, P., et al. (2008). "Bone marrow–derived mesenchymal stem cells facilitate engineering of long-lasting functional vasculature." Blood, The Journal of the American Society of Hematology **111**(9): 4551-4558.

Baasanjav, S., et al. (2011). "Faulty initiation of proteoglycan synthesis causes cardiac and joint defects." The American Journal of Human Genetics **89**(1): 15-27.

Badylak, S., et al. (2003). Extracellular matrix for myocardial repair. The heart surgery forum.

Bayrak, A., et al. (2010). "Human immune responses to porcine xenogeneic matrices and their extracellular matrix constituents in vitro." Biomaterials **31**(14): 3793-3803.

Bibevski, S., et al. (2017). "Mitral valve replacement using a handmade construct in an infant." Interactive cardiovascular and thoracic surgery **24**(4): 639-640.

Bibevski, S. and F. G. Scholl (2015). "Feasibility and early effectiveness of a custom, hand-made systemic atrioventricular valve using porcine extracellular matrix (CorMatrix) in a 4-month-old infant." The Annals of thoracic surgery **99**(2): 710-712.

Bilodeau, K., et al. (2005). "Design of a perfusion bioreactor specific to the regeneration of vascular tissues under mechanical stresses." Artificial organs **29**(11): 906-912.

Blum, K. M., et al. (2018). "Tissue-engineered heart valves: a call for mechanistic studies." Tissue Engineering Part B: Reviews **24**(3): 240-253.

Boni, L., et al. (2012). "Reconstruction of pulmonary artery with porcine small intestinal submucosa in a lamb surgical model: Viability and growth potential." The Journal of thoracic and cardiovascular surgery **144**(4): 963-969. e961.

Bourgine, P. E., et al. (2018). "In vitro biomimetic engineering of a human hematopoietic niche with functional properties." Proceedings of the National Academy of Sciences **115**(25): E5688-E5695.

Boyd, W., et al. (2010). Pericardial reconstruction using an extracellular matrix implant correlates with reduced risk of postoperative atrial fibrillation in coronary artery bypass surgery patients. Heart Surgery Forum.

Brazile, B., et al. (2015). "On the bending properties of porcine mitral, tricuspid, aortic, and pulmonary valve leaflets." Journal of long-term effects of medical implants **25**(1-2).

Castellanos, G., et al. (2018). "Stem Cell cytoskeletal responses to pulsatile flow in heart valve tissue engineering studies." Frontiers in cardiovascular medicine **5**: 58.

Cheung, D. Y., et al. (2015). "Current progress in tissue engineering of heart valves: multiscale problems, multiscale solutions." Expert opinion on biological therapy **15**(8): 1155-1172.

Clarke, D. (1999). The SynerGraft Valve: A New Acellular (Nonglutaraldehyde-Fixed) Tissue Heart Valve for Autologous Recellularization First. Seminars in thoracic and cardiovascular surgery.

Cua, C. L., et al. (2014). "Echocardiographic analysis of an extracellular matrix tricuspid valve." Echocardiography **31**(8): E264-E266.

Daamen, W. F., et al. (2007). "Elastin as a biomaterial for tissue engineering." Biomaterials **28**(30): 4378-4398.

Dal-Bianco, J. P. and R. A. Levine (2013). "Anatomy of the mitral valve apparatus: role of 2D and 3D echocardiography." Cardiology clinics **31**(2): 151-164.

Dan, P., et al. (2015). "The role of mechanical stimuli in the vascular differentiation of mesenchymal stem cells." Journal of Cell Science **128**(14): 2415-2422.

Dohmen, P., et al. (2005). Results of a decellularized porcine heart valve implanted into the juvenile sheep model. The heart surgery forum.

Dohmen, P. M., et al. (2011). "Ten years of clinical results with a tissue-engineered pulmonary valve." The Annals of thoracic surgery **92**(4): 1308-1314.

DuBose, J. J. and A. Azizzadeh (2015). "Utilization of a tubularized CorMatrix extracellular matrix for repair of an arteriovenous fistula aneurysm." Annals of vascular surgery **29**(2): 366. e361-366. e364.

Dudzinski, D. M. and J. Hung (2014). "Echocardiographic assessment of ischemic mitral regurgitation." Cardiovascular ultrasound **12**(1): 46.

Eckhauser, A. W., et al. (2013). "Repair of traumatic aortoinnominate disruption using CorMatrix." The Annals of thoracic surgery **95**(4): e99-e101.

Ellis, S., et al. (2018). "Immunology of wound healing." Current dermatology reports **7**(4): 350-358.

Emmert, M. Y. and S. P. Hoerstrup (2016). Tissue engineered heart valves: moving towards clinical translation, Taylor & Francis.

Engelmayr Jr, G. C., et al. (2006). "Cyclic flexure and laminar flow synergistically accelerate mesenchymal stem cell-mediated engineered tissue formation: implications for engineered heart valve tissues." Biomaterials **27**(36): 6083-6095.

Eslami, M., et al. (2015). "Expression of COLLAGEN 1 and ELASTIN genes in mitral valvular interstitial cells within microfiber reinforced hydrogel." Cell Journal (Yakhteh) **17**(3): 478.

Etnel, J. R., et al. (2019). "Bioprosthetic aortic valve replacement in nonelderly adults: a systematic review, meta-analysis, and microsimulation." Circulation: Cardiovascular Quality and Outcomes **12**(2): e005481.

Fallon, A., et al. (2012). "Remodeling of extracellular matrix patch used for carotid artery repair." Journal of Surgical Research **175**(1): e25-e34.

Fallon, A. M., et al. (2014). "In vivo remodeling potential of a novel bioprosthetic tricuspid valve in an ovine model." The Journal of thoracic and cardiovascular surgery **148**(1): 333-340. e331.

Flameng, W., et al. (2014). "Coating with fibronectin and stromal cell–derived factor-1α of decellularized homografts used for right ventricular outflow tract reconstruction eliminates immune response–related degeneration." The Journal of thoracic and cardiovascular surgery **147**(4): 1398-1404. e1392.

Fu, Y., et al. (2017). "Trophic effects of mesenchymal stem cells in tissue regeneration." Tissue Engineering Part B: Reviews **23**(6): 515-528.

Gallina, C., et al. (2015). "A new paradigm in cardiac regeneration: the mesenchymal stem cell secretome." Stem cells international **2015**.

Gerdisch, M. W., et al. (2014). "Early experience treating tricuspid valve endocarditis with a novel extracellular matrix cylinder reconstruction." The Journal of thoracic and cardiovascular surgery **148**(6): 3042-3048.

Gerdisch, M. W., et al. (2014). "Clinical experience with CorMatrix extracellular matrix in the surgical treatment of mitral valve disease." The Journal of thoracic and cardiovascular surgery **148**(4): 1370-1378.

Gilbert, C. L., et al. (2011). "Novel use of extracellular matrix graft for creation of pulmonary valved conduit." World Journal for Pediatric and Congenital Heart Surgery **2**(3): 495-501.

Gonzalez, B., et al. (2018). "Recapitulation of human bio-scaffold mitral valve growth in the baboon model." Circulation **138**(Suppl_1): A11348-A11348.

Gonzalez, B. A., et al. (2020). "Physiologically Relevant Fluid-Induced Oscillatory Shear Stress Stimulation of Mesenchymal Stem Cells Enhances the Engineered Valve Matrix Phenotype." Frontiers in cardiovascular medicine **7**.

Gonzalez, B. A., et al. (2020). "Porcine small intestinal submucosa mitral valve material responses support acute somatic growth." Tissue Engineering Part A **26**(9-10): 475-489.

He, X. and D. N. Ku (1996). "Pulsatile flow in the human left coronary artery bifurcation: average conditions."

Henaine, R., et al. (2012). "Valve replacement in children: a challenge for a whole life." Archives of cardiovascular diseases **105**(10): 517-528.

Hinton, R. B. and K. E. Yutzey (2011). "Heart Valve Structure and Function in Development and Disease." Annual Review of Physiology **73**(1): 29-46.

Hoerstrup, S., et al. (2000). "Optimized growth conditions for tissue engineering of human cardiovascular structures." The International journal of artificial organs **23**(12): 817-823.

Hoerstrup, S. P., et al. (2000). "Functional living trileaflet heart valves grown in vitro." Circulation **102**(suppl_3): Iii-44-Iii-49.

Holliday, C. J., et al. (2011). "Discovery of shear-and side-specific mRNAs and miRNAs in human aortic valvular endothelial cells." American Journal of Physiology-Heart and Circulatory Physiology **301**(3): H856-H867.

Honge, J. L., et al. (2011). "Recellularization of aortic valves in pigs." European Journal of Cardio-Thoracic Surgery **39**(6): 829-834.

Hoshiba, T., et al. (2016). "Decellularized extracellular matrix as an in vitro model to study the comprehensive roles of the ECM in stem cell differentiation." Stem cells international **2016**.

Hynes, R. O. and A. Naba (2012). "Overview of the matrisome—an inventory of extracellular matrix constituents and functions." Cold Spring Harbor perspectives in biology **4**(1): a004903.

Kim, S. S., et al. (2006). "Tissue engineering of heart valves in vivo using bone marrow-derived cells." Artificial organs **30**(7): 554-557.

Kothapalli, C. R. and A. Ramamurthi (2009). "Biomimetic regeneration of elastin matrices using hyaluronan and copper ion cues." Tissue Engineering Part A **15**(1): 103-113.

Kusindarta, D. L. and H. Wihadmadyatami (2018). "The role of extracellular matrix in tissue regeneration." Tissue Regeneration: 65.

Laurens, N., et al. (2006). "Fibrin structure and wound healing." Journal of Thrombosis and Haemostasis **4**(5): 932-939.

Lauten, A., et al. (2015). "Transcatheter treatment of tricuspid regurgitation by caval valve implantation—experimental evaluation of decellularized tissue valves in central venous position." Catheterization and Cardiovascular Interventions **85**(1): 150-160.

Liu, A. C., et al. (2007). "The emerging role of valve interstitial cell phenotypes in regulating heart valve pathobiology." The American journal of pathology **171**(5): 1407-1418.

Matheny, R., et al. (2000). "Porcine small intestine submucosa as a pulmonary valve leaflet substitute." The Journal of heart valve disease **9**(6): 769-774; discussion 774-765.

McCarthy, K. P., et al. (2010). "Anatomy of the mitral valve: understanding the mitral valve complex in mitral regurgitation." European Journal of Echocardiography **11**(10): i3-i9.

Mosala Nezhad, Z., et al. (2016). "Small intestinal submucosa extracellular matrix (CorMatrix®) in cardiovascular surgery: a systematic review." Interactive cardiovascular and thoracic surgery **22**(6): 839-850.

Nejad, S. P., et al. (2016). "Biomechanical conditioning of tissue engineered heart valves: Too much of a good thing?" Advanced drug delivery reviews **96**: 161-175.

O'Brien, M. F., et al. (1999). The SynerGraft valve: a new acellular (nonglutaraldehyde-fixed) tissue heart valve for autologous recellularization first experimental studies before clinical implantation. Seminars in thoracic and cardiovascular surgery, WB SAUNDERS CO.

Olsson-Collentine, A., et al. (2019). "The prevalence of marginally significant results in psychology over time." Psychological Science **30**(4): 576-586.

Orimadegun, A. and A. Omisanjo (2014). "Evaluation of five formulae for estimating body surface area of Nigerian children." Annals of medical and health sciences research **4**(6): 889-898.

Ota, T., et al. (2007). "Novel method of decellularization of porcine valves using polyethylene glycol and gamma irradiation." The Annals of thoracic surgery **83**(4): 1501-1507.

Padalino, M. A., et al. (2012). "Extracellular matrix graft for vascular reconstructive surgery: evidence of autologous regeneration of the neoaorta in a murine model." European Journal of Cardio-Thoracic Surgery **42**(5): e128-e135.

Padalino, M. A., et al. (2015). "Early and mid-term clinical experience with extracellular matrix scaffold for congenital cardiac and vascular reconstructive surgery: a multicentric Italian study." Interactive cardiovascular and thoracic surgery **21**(1): 40-49.

Pavcnik, D., et al. (2009). "Angiographic evaluation of carotid artery grafting with prefabricated small-diameter, small-intestinal submucosa grafts in sheep." Cardiovascular and interventional radiology **32**(1): 106-113.

Pavcnik, D., et al. (2002). "Percutaneous bioprosthetic venous valve: a long-term study in sheep." Journal of vascular surgery **35**(3): 598-602.

Perez-Estenaga, I., et al. (2018). "Allogeneic mesenchymal stem cells and biomaterials: the perfect match for cardiac repair?" International journal of molecular sciences **19**(10): 3236.

Poulin, F., et al. (2013). "3-Dimensional Transesophageal Echocardiography–Guided Closure of a Gerbode Shunt Due to CorMatrix Patch Dehiscence." Journal of the American College of Cardiology **62**(3): e5.

Pour Issa, E. (2018). Evaluating the Acute In Vitro Hydrodynamic Functionality of the Porcine Small Intestinal Submucosa (PSIS) Mitral Valve Bioscaffolds in Adult and the Pediatric Cardiovascular Conditions. Department of Biomedical Engineering, Florida International University.

Pritschet, L., et al. (2016). "Marginally significant effects as evidence for hypotheses: Changing attitudes over four decades." Psychological Science **27**(7): 1036-1042.

Quarti, A., et al. (2011). "Preliminary experience in the use of an extracellular matrix to repair congenital heart diseases." Interactive cardiovascular and thoracic surgery **13**(6): 569-572.

Ramaswamy, S., et al. (2014). "A novel bioreactor for mechanobiological studies of engineered heart valve tissue formation under pulmonary arterial physiological flow conditions." Journal of biomechanical engineering **136**(12).

Rath, S., et al. (2015). "Differentiation and distribution of marrow stem cells in flex-flow environments demonstrate support of the valvular phenotype." PloS one **10**(11).

Redlarski, G., et al. (2016). "Body surface area formulae: an alarming ambiguity." Scientific reports **6**: 27966.

Rippel, R. A., et al. (2012). "Tissue-engineered heart valve: future of cardiac surgery." World journal of surgery **36**(7): 1581-1591.

Robotin-Johnson, M. C., et al. (1998). "An experimental model of small intestinal submucosa as a growing vascular graft." The Journal of thoracic and cardiovascular surgery **116**(5): 805-811.

Rosen, M., et al. (2005). "Small intestinal submucosa intracardiac patch: an experimental study." Surgical innovation **12**(3): 227-231.

Ruiz, C. E., et al. (2005). "Transcatheter placement of a low-profile biodegradable pulmonary valve made of small intestinal submucosa: a long-term study in a swine model." The Journal of thoracic and cardiovascular surgery **130**(2): 477. e471-477. e479.

Salinas, M. and S. Ramaswamy (2014). "Computational simulations predict a key role for oscillatory fluid shear stress in de novo valvular tissue formation." Journal of biomechanics **47**(14): 3517-3523.

Salinas, M., et al. (2016). "Relative effects of fluid oscillations and nutrient transport in the in vitro growth of valvular tissues." Cardiovascular engineering and technology **7**(2): 170-181.

Sandusky Jr, G., et al. (1992). "Histologic findings after in vivo placement of small intestine submucosal vascular grafts and saphenous vein grafts in the carotid artery in dogs." The American journal of pathology **140**(2): 317.

Scholl, F. G., et al. (2010). "Preliminary experience with cardiac reconstruction using decellularized porcine extracellular matrix scaffold: human applications in congenital heart disease." World Journal for Pediatric and Congenital Heart Surgery **1**(1): 132-136.

Slachman, F. N. (2014). "Constructive remodeling of CorMatrix extracellular matrix after aortic root repair in a 90-year-old woman." The Annals of thoracic surgery **97**(5): e129-e131.

Slaughter, M. S., et al. (2014). "Development of an extracellular matrix delivery system for effective intramyocardial injection in ischemic tissue." ASAIO journal **60**(6): 730-736.

Smith, J., et al. (2001). "Cyclic stretch induces the expression of vascular endothelial growth factor in vascular smooth muscle cells." Endothelium **8**(1): 41-48.

Sordelli, C., et al. (2014). "Echocardiographic assessment of heart valve prostheses." Journal of cardiovascular echography **24**(4): 103.

Soucy, K. G., et al. (2015). "Feasibility study of particulate extracellular matrix (P-ECM) and left ventricular assist device (HVAD) therapy in chronic ischemic heart failure bovine model." ASAIO journal **61**(2): 161-169.

Stelly, M. and T. C. Stelly (2013). "Histology of CorMatrix bioscaffold 5 years after pericardial closure." The Annals of thoracic surgery **96**(5): e127-e129.

Stock, U., et al. (2002). "Tissue engineering of heart valves-current aspects." The Thoracic and cardiovascular surgeon **50**(03): 184-193.

Sündermann, S. H., et al. (2014). "Use of extracellular matrix materials in patients with endocarditis." The Thoracic and cardiovascular surgeon **62**(01): 076-079.

Takagi, K., et al. (2006). "In vivo recellularization of plain decellularized xenografts with specific cell characterization in the systemic circulation: histological and immunohistochemical study." Artificial organs **30**(4): 233-241.

Toeg, H. D., et al. (2014). "Finding the ideal biomaterial for aortic valve repair with ex vivo porcine left heart simulator and finite element modeling." The Journal of thoracic and cardiovascular surgery **148**(4): 1739-1745. e1731.

VeDepo, M. C., et al. (2017). "Recellularization of decellularized heart valves: Progress toward the tissue-engineered heart valve." Journal of tissue engineering **8**: 2041731417726327.

Vermot, J., et al. (2009). "Reversing blood flows act through klf2a to ensure normal valvulogenesis in the developing heart." PLoS biology **7**(11).

Wallen, J. and V. Rao (2014). "Extensive tricuspid valve repair after endocarditis using CorMatrix extracellular matrix." The Annals of thoracic surgery **97**(3): 1048-1050.

Wang, H., et al. (2005). "Shear stress induces endothelial differentiation from a murine embryonic mesenchymal progenitor cell line." Arteriosclerosis, thrombosis, and vascular biology **25**(9): 1817-1823.

Wang, X., et al. (2019). "Emerging roles of proteoglycans in cardiac remodeling." International journal of cardiology **278**: 192-198.

Wang, Y., et al. (2019). Development of Small Intestinal Submucosa as Biomaterial in Tissue Engineering. IOP Conference Series: Materials Science and Engineering, IOP Publishing.

Weber, B., et al. (2012). "Stem cells for heart valve regeneration." Swiss medical weekly **142**: w13622.

White, J. K., et al. (2005). "A stentless trileaflet valve from a sheet of decellularized porcine small intestinal submucosa." The Annals of thoracic surgery **80**(2): 704-707.

Williams, A., et al. (2017). "A “sweet-spot” for fluid-induced oscillations in the conditioning of stem cell-based engineered heart valve tissues." Journal of biomechanics **65**: 40-48.

Williams, D. F. (2014). "The biomaterials conundrum in tissue engineering." Tissue Engineering Part A **20**(7-8): 1129-1131.

Witt, R. G., et al. (2013). "Short-term experience of porcine small intestinal submucosa patches in paediatric cardiovascular surgery." European Journal of Cardio-Thoracic Surgery **44**(1): 72-76.

Woo, J. S., et al. (2016). "Histologic examination of decellularized porcine intestinal submucosa extracellular matrix (CorMatrix) in pediatric congenital heart surgery." Cardiovascular Pathology **25**(1): 12-17.

Xing, Y., et al. (2004). "Effects of constant static pressure on the biological properties of porcine aortic valve leaflets." Annals of biomedical engineering **32**(4): 555-562.

Xu, Y., et al. (2001). "High toughness, 3D textile, SiC/SiC composites by chemical vapor infiltration." Materials Science and Engineering: A **318**(1-2): 183-188.

Yanagawa, B., et al. (2013). "Initial experience with intraventricular repair using CorMatrix extracellular matrix." Innovations **8**(5): 348-352.

Yanagawa, B., et al. (2014). "Potential myocardial regeneration with CorMatrix ECM: a case report." The Journal of thoracic and cardiovascular surgery **147**(4): e41-e43.

Yavuz, K., et al. (2006). "Comparison of the endothelialization of small intestinal submucosa, dacron, and expanded polytetrafluoroethylene suspended in the thoracoabdominal aorta in sheep." Journal of vascular and interventional radiology **17**(5): 873-882.

Yin, X., et al. (2017). "Fibre-reinforced multifunctional SiC matrix composite materials." International Materials Reviews **62**(3): 117-172.

Zafar, F., et al. (2015). "Physiological growth, remodeling potential, and preserved function of a novel bioprosthetic tricuspid valve: tubular bioprosthesis made of small intestinal submucosa-derived extracellular matrix." Journal of the American College of Cardiology **66**(8): 877-888.

Zaidi, A. H., et al. (2014). "Preliminary experience with porcine intestinal submucosa (CorMatrix) for valve reconstruction in congenital heart disease:

histologic evaluation of explanted valves." The Journal of thoracic and cardiovascular surgery **148**(5): 2216-2225. e2211.

Zhang, G., et al. (2006). "A PEGylated fibrin patch for mesenchymal stem cell delivery." Tissue engineering **12**(1): 9-19.

Zhou, J., et al. (2010). "Impact of heart valve decellularization on 3-D ultrastructure, immunogenicity and thrombogenicity." Biomaterials **31**(9): 2549-2554.

Zilla, P., et al. (2020). Progressive Reinvention or Destination Lost? Half a Century of Cardiovascular Tissue Engineering. *Frontiers in Cardiovascular Medicine*, *7*.

APPENDIX A: TENSILE TESTING

MATLAB script used for section 3.3.2.1 Tensile Testing (page 31) and to produce Figure 7 (page 32). Script below was for fatigue samples but same applies for non-fatigue samples.

```
%-------------------------------------------------------------------------
% First 4 samples are 4ply F, last 4 are 2ply F
% Sample 1
figure(1);
% Type in filename of excel sheet want to read
filename = 'FTensile020218_S1_2.xlsx';
[num, ~, raw] = xlsread(filename);
% get values in excel for force; force is in Newtons
force = num(1:end,5);
% area is in mm squared
a = 0.11; %the thickness of the samples
area = (a * 10); % 100 um to mm, 1 cm to mm (cross sectional area)
% get values in excel for the change of length; length in mm
changeLength = num(1:end,4);
b = 5; % changes based on tensile (T) or fatigue(F) testing (T=5, F=18)
OrigLength = b; % in mm (distance between grips in Bose System set up)
% calculate change in length for strain purposes
change = (OrigLength - abs(changeLength));
% calculate stress and strain; stress in MPa
stress = (force./area);
strain = (change./OrigLength);

% find the point of max failure and get matching strain value
[FailStress, index] = max(stress);
FailStrain = strain(index);

%Continue on the same script for all your samples and then when you
want to plot you at this…

% creates on graph with multiple samples on it
subplot(1,2,1);
plot(strain,stress,'b'); % plot first sample in blue
hold on % holds on next sample plotted together with previous sample
plot(strain2,stress2,'r'); % plot first sample in red
hold on % holds on next sample plotted together with previous sample
plot(strain3,stress3,'g'); % plot first sample in green
hold on % holds on next sample plotted together with previous sample
plot(strain4,stress4,'m'); % plot first sample in magenta
hold on % holds on next sample plotted together with previous sample

xlabel('Strain '); % labels x-axis
ylabel('Stress (MPa)'); % labels y-axis
title('4ply Fatigue Stress vs Strain'); % creates title of graph
% set limits of your x and y axis
xlim([0 1]);
ylim([0 45]);
%-------------------------------------------------------------------------
```

APPENDIX B: DECELLULARIZED PSIS SCAFFOLD BEFORE IMPLANTATION

Raw decellularized scaffold with remaining porcine cells before implantation from Section 4.2.2 (page 47)

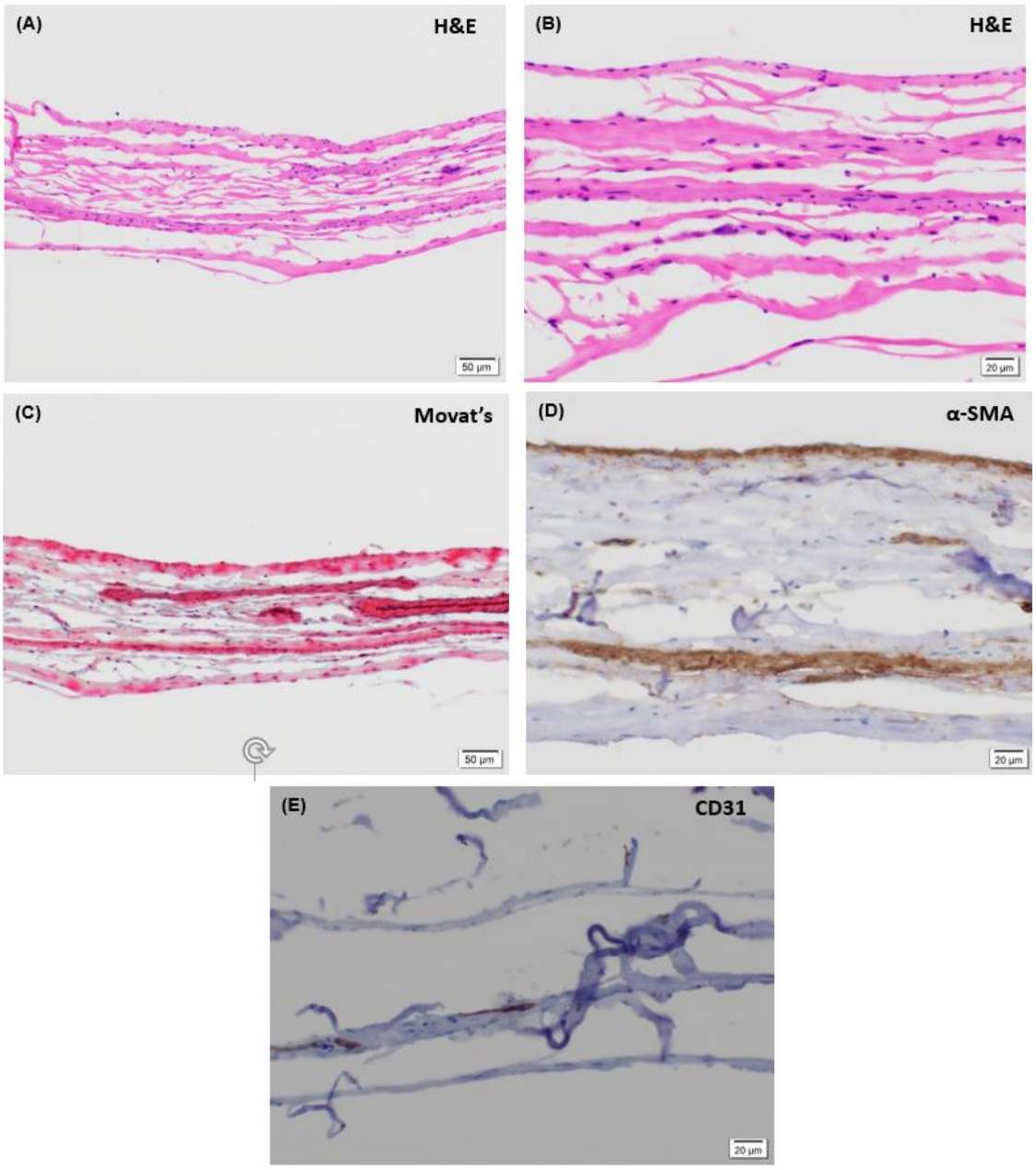

Raw decellularized PSIS Matrix (Cormatrix, Roswell, GA) with presence of cells showing dark blue nuclei against a collagen background (pink) (**A**-20x, **B**-40x; H&E). The bioscaffold is predominantly composed of collagen with rare small vessels and scattered spindle cells **(C**-20x; Movat's**).** There is a presence of α-SMA (smooth muscle cells) and fibroblast type cells in brown (**D**-40x) in collagen matrix with rare CD31 positive cells (endothelial cells stain brown) predominantly in small vessels and along the surface (**E**-40x).

APPENDIX C: SPATIAL INTENSITY MAPS OF EXPLANT BABOON MITRAL VALVES AT LEAFLET SITE

ECM quantification for all of the baboon explants (native, 3-, 11-, 20-months PSIS) at the leaflet location from Section 4.2.3

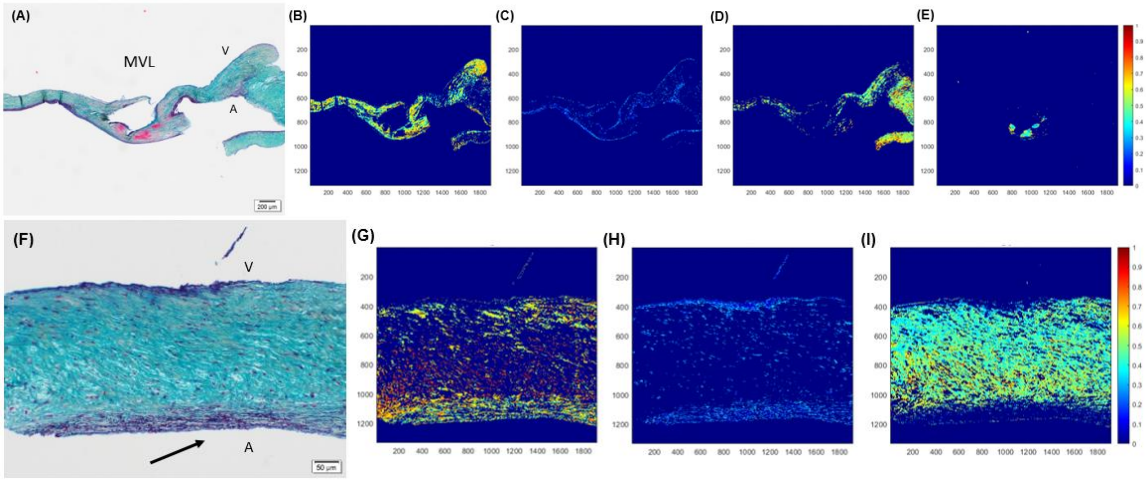

C.1: *ECM components of native juvenile baboon mitral valve explant at 14-months.* Native mitral valve leaflet (**MVL**) (**A**-4x; Movat's) demonstrating matrix proteins of collagen (**B**), elastin (**C**) proteoglycans (**D**) and fibrin (**E**) (yellow/green, black, blue and dark pink, respectively), with 36%, 15%, 45% and 3%, respectively of each ECM protein. Zoomed in area of the leaflet (**F**-20x; Movat's) with (**G**) 23%, (**H**) 11% and (**I**) 65%, respectively of each ECM protein (absence of fibrin). Note elastic deposition along the atrialis layer (arrow). A depicts the atrialis and V depicts the ventricularis layers of the mitral valve.

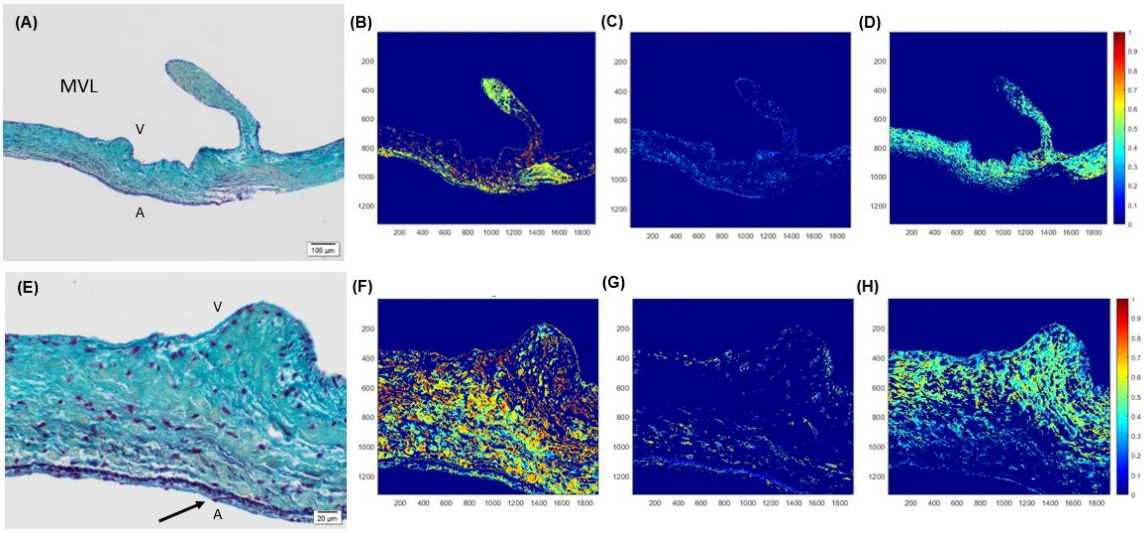

C.1.2: *ECM components of native juvenile baboon mitral valve explant at 14-months.* Native mitral valve leaflet (**MVL**) (**A**-10x; Movat's) demonstrating matrix proteins of collagen (**B**), elastin (**C**) proteoglycans (**D**) and fibrin (**E**) (yellow/green, black, blue and dark pink, respectively), with 54%, 15%, and 31%, respectively of each ECM protein. Zoomed in area of the leaflet (**E**-40x; Movat's) with (**F**) 50%, (**G**) 7% and (**H**) 42%, respectively of each ECM protein. Note elastic deposition along the atrialis layer (arrow). A depicts the atrialis and V depicts the ventricularis layers of the mitral valve.

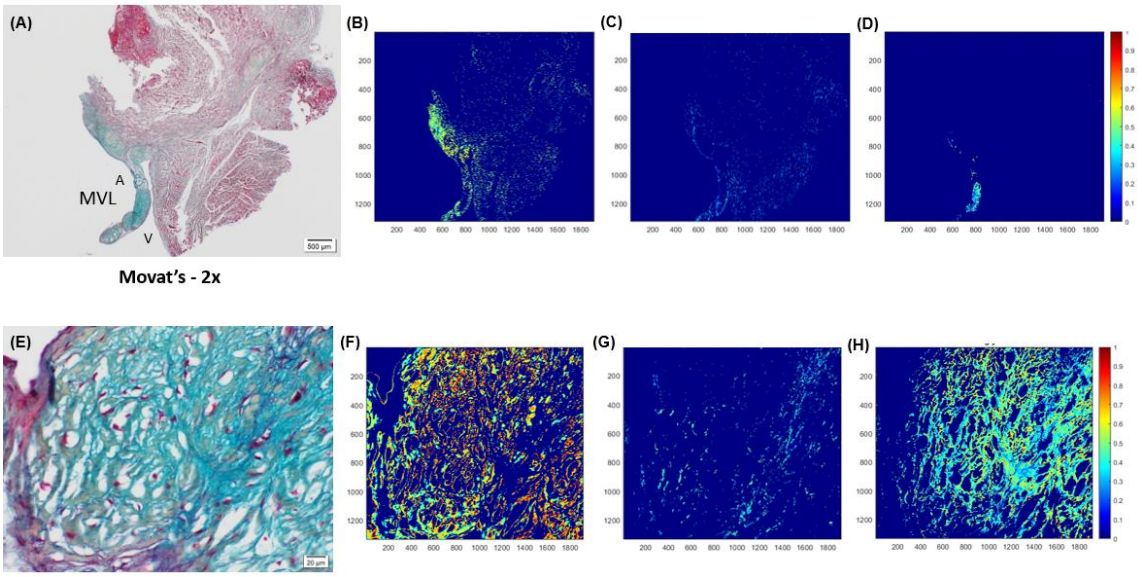

C.2: *ECM components of PSIS mitral valve explanted at 3-month post implantation.* PSIS mitral valve leaflet (**MVL**) (**A**-2x; Movat's) demonstrating matrix proteins of collagen (**B**), scattered elastin (**C**) and proteoglycans (**D**) (yellow/green, black, blue respectively), with 57%, 9% and 3%, respectively of each ECM protein. Zoomed in area of the leaflet (**E**-40x; Movat's) with (**F**) 34%, (**G**) 4% and (**H**) 44%, respectively of ECM proteins.

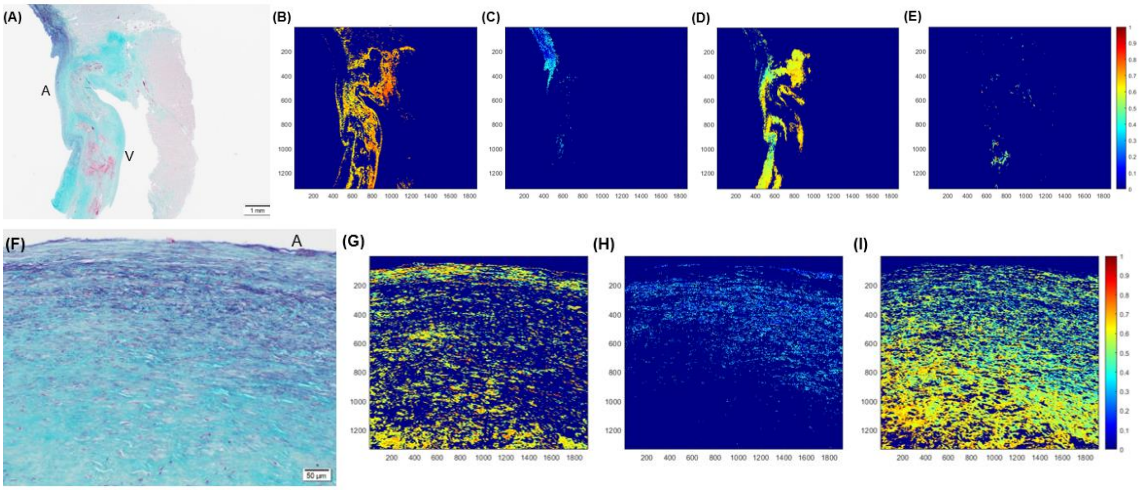

C.3: *ECM components of PSIS mitral valve explanted at 11-month post implantation.* PSIS mitral valve leaflet (**MVL**) (**A**-1.25x; Movat's) demonstrating matrix proteins of collagen (**B**), elastin (**C**), proteoglycans (**D**) and fibrin (**E**) (yellow/green, black, blue, dark pink respectively), with 47%, 13%, 38% and 2%, respectively of each ECM protein. Zoomed in area of the leaflet (**F**-20x; Movat's) with (**G**) 34%, (**H**) 4% and (**I**) 44%, respectively of ECM proteins. A depicts the atrialis and V depicts the ventricularis layers of the mitral valve.

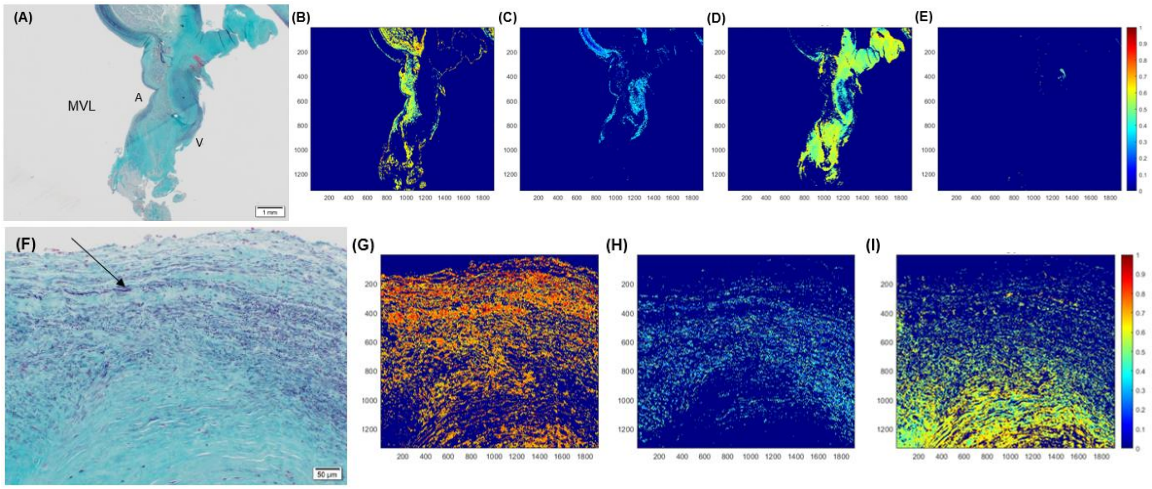

C.3.2: *ECM components of PSIS mitral valve explanted at 11-month post implantation.* PSIS mitral valve leaflet (**MVL**) (**A**-1.25x; Movat's) demonstrating matrix proteins of collagen (**B**), elastin (**C**), proteoglycans (**D**) and fibrin (**E**) (yellow/green, black, blue, dark pink respectively), with 28%, 15%, 56% and 1%, respectively of each ECM protein. Zoomed in area of the leaflet (**F**-20x; Movat's) with (**G**) 67%, (**H**) 6% and (**I**) 27%, respectively of ECM proteins. A depicts the atrialis and V depicts the ventricularis layers of the mitral valve.

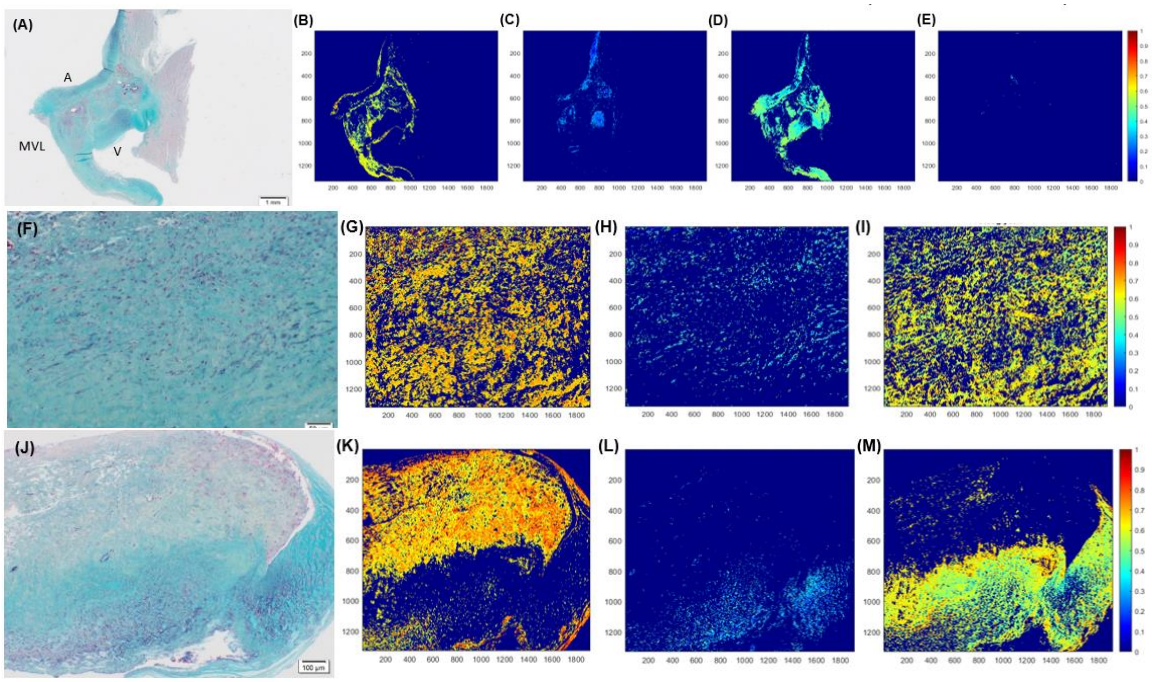

C.3.3: *ECM components of PSIS mitral valve explanted at 11-month post implantation.* PSIS mitral valve leaflet (**MVL**) (**A**-1.25x; Movat's) demonstrating matrix proteins of collagen (**B**), elastin (**C**), proteoglycans (**D**) and fibrin (**E**) (yellow/green, black, blue, dark pink respectively), with 33%, 15%, 52% and 0.4%, respectively of each ECM protein. Zoomed in area of the leaflet (**F**-20x; Movat's) with (**G**) 47%, (**H**) 7% and (**I**) 47%, respectively of ECM proteins. Another zoomed in area of the leaflet tip (J-10x; Movat's) with (K) 51% (L) 7% and (M) 41%, respectively. A depicts the atrialis and V depicts the ventricularis layers of the mitral valve.

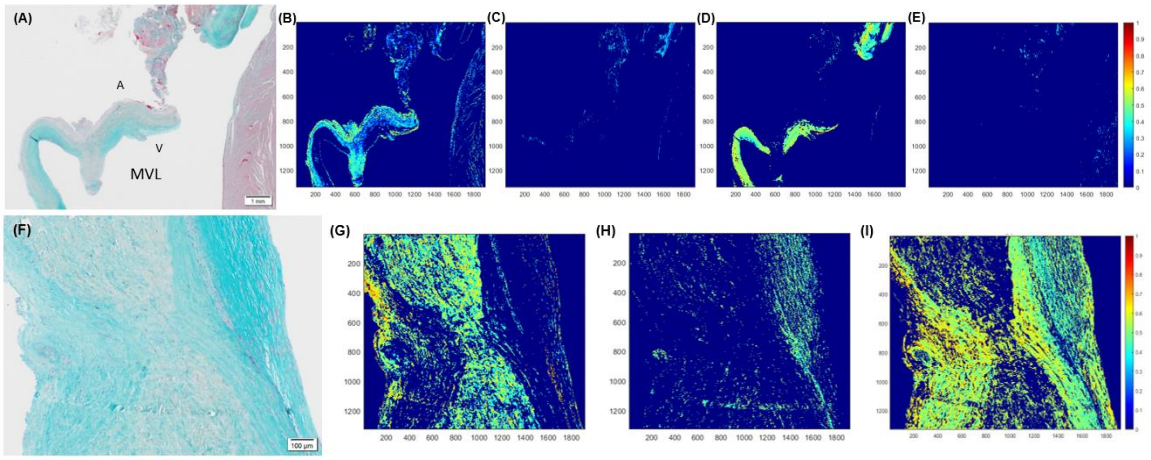

C.4: *ECM components of PSIS mitral valve explanted at 20-month post implantation.* PSIS mitral valve leaflet (**MVL**) (**A**-1.25x; Movat's) demonstrating matrix proteins of collagen (**B**), elastin (**C**), proteoglycans (**D**) and fibrin (**E**) (yellow/green, black, blue, dark pink respectively), with 61%, 6%, 30% and 3%, respectively of each ECM protein. (**F**-10x; Movat's) with (**G**) 36%, (**H**) 9% and (**I**) 54%, respectively of ECM proteins. A depicts the atrialis and V depicts the ventricularis layers of the mitral valve.

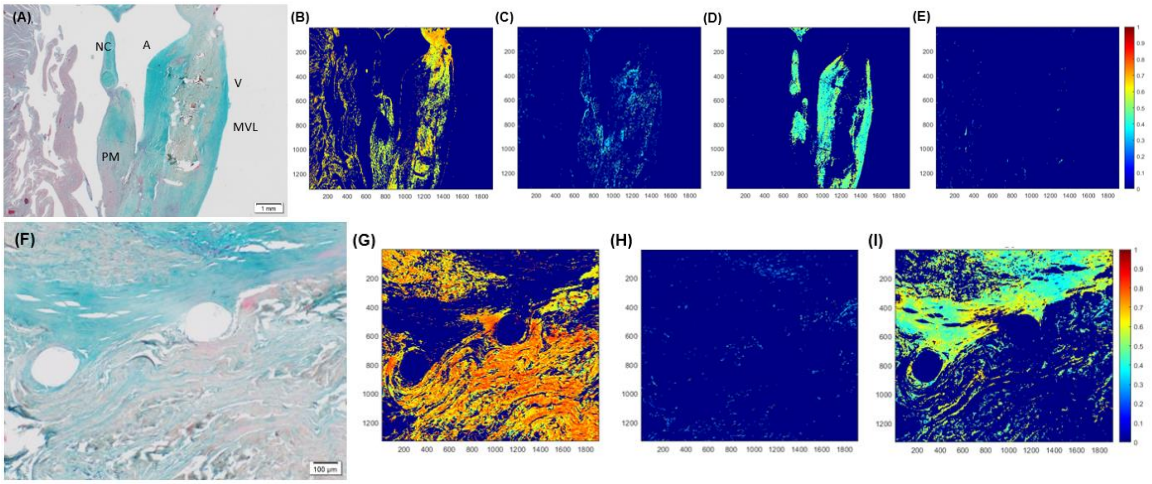

C.4.2: *ECM components of PSIS mitral valve explanted at 20-month post implantation.* PSIS mitral valve leaflet (**MVL**) (**A**-1.25x; Movat's) demonstrating matrix proteins of collagen (**B**), elastin (**C**), proteoglycans (**D**) and fibrin (**E**) (yellow/green, black, blue, dark pink respectively), with 49%, 11%, 38% and 1%, respectively of each ECM protein. (**F**-10x; Movat's) with (**G**) 41%, (**H**) 10% and (**I**) 45%, respectively of ECM proteins. A depicts the atrialis and V depicts the ventricularis layers of the mitral valve. NC is neochordae and PM is papillary muscle

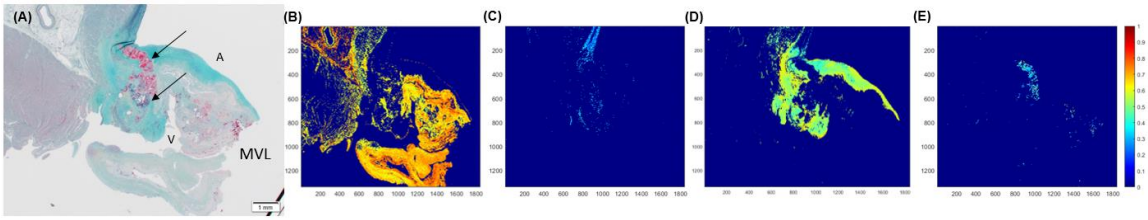

C.4.3: *ECM components of PSIS mitral valve explanted at 20-month post implantation.* PSIS mitral valve leaflet (**MVL**) (**A**-1.25x; Movat's) demonstrating matrix proteins of collagen (**B**), elastin (**C**), proteoglycans (**D**) and fibrin (**E**) (yellow/green, black, blue, dark pink respectively), with 70%, 3%, 25% and 2%, respectively of each ECM protein. A depicts the atrialis and V depicts the ventricularis layers of the mitral valve.

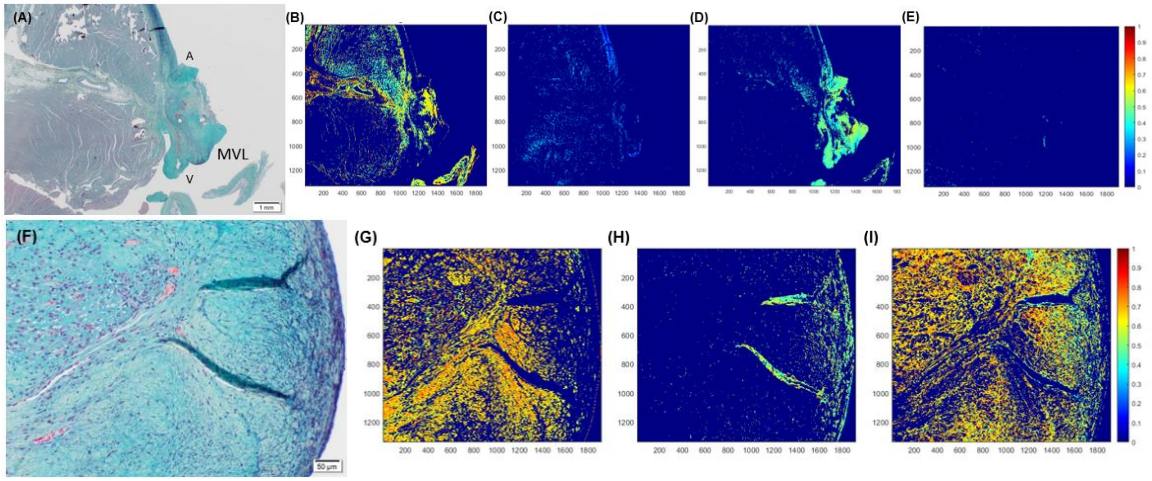

C.4.4: *ECM components of PSIS mitral valve explanted at 20-month post implantation.* PSIS mitral valve leaflet (**MVL**) (**A**-1.25x; Movat's) demonstrating matrix proteins of collagen (**B**), elastin (**C**), proteoglycans (**D**) and fibrin (**E**) (yellow/green, black, blue, dark pink respective), with 57%, 14%, 28% and 1%, respectively of each ECM protein. Zoomed in area of the leaflet (**F**-20x; Movat's) with (**G**) 37%, (**H**) 12% and (**I**) 47%, respectively of ECM proteins. A depicts the atrialis and V depicts the ventricularis layers of the mitral valve.

APPENDIX D: SPATIAL INTENSITY MAPS OF EXPLANT BABOON MITRAL VALVES AT ANNULUS SITE

ECM quantification for all of the baboon explants (3-, 11-, 20-months PSIS) at the annulus location from Section 4.2.3

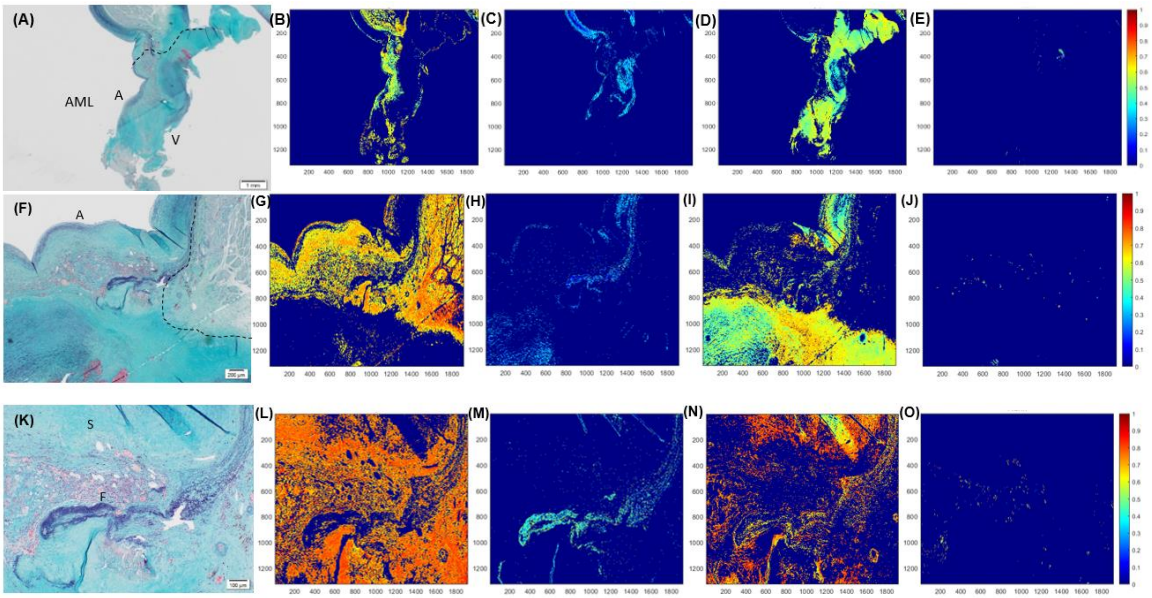

D.1: *ECM components of PSIS mitral valve explanted at 11-month post implantation focused at the annulus.* PSIS mitral valve leaflet (**MVL**) (**A**-1.25x; Movat's) demonstrating matrix proteins of collagen (**B**), elastin (**C**) proteoglycans (**D**) and faint fibrin (E) (yellow/green, black, blue and dark pink respectively), with 28%, 15%, 56% and 1%, respectively of each ECM protein. Zoomed in area at annulus edge (**F**-4x; Movat's) with (**G**) 48%, (**H**) 6%, (**I**) 46% and (**J**) 0.3%, respectively of ECM proteins. Higher magnification at location F, (**K**-10x; Moavt's) with ECM proteins of (**L**) 43%, (**M**) 17%, (**N**) 40% and (**O**) 0.1% of collagen, elastin, proteoglycans and fibrin, respectively. A depicts the atrialis and V depicts the ventricularis layers of the mitral valve.

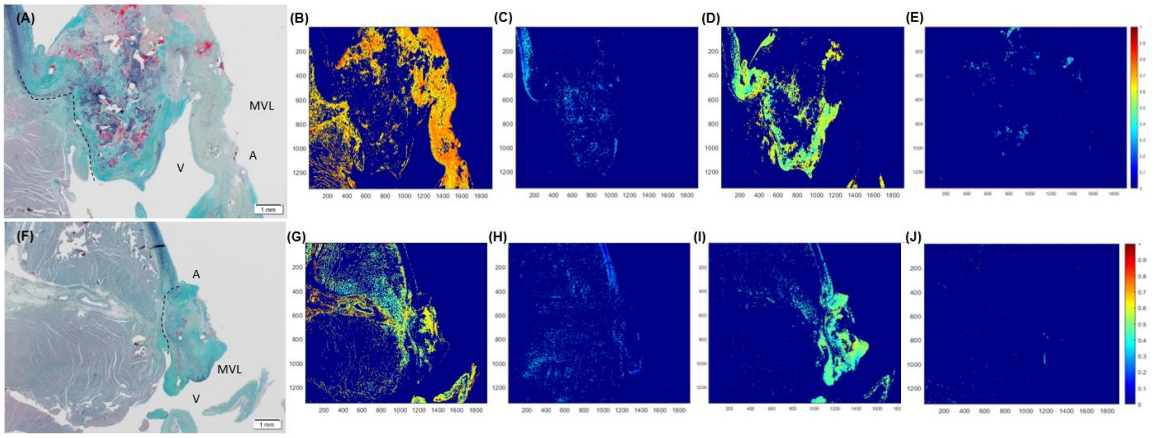

D.2: *ECM components of PSIS mitral valve explanted at 20-month post implantation focused at the annulus.* PSIS mitral valve leaflet (**MVL**) (**A**-1.25x; Movat's) zoomed at the annulus, where endocarditis occurred, demonstrating matrix proteins of collagen (**B**), elastin (**C**), proteoglycans (**D**), anf fibrin (E) (yellow/green, black, blue and dark pink, respectively), with 58%, 2%, 40% and 1%, respectively of each ECM protein. Another area of the annulus (**F**-1.25x; Movat's) with (**G**) 57%, (**H**) 14%, (**I**) 28% and (**J**) 1%, respectively of ECM proteins.

APPENDIX E: SPATIAL INTENSITY MAPS OF EXPLANT BABOON MITRAL VALVES AT NEOCHORDAE SITE

ECM quantification for all of the baboon explants (11-, 20-months PSIS) at the neochordae to papillary muscle location from Section 4.2.3

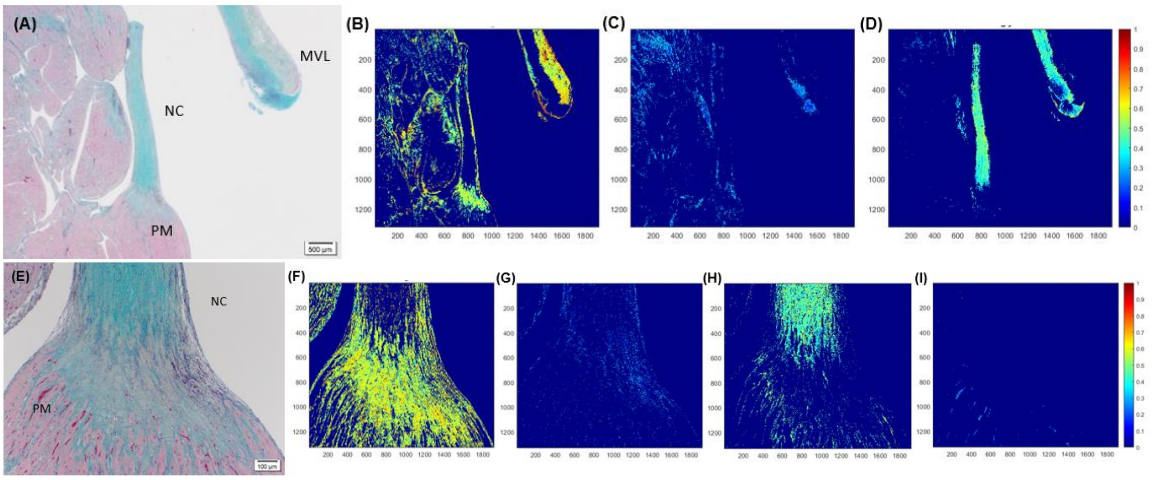

E.1: *ECM components of PSIS mitral valve explanted at 11-month post implantation focused at the neochordae and papillary muscle point.* PSIS mitral valve (**MVL**) (**A**-2x; Movat's) showing neochordae (NC), integrated to papillary muscle (PM) with matrix proteins of collagen (**B**), elastin (**C**) and proteoglycans (**D**) (yellow/green, black, blue respective), with 52%, 20% and 28%, respectively of each ECM protein. Higher magnification (**E**-10x; Movat's) zoomed at the NC demonstrating matrix proteins of collagen (**F**), elastin (**G**), proteoglycans (**H**) and fibrin (I) (yellow/green, black, blue and dark pink respectively), with 70%, 7%, 23% and 1%, respectively of each ECM protein.

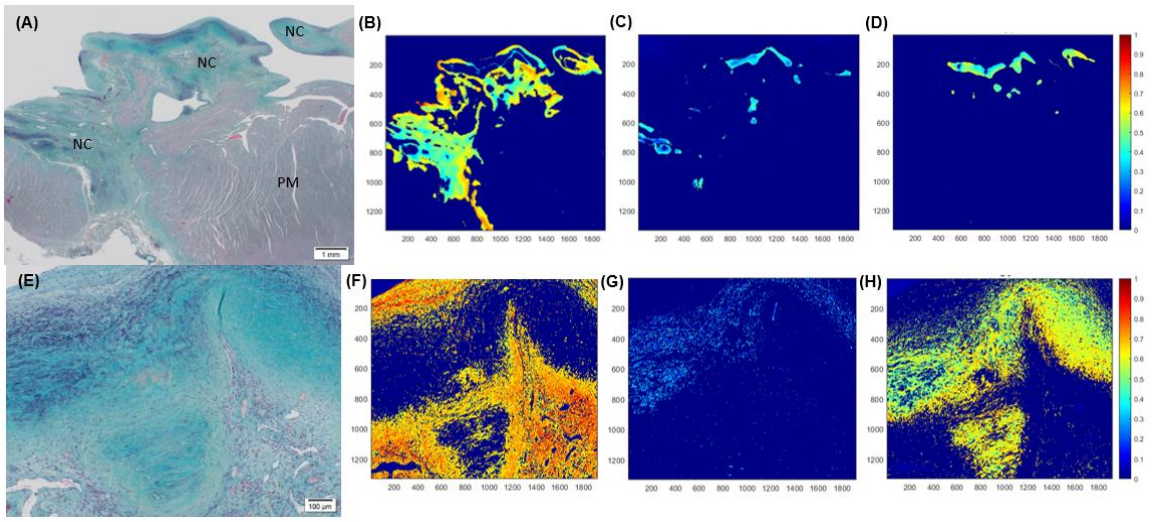

E.1.2: *ECM components of PSIS mitral valve explanted at 11-month post implantation focused at the neochordae and papillary muscle point.* PSIS mitral valve (**A**-1.25x; Movat's) showing neochordae (NC), integrated to papillary muscle (PM) with matrix proteins of collagen (**B**), elastin (**C**) and proteoglycans (**D**) (yellow/green, black, blue respectively), with 79%, 10% and 10%, respectively of each ECM protein. Higher magnification (**E**-10x; Movat's) zoomed at the NC demonstrating matrix proteins of collagen (**F**), elastin (**G**) and proteoglycans (**H**) (yellow/green, black, blue, respectively), with 47%, 6%, and 40%, respectively of each ECM protein.

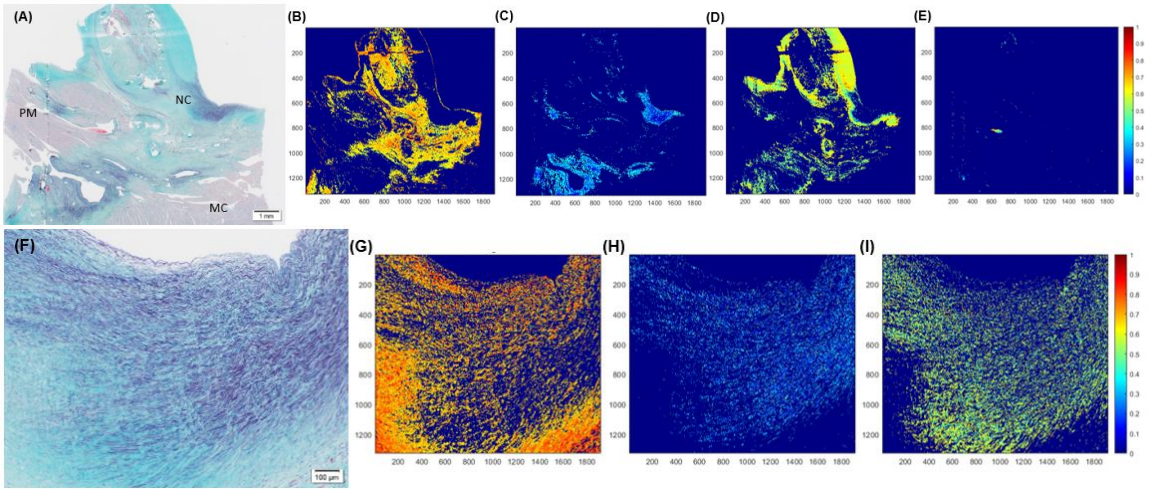

E.1.3: *ECM components of PSIS mitral valve explanted at 11-month post implantation focused at the neochordae and papillary muscle point.* PSIS mitral valve (**A**-1.25x; Movat's) showing neochordae (NC), integrated to myocardium (MC) with matrix proteins of collagen (**B**), elastin (**C**) proteoglycans (**D**) and fibrin (E) (yellow/green, black, blue and dark pink respectively), with 49%, 16% 34% and 1%, respectively of each ECM protein. Higher magnification (**F**-10x; Movat's) zoomed at the NC demonstrating matrix proteins of collagen (**G**), elastin (**H**), proteoglycans (**I**) (yellow/green, black, blue, respectively), with 49%, 19% and 33%, respectively of each ECM protein.

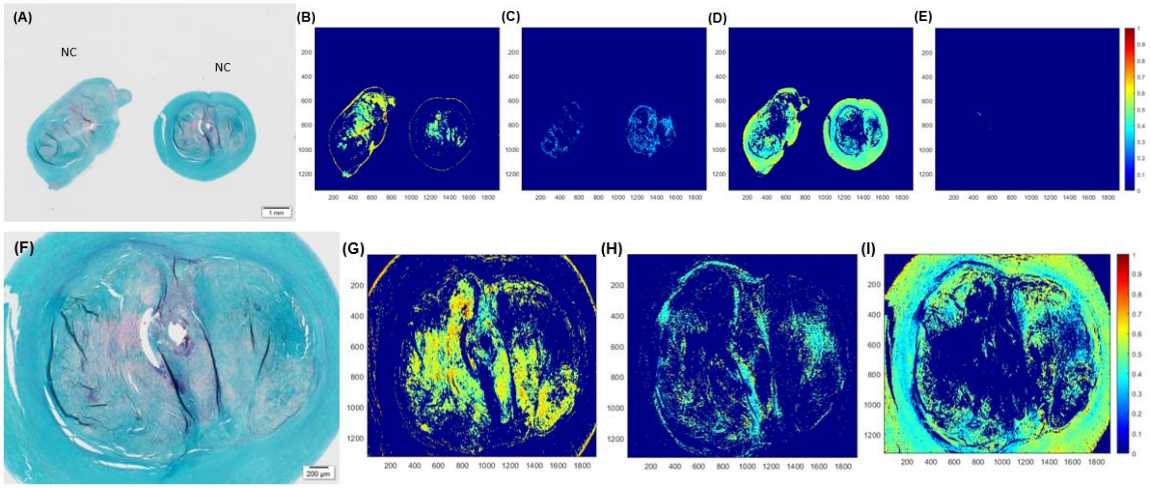

E.1.4: *ECM components of PSIS mitral valve explanted at 11-month post implantation focused at the neochordae and papillary muscle point.* PSIS mitral valve cross-section of (**A**-1.25x; Movat's) neochordae (NC), with matrix proteins of collagen (**B**), elastin (**C**) proteoglycans (**D**) and (**E**) fibrin (yellow/green, black, blue and dark pink respectively), with 23%, 10%, 67% and 0.04%, respectively of each ECM protein. Higher magnification (**F**-4x; Movat's) zoomed at the NC demonstrating matrix proteins of collagen (**G**), elastin (**H**) and proteoglycans (**I**) (yellow/green, black, blue, respectively), with 32%, 2%, and 66%, respectively of each ECM protein.

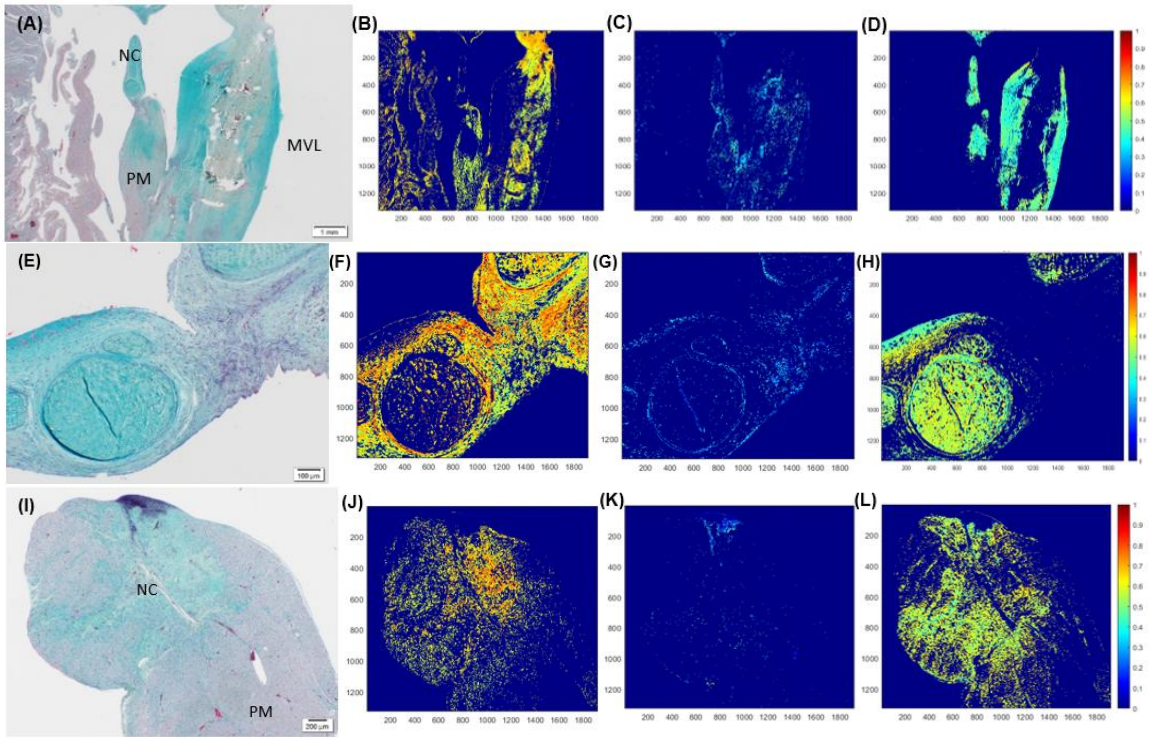

E.2: *ECM components of PSIS mitral valve explanted at 20-month post implantation focused at the neochordae and papillary muscle point.* PSIS mitral valve (**MVL**) (**A**-1.25x; Movat's) with neochordae (NC) and papillary muscle (PM) demonstrating matrix proteins of collagen (**B**), elastin (**C**) and proteoglycans (**D**) (yellow/green, black, blue, respectively), with 49%, 11 and 38%, respectively of each ECM protein. Higher magnification (**E**-10x; Movat's) zoomed at the NC demonstrating matrix proteins of collagen (**F**), elastin (**G**), proteoglycans (**H**) (yellow/green, black, blue, respectively), with 58%, 8% and 34%, respectively of each ECM protein. Another area of the NC (**I**-4x; Movat's) with (**J**) 35% collagen, (**K**) 10% elastin and (**L**) 55% proteoglycans.

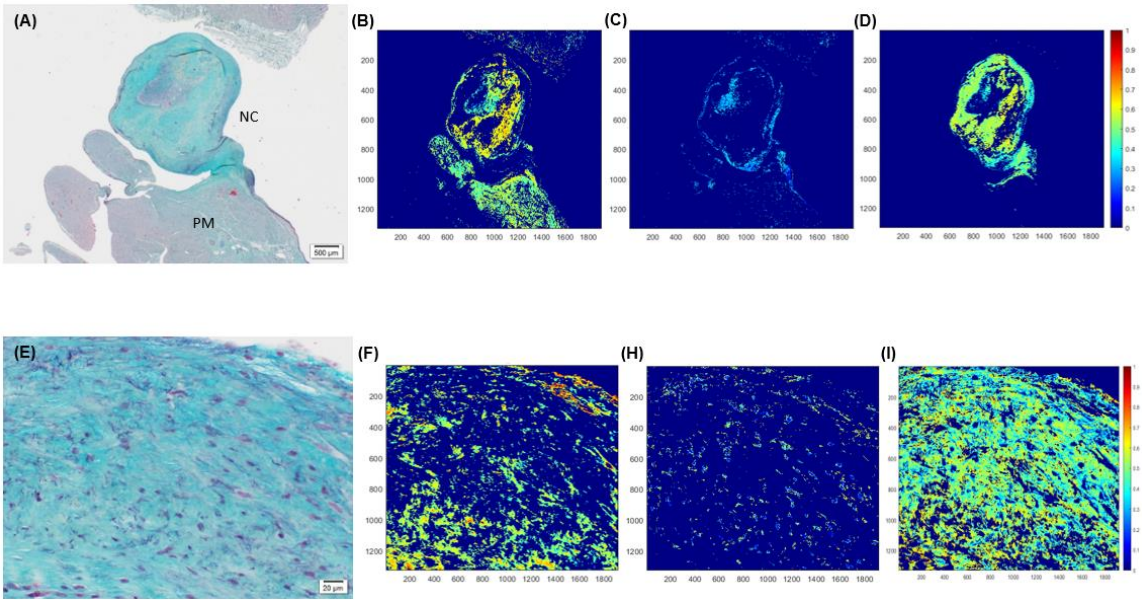

E.2.2: *ECM components of PSIS mitral valve explanted at 20-month post implantation focused at the neochordae and papillary muscle point.* PSIS mitral valve (**MVL**) (**A**-2x; Movat's) zoomed at the neochordae (NC) integrating with papillary muscle (PM) demonstrating matrix proteins of collagen (**B**), elastin (**C**) and proteoglycans (**D**) (yellow/green, black, blue respectively), with 49%, 12% and 39%, respectively of each ECM protein. Higher magnification (**E**-40x; Movat's) zoomed at the NC demonstrating matrix proteins of collagen (**F**), elastin (**G**), proteoglycans (**H**) (yellow/green, black, blue, respectively), with 25%, 6% and 69%, respectively of each ECM protein.

APPENDIX F: TORPEDO BIOREACTOR DESIGN

Design of all of the different parts of our laboratories custom-built, in-house, torpedo bioreactor from Section 5.1 (page 69)

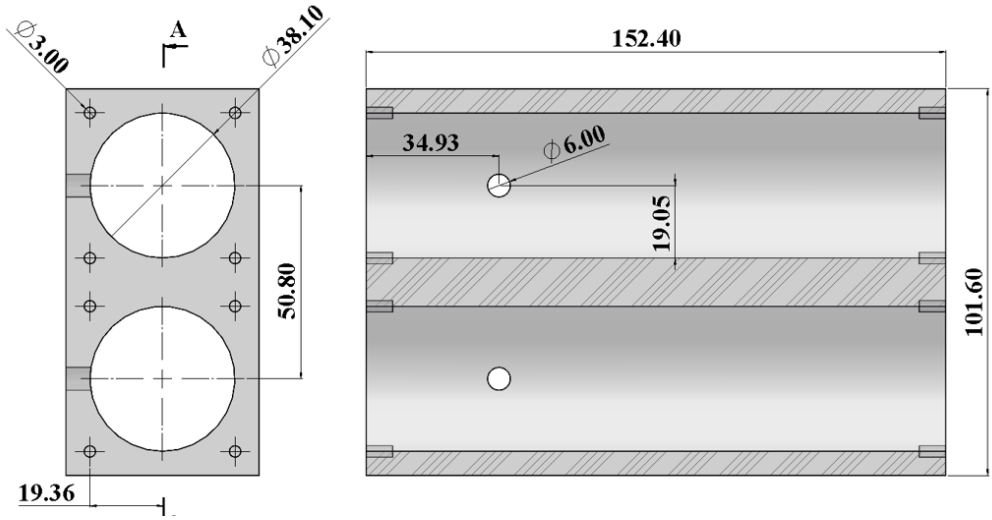

F.1 *Design of the main chamber of our laboratories custom-built, in-house, torpedo bioreactor*. The bioreactor is a U-shaped bioreactor made of acrylic. All dimensions are in mm.

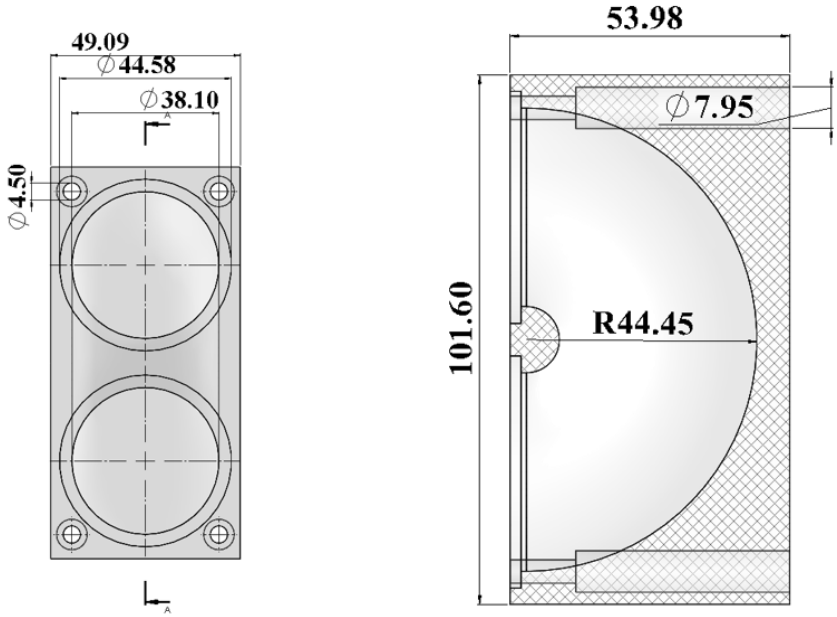

F.1.2 *Design of the U-shaped tube of our laboratories custom-built, in-house, torpedo bioreactor*. This is the U-shaped tube that is attached to the main chamber of the torpedo bioreactor, also made of acrylic. This design allows for higher fluid velocities and shear stress while still remaining in laminar flow. All dimensions are in mm.

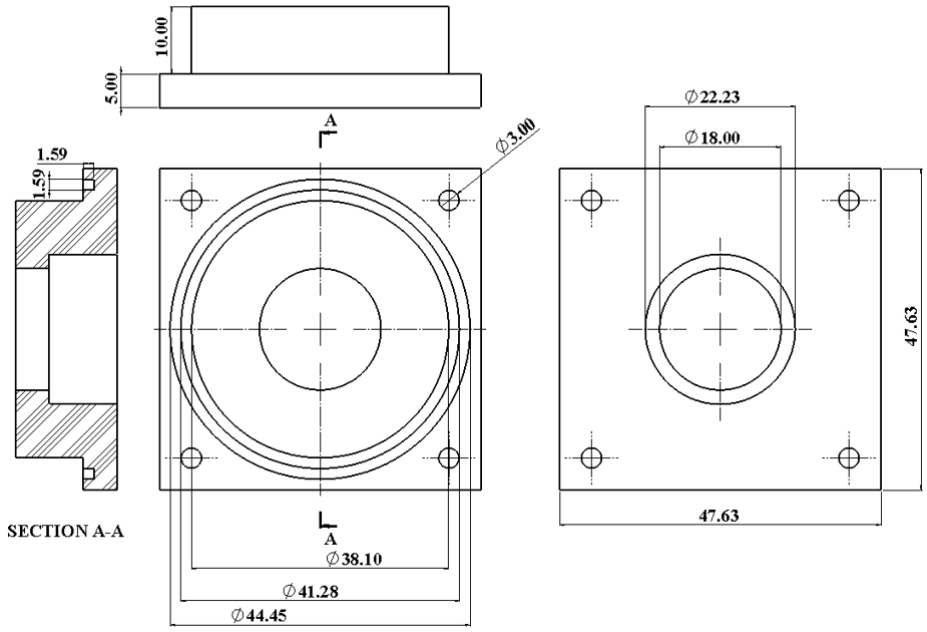

F.1.3 *Design of the caps of our laboratories custom-built, in-house, torpedo bioreactor*. These acrylic caps are used to seal the torpedo bioreactor; they are connected to the inlet tubing (which is supplied from the pump) and the outlet tubing (which is emptied out to the reservoir). All dimensions are in mm.

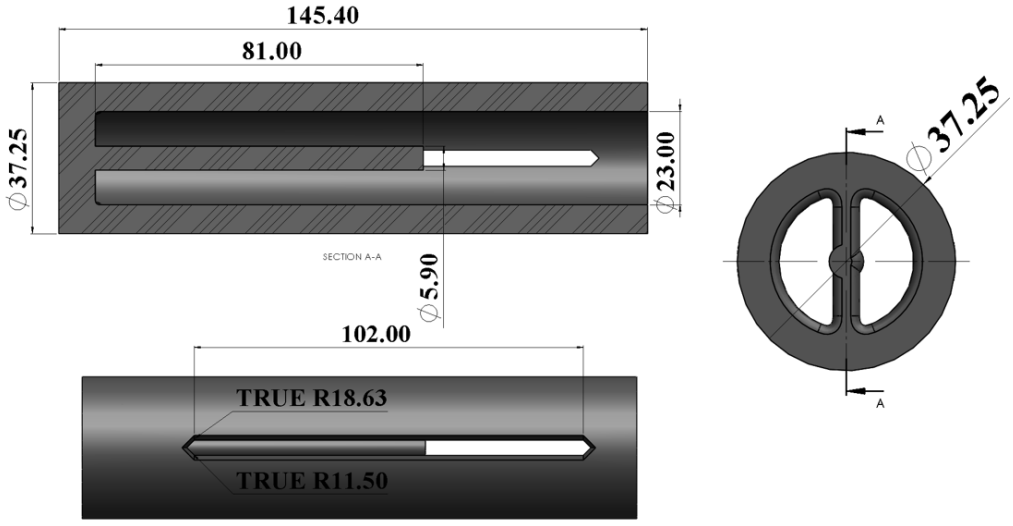

F.2 *Design of the internal chamber of our laboratories custom-built, in-house, torpedo bioreactor*. The internal chamber is made of PLA and houses our main component, the “torpedo”, which hold the scaffolds in place. All dimensions are in mm.

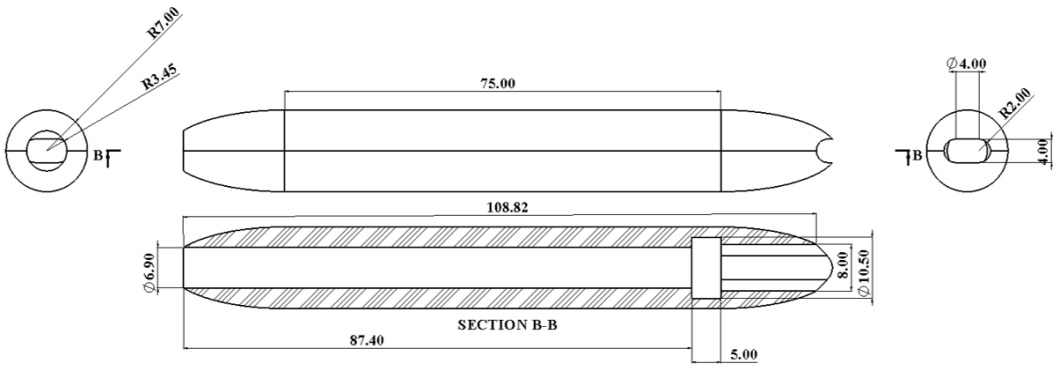

F.2.2 *Design of the torpedo of our laboratories custom-built, in-house, torpedo bioreactor*. The torpedo is housed inside of the internal chamber (Appendix F.2) and is made of PLA. The scaffolds are placed onto the torpedo so that the scaffold does not move due to the flow. All dimensions are in mm.

APPENDIX G: SPATIAL INTENSITY MAPS FOR ECM QUANTIFICATION OF STATIC IN VITRO PSIS TUBULAR VALVES

ECM quantification of different depths of “static” control group of tissue that was left in rotisserie culture for 22 days (Section 5.2.3).

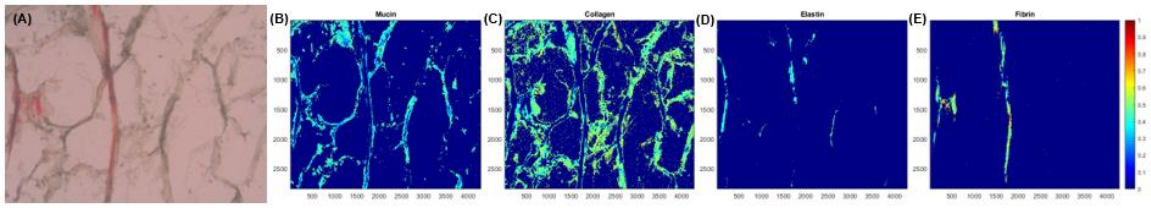

G.1: *ECM quantification of static PSIS valves*. (**A**) static PSIS valves were assessed for ECM quantification via spatial intensity maps (**B-E**). Spatial intensity maps for these static PSIS valves at a depth of (**A**) 112 µm were computed. There was (**B**) 11% mucins, (**C**) 17% collagen, (**D**) 1% elastin and (**E**) 2% fibrin present. Magnification 50x.

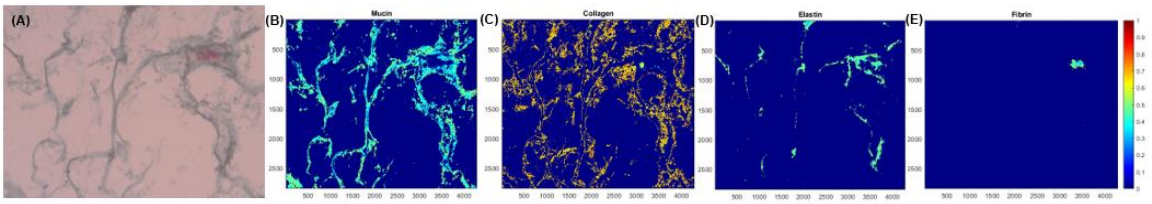

G.2: *ECM quantification of static PSIS valves*. (**A**) static PSIS valves were assessed for ECM quantification via spatial intensity maps (**B-E**). Spatial intensity maps for these static PSIS valves at a depth of (**A**) 208 µm were computed. There was (**B**) 14% mucins, (**C**) 14% collagen, (**D**) 3% elastin and (**E**) 0.3% fibrin present. Magnification 50x.

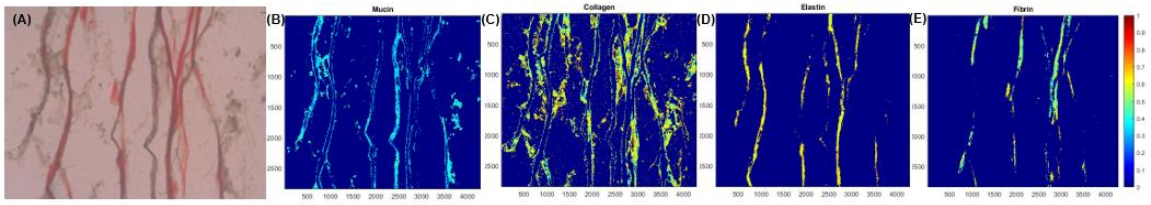

G.3: *ECM quantification of static PSIS valves*. (**A**) static PSIS valves were assessed for ECM quantification via spatial intensity maps (**B-E**). Spatial intensity maps for these static PSIS valves at a depth of (**A**) 400 µm were computed. There was (**B**) 8% mucins, (**C**) 16% collagen, (**D**) 3% elastin and (**E**) 3% fibrin present. Magnification 50x.

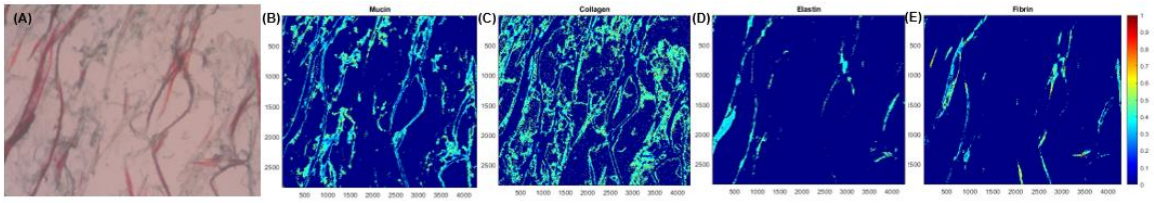

G.4: *ECM quantification of static PSIS valves*. (**A**) static PSIS valves were assessed for ECM quantification via spatial intensity maps (**B-E**). Spatial intensity maps for these static PSIS valves at a depth of (**A**) 496 µm were computed. There was (**B**) 16% mucins, (**C**) 27% collagen, (**D**) 3% elastin and (**E**) 4% fibrin present. Magnification 50x.

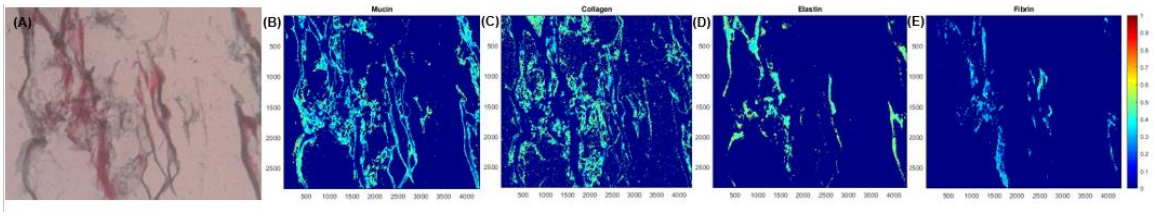

G.5: *ECM quantification of static PSIS valves*. (**A**) static PSIS valves were assessed for ECM quantification via spatial intensity maps (**B-E**). Spatial intensity maps for these static PSIS valves at a depth of (**A**) 688 µm were computed. There was (**B**) 16% mucins, (**C**) 17% collagen, (**D**) 6% elastin and (**E**) 3% fibrin present. Magnification 50x.

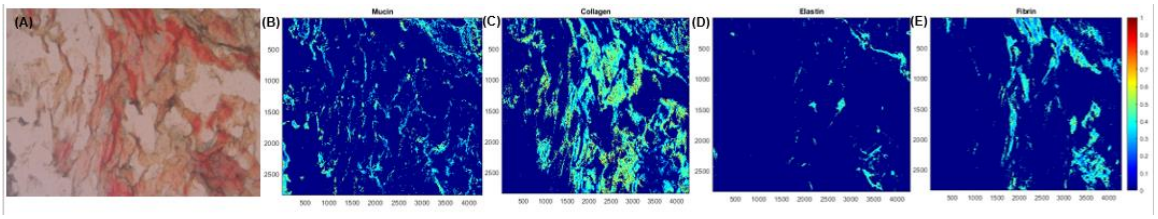

G.6: *ECM quantification of static PSIS valves*. (**A**) static PSIS valves were assessed for ECM quantification via spatial intensity maps (**B-E**). Spatial intensity maps for these static PSIS valves at a depth of (**A**) 784 µm were computed. There was (**B**) 10% mucins, (**C**) 29% collagen, (**D**) 2% elastin and (**E**) 11% fibrin present. Magnification 50x.

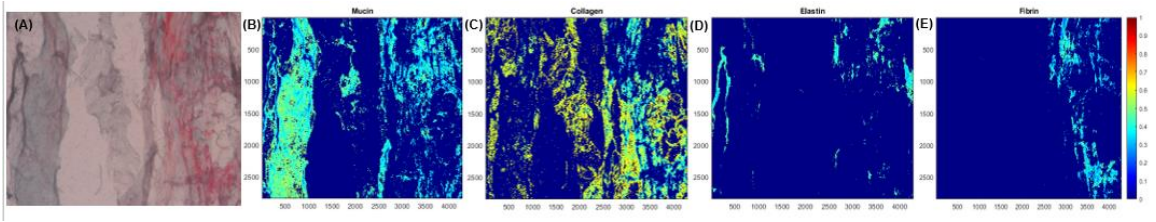

G.7: *ECM quantification of static PSIS valves*. (**A**) static PSIS valves were assessed for ECM quantification via spatial intensity maps (**B-E**). Spatial intensity maps for these static PSIS valves at a depth of (**A**) 976 µm were computed. There was (**B**) 29% mucins, (**C**) 28% collagen, (**D**) 4% elastin and (**E**) 6% fibrin present. Magnification 50x.

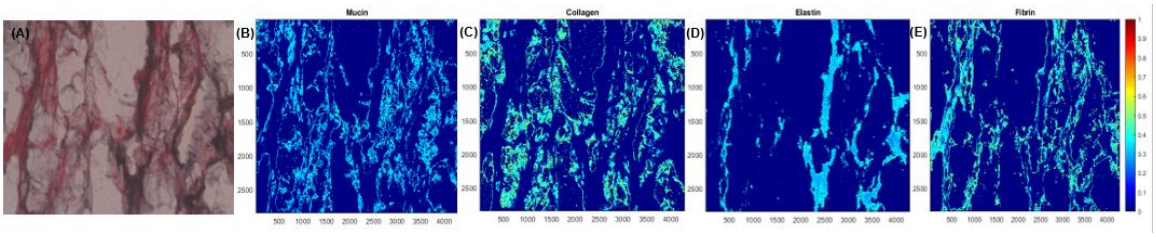

G.8: *ECM quantification of static PSIS valves*. (**A**) static PSIS valves were assessed for ECM quantification via spatial intensity maps (**B-E**). Spatial intensity maps for these static PSIS valves at a depth of (**A**) 1072 µm were computed. There was (**B**) 21% mucins, (**C**) 20% collagen, (**D**) 10% elastin and (**E**) 18% fibrin present. Magnification 50x.

APPENDIX H: SPATIAL INTENSITY MAPS FOR ECM QUANTIFICATION OF DYNAMIC IN VITRO PSIS TUBULAR VALVES

ECM quantification of different depths of dynamic group of tissue that was seeded for 8 days in rotisserie and in the torpedo bioreactor for 14 days (Section 5.2.3).

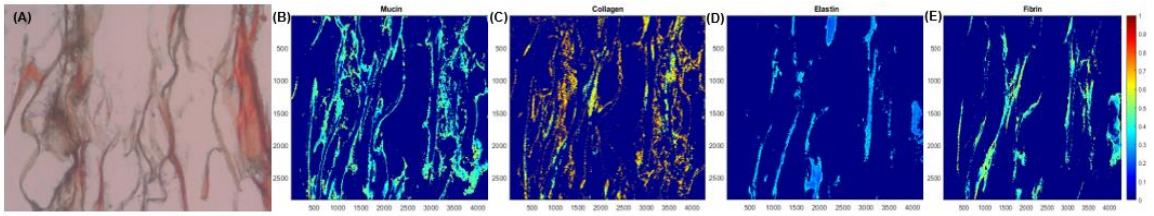

H.1: *ECM quantification of dynamic PSIS valves*. (**A**) dynamic PSIS valves were assessed for ECM quantification via spatial intensity maps (**B-E**). Spatial intensity maps for these dynamic PSIS valves at a depth of (**A**) 112 µm were computed. There was (**B**) 17% mucins, (**C**) 12% collagen, (**D**) 7% elastin and (**E**) 8% fibrin present. Magnification 50x.

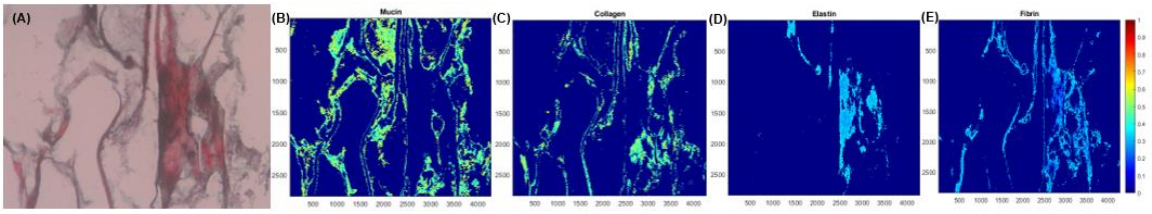

H.2: *ECM quantification of dynamic PSIS valves*. (**A**) dynamic PSIS valves were assessed for ECM quantification via spatial intensity maps (**B-E**). Spatial intensity maps for these dynamic PSIS valves at a depth of (**A**) 208 µm were computed. There was (**B**) 17% mucins, (**C**) 9% collagen, (**D**) 5% elastin and (**E**) 10% fibrin present. Magnification 50x.

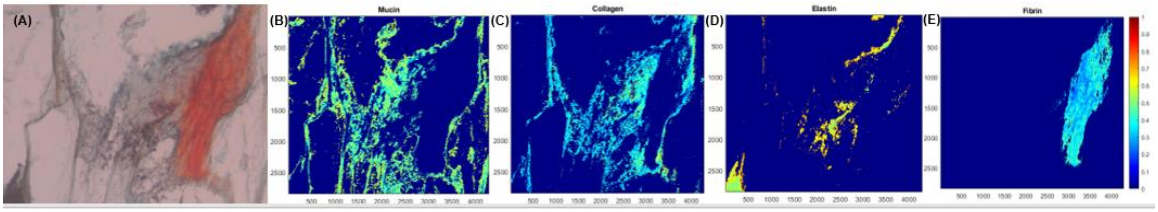

H.3: *ECM quantification of dynamic PSIS valves*. (**A**) dynamic PSIS valves were assessed for ECM quantification via spatial intensity maps (**B-E**). Spatial intensity maps for these dynamic PSIS valves at a depth of (**A**) 400 µm were computed. There was (**B**) 21% mucins, (**C**) 16% collagen, (**D**) 8% elastin and (**E**) 10% fibrin present. Magnification 50x.

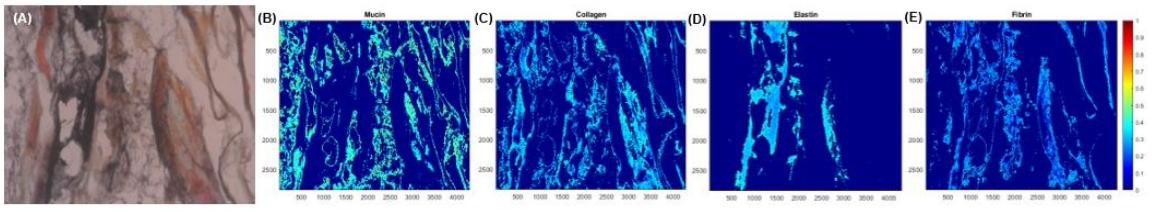

H.4: *ECM quantification of dynamic PSIS valves*. (**A**) dynamic PSIS valves were assessed for ECM quantification via spatial intensity maps (**B-E**). Spatial intensity maps for these dynamic PSIS valves at a depth of (**A**) 496 µm were computed. There was (**B**) 23% mucins, (**C**) 22% collagen, (**D**) 10% elastin and (**E**) 17% fibrin present. Magnification 50x.

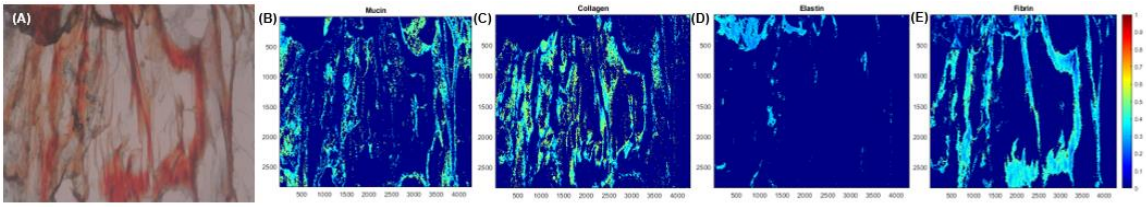

H.5: *ECM quantification of dynamic PSIS valves*. (**A**) dynamic PSIS valves were assessed for ECM quantification via spatial intensity maps (**B-E**). Spatial intensity maps for these dynamic PSIS valves at a depth of (**A**) 688 µm were computed. There was (**B**) 18% mucins, (**C**) 19% collagen, (**D**) 5% elastin and (**E**) 23% fibrin present. Magnification 50x.

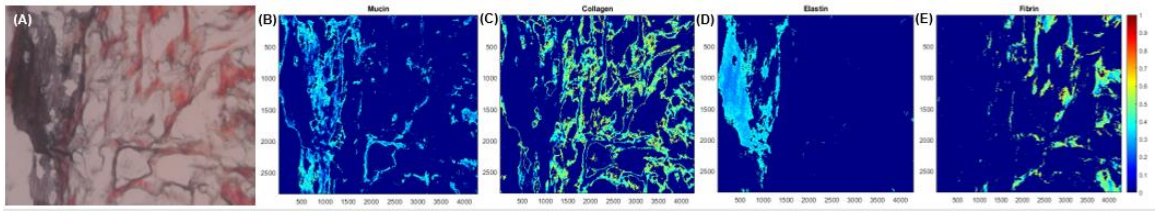

H.6: *ECM quantification of dynamic PSIS valves*. (**A**) dynamic PSIS valves were assessed for ECM quantification via spatial intensity maps (**B-E**). Spatial intensity maps for these dynamic PSIS valves at a depth of (**A**) 784 µm were computed. There was (**B**) 14% mucins, (**C**) 24% collagen, (**D**) 13% elastin and (**E**) 10% fibrin present. Magnification 50x.

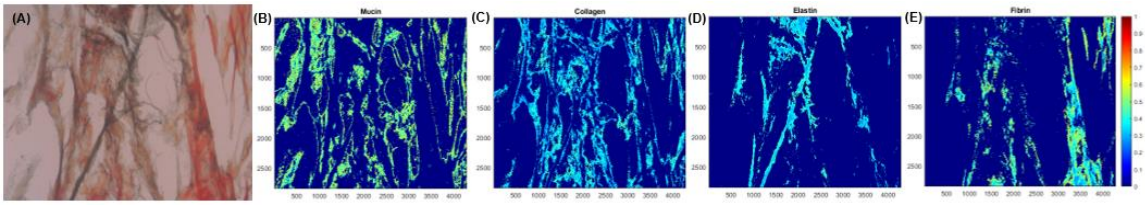

H.7: *ECM quantification of dynamic PSIS valves*. (**A**) dynamic PSIS valves were assessed for ECM quantification via spatial intensity maps (**B-E**). Spatial intensity maps for these dynamic PSIS valves at a depth of (**A**) 976 µm were computed. There was (**B**) 21% mucins, (**C**) 22% collagen, (**D**) 10% elastin and (**E**) 12% fibrin present. Magnification 50x.

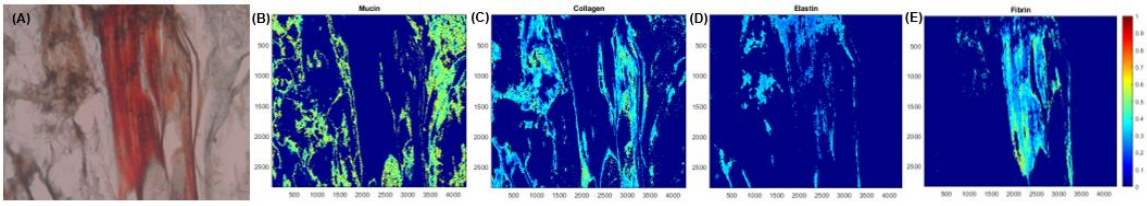

H.8: *ECM quantification of dynamic PSIS valves*. (**A**) dynamic PSIS valves were assessed for ECM quantification via spatial intensity maps (**B-E**). Spatial intensity maps for these dynamic PSIS valves at a depth of (**A**) 1072 µm were computed. There was (**B**) 24% mucins, (**C**) 24% collagen, (**D**) 9% elastin and (**E**) 14% fibrin present. Magnification 50x.

VITA

BRITTANY A. GONZALEZ

Born, Miami, Florida

2011-2013	A.A, Engineering-Science Miami Dade College Honors College Miami, Florida
2013-2015	B.S., Biomedical Engineering Minor, Health, Medicine & Society Georgia Institute of Technology Atlanta, Georgia
2015	Research Experiences for Undergraduates (REU) University of Nebraska-Lincoln Bio/Flow Systems Research Laboratory Lincoln, Nebraska
	Undergraduate Research Volunteer Georgia Institute of Technology Tissue Mechanics Lab (TML) Atlanta, Georgia
2016-2018	NSF Bridge to Doctorate Fellowship Florida International University Miami, Florida
2018-2019	Teaching Assistant Florida International University Miami, Florida
2019-2020	Doctoral Candidate Florida International University Miami, Florida
2020	Dissertation Year Fellowship Florida International University Miami, Florida

PUBLICATIONS AND PRESENTATIONS

Gonzalez B.A, Gonzalez-Perez, M., Mirza, A., Scholl, F., Bibevski, S., Rivas-Wagner, K., Bibevski, J., Hernandez, L., Ladich, E., Brehier, V., Casares, M.,

Morales, P., Lopez, J., Wagner, J., Ramaswamy, S: Extracellular Matrix Quantification of Fully Regenerated Neochordae after Bio-scaffold Mitral Valve Implantatio in a Juvenille Non-human Primate Model, American Heart Association's (AHA's) Scientific Sessions Conference, November 14th-16th, Virtual Meeting, 2020.

Gonzalez, B. A., Perez-Nevarez, M., Mirza, A., Perez, M. G., Lin, Y. M., Hsu, C. P. D., ... & George, F. (2020). Physiologically Relevant Fluid-Induced Oscillatory Shear Stress Stimulation of Mesenchymal Stem Cells Enhances the Engineered Valve Matrix Phenotype. *Frontiers in Cardiovascular Medicine*, *7*.

Gonzalez, B. A., Pour Issa, E., Mankame, O. V., Bustillos, J., Cuellar, A., Rodriguez, A. J., ... & Casares, M. (2020). Porcine small intestinal submucosa mitral valve material responses support acute somatic growth. *Tissue Engineering Part A*, *26*(9-10), 475-489.

Gonzalez, B., Hernandez, L., Bibevski, S., Scholl, F., Brehier, V., Casares, M., Bibevski, J., Rivas, K., Morales, P., Wagner, J., Lopez, J., Ramaswamy, S. Abstract 11348: Recapitulation of Human Bio-Scaffold Mitral Valve Growth in the Baboon Model. Circulation, Vol 138, Issue Suppl_1, 2018.

Gonzalez B.A, Scholl, F., Bibevski, S., Rivas, K., Bibevski, J., Hernandez, L., Ladich, E., Brehier, V., Casares, M., Morales, P., Lopez, J., Wagner, J., Ramaswamy, S (VIRTUAL VIDEO): Complete Regeneration of Neochordae Component of Bio-scaffold Mitral Valve Apparatus in a Non-human Primate Model, Summer Biomechanics, Bioengineering and Biotransport (SB3C), June 17th- 20th, Virtual Meeting, 2020.

Gonzalez B, Scholl, F., Bibevski, S., Hernandez, L., Brehier, V., Casares, M., Rivas, K., Morales, P., Lopez, J., Wagner, J., Bibevski, J., Ramaswamy, S (ORAL): Longitudinal Tissue Engineered Mitral Heart Valve Growth Estimation in a Nonhuman Primate Model, Biomedical Engineering Society Annual Fall Meeting (BMES), October 16-19th, Philadelphia, PA, 2019.

Gonzalez B, Bustillos J, Shaver M, Rodriguez A, Cuellar A, Agarwal A, Ramaswamy S (POSTER): Leaflet Extensions in Porcine Small Intestinal Submucosa Bio-Scaffolds for Heart Valve Regenerative Applications, Biomedical Engineering Society Annual Fall Meeting (BMES), October 17-20th, Atlanta, GA, 2018.

Gonzalez B, Hernandez L, Bibevski S, Scholl F, Brehier V, Casares M, Bibevski J, Rivas K, Morales P, Wagner J, Lopez J, Ramaswamy S (ORAL): Assessment of Growth of Mitral Valves Fabricated from Porcine Small Intestinal Submucosa in a Nonhuman Primate Model. 8th World Congress of Biomechanics, July 8-12, Dublin, Ireland 2018.